Acoustofluidic rare cell sample preparation

Antfolk, Maria

2015

Acoustofluidic rare cell sample preparation

Maria Antfolk

LUND
UNIVERSITY

DOCTORAL DISSERTATION
by due permission of the Faculty of Engineering, Lund University, Sweden. To be defended in E:1406, Ole Römers väg 3, Lund, on December 11th at 09:15.

Faculty opponent
Professor Abraham Lee, University of California, Irvine

Organization LUND UNIVERSITY Department of Biomedical Engineering P.O. Box 118, S-221 00 Lund, Sweden	Document name DOCTORAL DISSERTATION Date of issue: November 17th, 2015
Author: Maria Antfolk	Sponsoring organization: VR, Vinnova, SSF, KAW
Title: Acoustofluidic rare cell sample preparation	

Abstract: Acoustofluidics utilizes a combination of acoustics, in the form of ultrasound, and microfluidics to manipulate cells and particles. This has proven to be a versatile method that is gentle to the cells. In this thesis acoustofluidics has been used for processing rare cells in continuous flow. Rare cells are within this thesis defined as cells that are present in numbers of 1-1000 per mL in a much larger population of background cells. Rare cells present in blood have been of particular interest, and cancer cells and bacteria have been used as model cells. In this thesis acoustofluidics has first been used to concentrate cells. This was done by using two-dimensional focusing and a multistage acoustofluidic device where sequential concentration steps, generating moderate concentration factors, could be multiplied into large concentration factors. The usefulness of the method was then extended as the critical particle focusing size was lowered to also allow focusing of bacteria. This was done through using two-dimensional focusing, which was shown to change the acoustic streaming pattern to no longer counteract the primary acoustic radiation force. The new critical particle focusing size was determined to be between 0.5 µm and 0.24 µm in particle diameter for polystyrene-like particles. In the third paper a simplyfied acoustofluidic device, that does not rely on a clean fluid sheath flow to prealign the cells or particles before the separation, was presented. To be able to do this the device used only two-dimensional focusing to prealign the cells. The usefulness of the device was in turn demonstrated with the separation of cancer cells from white blood cells where it was shown to perform comparably to previously presented devices. In the fourth paper a separation method was combined with the concentration method presented in the first paper on an integrated device. The device was shown to be able to simultaneously separate and concentrate cancer cells from white blood cells. Finally, the previously proposed concentration device was integrated with a DEP single cell trapping device further showing the usefulness of the acoustofluidic method. Standing alone, the DEP trapping device could only process sample at a flow rate of 4 µL/min while still maintaining a high trapping efficiency.By integrating the DEP trapping device with the acoustofluidic concentrator device a higher sample inflow rate could be used as the acoustofluidic device could gear down the flow rate before the sample entered the DEP trapping device. Together samples could be processed ~10 times faster than using the DEP trapping device alone, while still recovering over 90% of the cells.

Key words: Acoustophoresis, acoustofluidics, ultrasound, microfluidics, cell separation, volume concentration, Lab-on-a-Chip	
Classification system and/or index terms (if any)	
Supplementary bibliographical information: ISRN: LUTEDX/TEEM - 1099 – SE Report-nr: 3/15	Language: English
ISSN and key title	ISBN: 978-91-7623-526-3 (print) ISBN: 978-91-7623-527-0 (pdf)
Recipient´s notes	Number of pages: 138 / Price Security classification

Distribution by Maria Antfolk, Department of Biomedical Engineering, P.O. Box 118, S-221 00 Lund, Sweden

To Christian and Ellen, my buoys in the bay

Everything counts in large amounts
-Depeche Mode

Cover illustration
Illustration of a multistage acoustophoresis device used for concentrating cancer cells (Paper I)

Public defence
December 11th, 2015, 09.15 in E:1406, E-huset, LTH, Lund University, Ole Römers väg 3, 223 63 Lund, Sweden

Advisors
Professor Thomas Laurell
Dr. Per Augustsson
Dr. Andreas Lenshof
Department of Biomedical Engineering, Lund University, Sweden

Faculty opponent
Professor Abraham Lee
Department of Biomedical Engineering, University of California, Irvine, USA

Examination board
Associate Professor Lisa Rydén
Department of Clinical Sciences, Lund University, Sweden
Associate Professor David Bryder
Department of Laboratory Medicine, Lund University, Sweden
Associate Professor Aman Russom
School of Biotechnology, Royal Institute of Technology, Sweden
Deputy member: Professor Tautgirdas Ruzgas
Department of Biomedical Science, Malmö University, Sweden
Deputy member: Dr. Edith Hammer
Department of Biology, Lund University, Sweden

Chairman
Associate Professor Johan Nilsson
Department of Biomedical Engineering, Lund University, Sweden

ISBN: 978-91-7623-526-3 (print)
ISBN: 978-91-7623-527-0 (pdf)
Report-nr: 3/15
Printed in November 2015 by Tryckeriet i E-huset, Lund, Sweden

List of publications

I **Two-hundredfold volume concentration of dilute cell and particle suspensions using chip integrated multistage acoustophoresis**
Maria Nordin, and Thomas Laurell,
Lab on a Chip, 2012, 12(22), 4610-4616,

Authors contribution: Developed the idea, fabricated the device, performed the experiments, major part of writing.

II **Focusing of sub-micrometer particles and bacteria enabled by two-dimensional acoustophoresis**
Maria Antfolk, Peter B Muller, Per Augustsson, Henrik Bruus, and Thomas Laurell,
Lab on a Chip, 2014, 14(15), 2791-2799

Authors contribution: Developed the idea, fabricated the device, performed the experiments, major part of writing.

III **A single inlet two-stage acoustophoresis chip enabling tumor cell enrichment from white blood cells**
Maria Antfolk, Christian Antfolk, Hans Lilja, Thomas Laurell, and Per Augustsson,
Lab on a Chip, 2015, 15(9), 2102-2109

Authors contribution: Part of developing the idea, fabricated the device, performed the experiments, major part of writing.

IV **Acoustofluidic, label-free separation and simultaneous concentration of rare tumor cells from white blood cells**
Maria Antfolk, Cecilia Magnusson, Per Augustsson, Hans Lilja, and Thomas Laurell
Analytical Chemistry, 2015, 87(18), 9322-9328

Authors contribution: Developed the idea, part of fabricated the device, performed major part of the experiments, major part of writing.

V **Highly efficient single cell arraying by integrating acoustophoretic cell pre-concentration and dielectrophoretic cell trapping**
Soo Hyeon Kim*, Maria Antfolk*, Marina Kobayashi, Shohei Kaneda, Thomas Laurell, and Teruo Fujii
Lab on a Chip, 2015, 15(22), 4356-4363
*Authors contributed equally to this work.

Authors contribution: Part of developing the idea, fabricated acoustophoresis device, performed proof-of-concept experiments, tech-transfer to Japan, part of writing.

Related papers

VI **Microfluidic, label-free enrichment of prostate cancer cells in blood based on acoustophoresis**
Per Augustsson*, Cecilia Magnusson*, Maria Nordin, Hans Lilja, and Thomas Laurell
Analytical Chemistry, 2012, 84(18), 7954-7962
*Authors contributed equally to this work.

VII **Microchannel acoustophoresis does not impact survival or function of microglia, leukocytes or tumor cells**
Miguel Burguillos*, Cecilia Magnusson*, Maria Nordin*, Andreas Lenshof, Per Augustsson, Magnus Hansson, Eskil Elmér, Hans Lilja, Patrik Brundin, Thomas Laurell, and Tomas Deierborg
PLoS ONE, 2013, 8(5), e64233
*Authors contributed equally to this work.

VIII **Acoustic actuated fluorescence activated sorting of microparticles**
Ola Jakobsson, Carl Grenvall, Maria Nordin, Mikael Evander, and Thomas Laurell
Lab on a Chip, 2014,14(11) 1943-1950

IX **Continuous flow two-dimensional acoustic orientation of nonspherical cells**
Ola Jakobsson, Maria Antfolk, and Thomas Laurell
Analytical Chemistry, 2014, 86(12), 6111-6114

X **Thousand-fold volumetric concentration of live cells with a recirculating acoustofluidic device**
Ola Jakobsson, Seung Soo Oh, Maria Antfolk, Michael Eisenstein, Thomas Laurell, and H. Tom Soh
Analytical Chemistry, 2015, 87(16), 8497-8502

Contents

1

Introduction

An early encounter with rare cells was done by pathologist Thomas Ashworth, in 1869, when he noticed some unusual cells in the blood of a deceased cancer patient. The cells he had found did not look like normal blood cells but where instead similar to the cells found in the numerous cancer tumors in the patient's body. Ashworth speculated that these cells were derived from the tumors and would explain the amount of tumors found in the patient[1]. Since then cancer cells found in blood, known as circulating tumor cells, have been proven to be derived from the cancer tumors but science has not yet come to an agreement of whether all of these cells or just a few of them have the potential to form new secondary tumors. Nevertheless, they are recognized for their diagnostic and prognostic value, as are many other rare cell populations.

The advent of the Lab-on-a-Chip and Micro Total Analysis System (μTAS) concept in the early 1990s, where the aim is to shrink an entire laboratory with all its functions onto a microchip (Figure 1.1), eventually presented new tools for the rare cell research area. This thesis' contribution to this research area is a few operation units that can be further integrated together with other sample preparation or analysis units to be parts of a true μTAS.

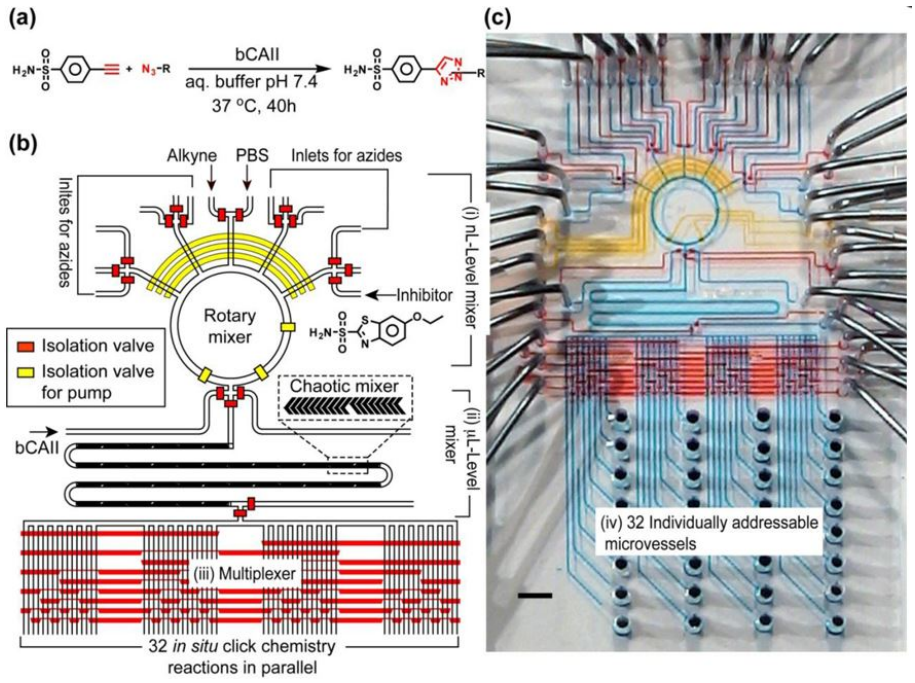

Figure 1.1: Example of a lab on a chip device used for in situ click chemistry reactions. Reprinted from Nano Today, 4(6) Lin, W.-Y., Wang, Y., Wang, S., and Tseng, H.-R. Integrated Microfluidic Reactors, 470-481[2]. Copyright 2009, with permission from Elsevier.

2

Rare cells - definition and importance

Rare cells are cells that are low in abundance compared to another much larger population of background cells. Throughout this thesis a rare cell will also be defined as a cell with an abundance of less than 1000 cells/mL.

2.1 Types of rare cells

Rare cell populations are sought after for different reasons such as disease monitoring, diagnosis, or the development of personalized medicine, where the study of rare cells could provide opportunities to more specifically target treatments. Many interesting rare cells are derived from blood. These cells include circulating tumor cells, fetal cells in maternal blood, endothelial progenitor cells or circulating endothelial cells, stem cells, bacteria, or cells infected by parasites, bacteria or viruses. Each cell type has its own characteristics and separation challenges.

Circulating tumor cells

Circulating tumor cells (CTCs) are cancer cells shed from cancer tumors into the blood stream. Travelling with the blood stream, they can reach other tissues and potentially form secondary tumors, metastases. The cancer cells are mostly found in quantities of only 1-10 CTCs/mL in a background of about some billion erythrocytes, some 100 million thrombocytes, and some million leukocytes (Figure 2.1). These cancer cells are of interest to clinicians for their value as prognostic and diagnostic markers. If studied over a period of time they can also give insights into the evolution of the cancer tumor during the disease progression and indicate the response to treatment. They may also provide information that can lead to better drugs for a more targeted and personalized treatment[3,4]. CTCs have been detected in the blood from patients harbouring all major cancer types that have reached advanced metastatic stages but are very rarely detected in healthy subjects[3,5,6]. The quantities of CTCs found in the blood have been shown to be an independent predictor of disease progression in many types of cancers[4].

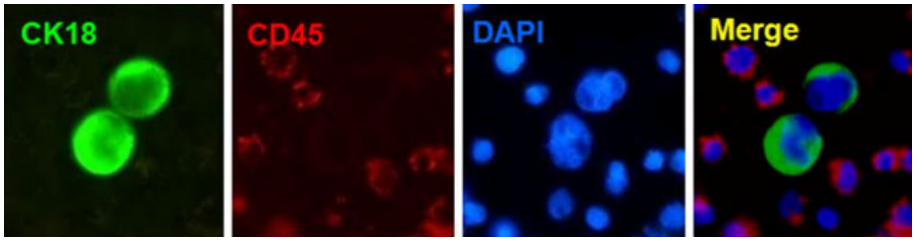

Figure 2.1: H1975 cells identified among WBCs by being positive for CK18 and negative for CD45. Cell nuclei are visualized by counterstaining with DAPI. Reprinted from: Ran, R., Li, L., Wang, M., Wang, S., Zheng, Z., & Lin, P. P. (2013). Determination of EGFR mutations in single cells microdissected from enriched lung tumor cells in peripheral blood. Analytical and Bioanalytical Chemistry, 405(23), 7377-82[7]. Reprinted with kind permission from Springer Science and Business Media.

Most attempts to isolate CTCs have been made on samples derived from carcinoma patients. This is due to the common nature of these cancers and because they express specific biomarkers that can be used to facilitate their isolation and detection. No other cancer forms have so far provided any specific biomarker for detection, although vimentin expressed at the cell surface have recently been reported as a biomarker for sarcoma[8]. CTCs originating from carcinomas are commonly isolated and detected using epithelial cell specific markers, such as epithelial cell adhesion molecule (EpCAM) in combination with cytokeratins. The use of epithelial cell markers may, however, lead to that subpopulations of cancer cells low in expression of EpCAM or cytokeratins remain undetected. For epithelial cell cancers to shed circulating tumor cells the cancer cells have to undergo an epithelial-mesenchymal transition. This is considered a crucial event where the cancer cells adopt a more mesenchymal-like migratory phenotype, which allows them to migrate from the original tumor into the blood stream. This transition might lead to the loss of epithelial cell

markers, which thereby disables the detection of these cells by methods relying on epithelial cell markers[9].

Fetal cells in maternal blood

During a pregnancy, cells from the fetus enter into the maternal bloodstream. A range of cell types such as fetal lymphocytes, granulocytes, trophoblasts, and nucleated red blood cells (nRBCs) have been found[10]. From these, the fetal nucleated red blood cells have been attracting most interest so far. Although rare and found in numbers as low as 1-2 cells/mL, these cells are among the most abundant of the fetal cells found in the maternal circulations. Another advantage is their relatively short lifespan, which makes them unlikely to persist between pregnancies, like other cell types may do[11].

By isolating fetal cells from maternal blood fetal genetic or chromosomal disorders such as sickle cell anaemia or trisomy 13, 18, and 21 can be identified, without the use of amniocentesis or chorionic villus sampling (CVS), in a less invasive way[10]. Sampling from the uterus can sometimes lead to miscarriage, infections or needle injury of the foetus. Even though rare, the risk of miscarriage after amniocentesis is about 1% and after CVS about 2%[12]. Needless to say, this is a risk that all parents would like to avoid as far as possible.

The isolation of fetal cells from the maternal circulation is complicated by the fact that there are no specific cell markers that are common to all the fetal cells found in the maternal circulation. Specific surface markers have, however, recently been proposed for the fetal nucleated red blood cells[13] and the trophoblasts[14]. Furthermore, the trophoblasts have also been successfully expanded *in vitro* after isolation[15].

Bacteria

Bacteria may be found in matrixes such as blood, water, or food. When bacteria are found in the blood stream there is a risk of developing bacteraemia or sepsis, especially critical to immunodeficient patients, elderly, or infants. Once sepsis have been developed the time it takes to identify the pathogen and administrate the right antibiotics is of great importance as the mortality rises with every hour that the patient goes untreated. The overall mortality (in North America) is as high as 30% and increasing to 50% if the patient develops the more severe syndrome, septic shock[16].

The rarity of the bacteria makes the identification of them time consuming as it is commonly relying on blood culture and expansion of the bacteria before any analysis can be performed[17]. The identification process commonly takes one day but may take as much as four days if the bacteria are slow growing. Adding to this time the samples often has to be sent to a central microbiology laboratory for the identification. During this time a broad spectrum of antibiotics is usually administered to the patient in hopes of clearing the bacteria. Earlier identification would not only increase the overall survival rate but also decrease the unnecessary use of antibiotics that contributes to the development of antibiotics resistant bacteria.

Circulating endothelial cells and endothelial progenitor cells

Circulating endothelial cells (CECs) and endothelial progenitor cells (EPCs) can be found in blood, and their number has been shown to increase or decrease with disease progression[18]. CECs are associated with vascular injury while the EPCs are more associated with revascularization and endothelial regeneration[19].

Cardiovascular disease is the leading cause of death in the developed world and is projected to take over after infectious disease as the number one cause of death worldwide. 49% of all deaths in Europe and 30% of all deaths before the age of 65 years are caused by cardiovascular disease, making it a major contributor to the health care costs. A common denominator between many cardiovascular disease conditions is the loss of appropriate endothelial physiology from damage or injury, which leads to dysfunction. Although several risk factors for cardiovascular disease have been identified, such as obesity, insulin resistance and diabetes, smoking, hypertension, poor diet, and increasing age, up to half of the patients suffering from cardiovascular disease do not possess any of these traditional risk factors. Hence, it is of interest to identify other risk factors or biomarkers to asses for example vascular injury and to prevent cardiovascular disease to occur.

CECs enumeration in peripheral blood can be used to assess endothelial damage or other dysfunction. These cells are mature cells, as opposed to the EPCs, that have detached from the intimal monolayer in response to injury. Elevated numbers of CECs have been seen in some cardiovascular diseases. CECs have been shown to be positive for CD146, however, this marker may also be found on trophoblasts, mesenchymal stem cells, periodontal tissue, and some malignant tissues, making the use of additional markers necessary for positive identification[19].

EPCs have also been found in elevated levels in the blood of patients suffering from cardiovascular diseases but also in patients undergoing various angiogenic therapies to revascularize or heal injured vessels[20]. Vascularization is also a key step in the growth of a cancer tumor as well as for invasion and metastasis. New vessel formation involves the recruitment of EPCs from the bone marrow which results in elevated levels of EPCs in times of significant tumor growth making these cells interesting for cancer monitoring as well[21]. EPCs have been reported to specifically express the multiple markers CD31, vascular endothelial cadherin, von Willebrand factor, and vascular endothelial growth factor 2. There is, however, no consensus in their biomarker expression profile[18].

Stem cells

Stem cells have the potential to differentiate into mature tissue cells and are used for cell therapies, for tissue engineering applications, or for drug discovery. Embryonic stem cells are the most potent stem cells that can differentiate into all three different embryonic layers. There are, however, some ethical considerations about the use of these cells. In regards to this, adult stem cells are more attractive even though they are not as pluripotent. Among the different stem cells hematopoietic and mesenchymal stem cells are the most studied. Hematopoietic stem cells have been used for many years in therapeutic procedures of the blood system in several malignant and autoimmune disorders[22]. Mesenchymal stem cells

are of interest as they are capable of differentiating into connective tissue lineages, such as bone, cartilage, and adipose tissue, as well as smooth muscles, and are used for tissue engineering of musculoskeletal tissues[23].

Stem cells are commonly separated by depletion of other blood cells which may increase the risk of contaminated populations. CD34 has been used as a marker for the isolation of hematopoietic stem cells, and CD271 has been used for mesenchymal stem cell isolation; however, the use of this marker may not produce a homogenous cell population and additional isolation steps based on other markers may be needed[24].

Infected cells

Cells can be infected by viruses, bacteria, or parasites, such as HIV-infected T-cells, or malaria parasites infecting red blood cells (RBCs) (Figure 2.2), which may cause cell dysfunction and cell death and result in serious health complications. Early diagnosis is vital for effective treatment and disease control.

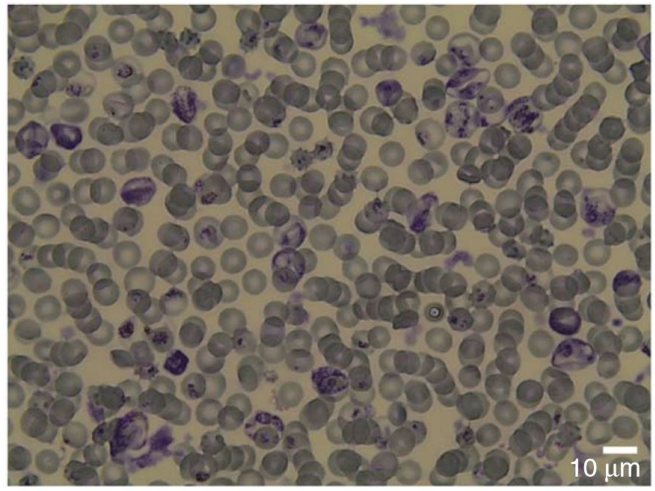

Figure 2.2: Microscopy image of *P. berghei*-infected blood extracted from infected mouse stained with Giemsa. Reprinted by permission from Macmillan Publishers Ltd: Nature Medicine, Peng, W. K., Kong, T. F., Ng, C. S., Chen, L., Huang, Y., Bhagat, A. A. S., Nguyen, N.-T., Preiser, P. R., & Han, J. (2014). Micromagnetic resonance relaxometry for rapid label-free malaria diagnosis. Nature Medicine, 20(9), 1069-73[25]. Copyright 2014.

The infected cells usually do not present any known biomarker that are different from what uninfected cells from the same population express. The infection, however, can induce changes in other cell properties, such as mechanical or biochemical properties[26]. For example, the deformability or change in paramagnetic properties of malaria-infected cells has been utilized as separation markers[27].

2.2 Needs and advantages for rare cell isolation

A general blood sample to be analysed would be around 5 mL. In one mL of this sample, composed of around 5 billion RBCs, 300 million platelets, and 5-10 million WBCs, 1-1000 rare cells can be found. Since it is not feasible to draw several decilitres of blood from a patient some needs and requirements must be fulfilled in order to successfully isolate the rare cells.

First of all, since the cells are low in numbers and the sample volume to be processed is limited, the recovery of them must be high. The recovery from a real sample can of course not be measured as it can never be known if all target cells are collected and detected. Recovery data is, therefore, generated with spiked cells. A high recovery will minimize the volume of sample that needs to be processed in order to collect a sufficient number of cells to enable analysis, and, thus, also the processing time of the sample. A high recovery will also ensure that the cells can be correctly enumerated when this is needed. It is not possible to specify a general recovery level needed, but the needed level is dependent on the subsequent analysis and will in turn determine how informative this analysis can be. A high recovery will also ensure that the collected cells are representative of the whole cell population and that the isolation method is not biased in any way.

It is worth noting that it can be misleading to compare recovery data between different experiments. Imagine a simple system composed of a piece of tubing connected to two syringes, pumping sample from one syringe to the other. The recovery of target cells should be 100% in the collecting syringe. A high recovery can, thus, be obtained without actively manipulating the sample at all. While some methods will produce 0% recovery when only pumping the samples through the system without actively manipulating them, other methods will in the same way recover some percentage of sample (with the same composition as the input sample) although without sorting it. This will obviously increase the chances for the latter method to generate higher recovery levels also when actively manipulating the samples. This will, however, be at the expense of the purity. To circumvent this, the term focusability, valid for acoustophoresis, was coined in paper II.

The second requirement is that the cells must be isolated with a high purity. If the purity is low it does not matter how high the recovery is, the isolated cells will not be further usable with a high background of other cells. If the purity is compromised subsequent analysis might also be. Comparing purity data directly between experiments is often misleading, as the purity also will depend on the composition of the sample to be processed *i.e.* the initial rarity of the target cells, as illustrated in Figure 2.3. The figure shows the purity of the target cell as a function of the initial cell concentration in RBC-depleted blood with a background of 5 million WBCs where the blue square indicates a purity that is acceptable for further enumeration and analysis of the rare cells. As with the recovery the acceptable purity depends on the subsequent analysis method and will also determine how informative the analysis results can be. It can be noted that the rarer the target cells the harder it is to obtain a high purity. The purity of a highly spiked sample will therefore often read higher than of a sample collected from a patient where the initial rare cell concentration is much lower. It can also be seen that removal of background cells is more critical to the

clinical relevance than a 10-20% drop in recovery as long as the chosen method is not biased. Consider *e.g.* that for CTCs, which are commonly found in quantities of only 1-10 cells/mL blood, the removal of WBCs have to be 99.9% or more to obtain a clinically relevant sample after the separation.

The third need is for a high throughput. As the cells are low in number per volume unit a relatively large sample may need to be processed in order to isolate a sufficient number of cells for further analysis. If the isolating system should have any clinical relevance it will need to be able to perform the isolation in a reasonable time frame. Preferably samples of around 5 mL of undiluted blood will have to be processed within an hour to ensure clinical relevance and high viability of the collected cells.

Furthermore, although not an actual need, it is an advantage if the processed sample gets concentrated in the process. Several methods used to isolate rare cells simultaneously dilute the sample through the use of sheath fluids. This imposes that the sample has to be subsequently concentrated in order to be able to analyse it, which is not always practically possible when handling samples with very low cell numbers.

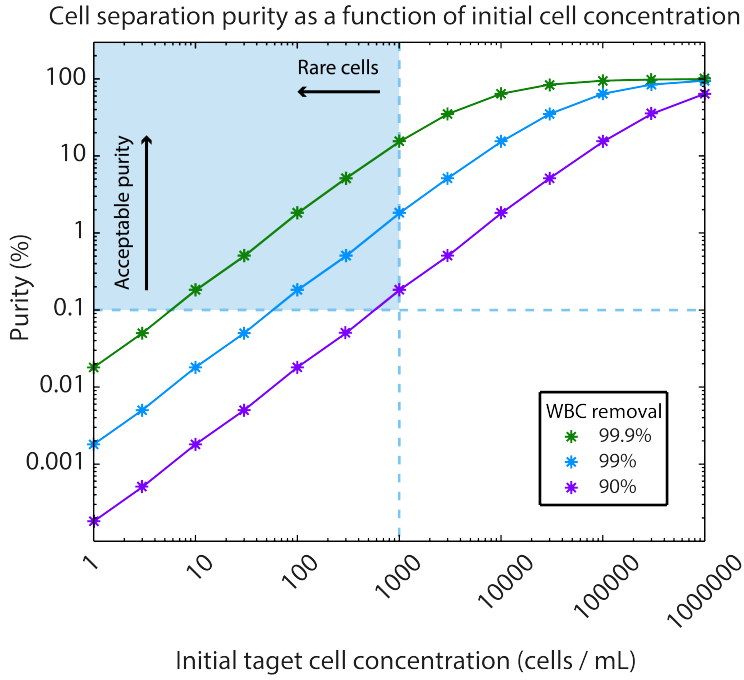

Figure 2.3: Purity of collected target rare cells as a function of initial cell concentration in blood where the RBCs have been previously depleted. The blue square indicates the area in which the purity of the collected rare cells is clinically relevant and acceptable for further enumeration and analysis. The WBC initial concentration was set to 5 000 000 / mL and the overall target cell recovery was set to 90%.

3

Conventional methods for cell processing

In many biomedical laboratories cell processing is performed using conventional methods that can be more or less laboursome, and cost intensive. The most commonly used methods include flow cytometry, magnetic separation, centrifugation, filtration, and cell culture.

3.1 Fluorescence activated cell sorting

Fluorescence activated cell sorting (FACS) sorts cells based on phenotypical differences in the form of different expression of specific biomarkers. In addition the method also displays the number of cells that express a certain marker and the level of expression for each cell. The method relies on fluorescent labelling of the specific markers.

In a commercial FACS the sample is commonly hydrodynamically focused before entering the fluorescence interrogation point where a laser is used to excite the fluorochromes, although the Attune^{TM} system relies on acoustic-assisted hydrodynamic focusing. When the cells enter the interrogation point the emitted light of the fluorochromes is then collected through a photomultiplier or detector and the information from both scatter and direct light is subsequently processed. Based on this information the cells are then distributed into droplets that are given different electrical charge dependent on their fluorescent profile. The formed drop should optimally contain a single cell. The drops are then sorted by deflecting them left or right by charged electrodes depending on the drops electrical charge. Finally, the drops can be collected in different sample tubes[28]. (Figure 3.1) Sorting rates up to input rates of 70 000 cells /sec have been performed, although few instruments can do this in reality with a maintained high purity[29]. The sorting rate is dependent on the characteristics of the cell to be sorted and the desired results in terms of purity versus recovery.

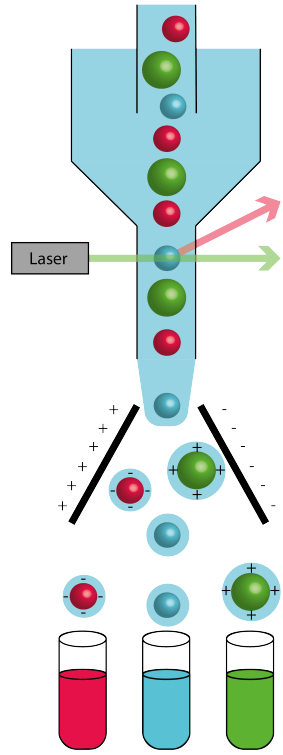

Figure 3.1: Schematic illustration of a FACS.

Bianchi *et al.*[30] showed that they could detect male DNA, in the form of the Y chromosomal sequence, in 75% of the cases where fetal RBCs where isolated from maternal blood using antibodies against the transferrin receptor. Although technically not true rare cells anymore, Swennenhius *et al.*[31] sorted circulating tumor cells from originally 7.5 mL of whole blood spiked with 500, 50, or 5 SKBR-3 cells, that had been pre-enriched using CellSearch. Although significantly enriched compared to the original sample only about 65% of the cells could be identified and 50% could be sorted.

Fluorescence activated cell sorting is widely used for many cell sorting applications and an advantage of the method is that cells can be sorted based on more than one marker at the same time. The sorting process might, however, expose the cells to high shear forces from the hydrodynamic focusing and the droplet generation, which may affect the cell viability. The relatively long processing times might also impair the viability and function of the cells. Also, as the sorting method is dependent on fluorescent signals the target population of interest must have a known specific marker different from the population of background cells. Recoveries tend to fall dramatically as small subpopulations (< 0.5% of total) are sorted. The recovery can be increased using certain strategies but at the cost of the purity.

The sorting performance will also depend on how different the expression of the target subpopulation is compared to the background population.

3.2 Immunomagnetic cell processing

Among the conventional macro scale methods immunomagnetic isolation has been most frequently used. As for FACS, the magnetic cell processing methods are also dependent on cell expression of specific markers, but instead of a fluorescent marker the cells are labelled with a magnetic bead.

Magnetic activated cell sorting

Magnetic activated cell sorting (MACS) uses magnetic forces to separate cells. After labelling the cells with antibody-coated magnetic beads or introducing magnetic nanoparticles into the cells, a magnetic field is applied to the whole sample. The labelled cells are then retained in the field while the unlabelled cells can pass through the field without being captured. After washing the captured cells to get rid of unspecifically bound cells, the magnetic field is removed and the captured cells can be eluated (Figure 3.2). Using MACS, cells can be isolated both through positive and negative selection (depletion). During positive selection the target cells are magnetically labelled and captured in the field while the background sample is not. During negative selection the background cells are instead magnetically labelled and captured while the target cells are not[32,33]. Which strategy to be used is dependent on the sample composition as well as the existence of cell specific markers for the different cells. The different isolation strategies can also be used in sequence.

The MACS system has been used for the isolation of rare cells, for example CTCs,[34–37] or nRBCs from blood[38]. CTCs have been isolated from white blood cells, both through positive (EpCAM-based) and negative (CD45-based) selection, where cytokeratine positive (CK+) cells could be found in some samples[37]. The use of only EpCAM as a marker may be problematic, as discussed above, why the used of both EpCAM-based and ErbB2-based positive selection has been suggested to be better[35]. After negative (CD45-based) selection Bluemke *et al.*[34] identified one CK+ and one CK- cancer cell population, identifiable as it was blue-stained by hemalaun. nRBCs have also been isolated from leukocytes through negative selection by depleting the leukocytes through the use of magnetic beads with anti-CD45- and anti-CD32-conjugated antibodies. This isolation process resulted in significant contamination of maternal cells in the fetal cell fraction preventing accurate analysis of the fetal cells[38].

Advantages of the MACS system is the relatively fast sorting time and the ability to process crude and highly concentrated samples. As it is reliant on biomarker expression the method is also gives a high specificity. In order to sort on more than one specific marker the process, however, have to be performed in sequence, which prolongs the sorting time. As the sorting is dependent on the availability of cell specific markers the method cannot be used for all sorting experiments. From the examples, where both positive and negative

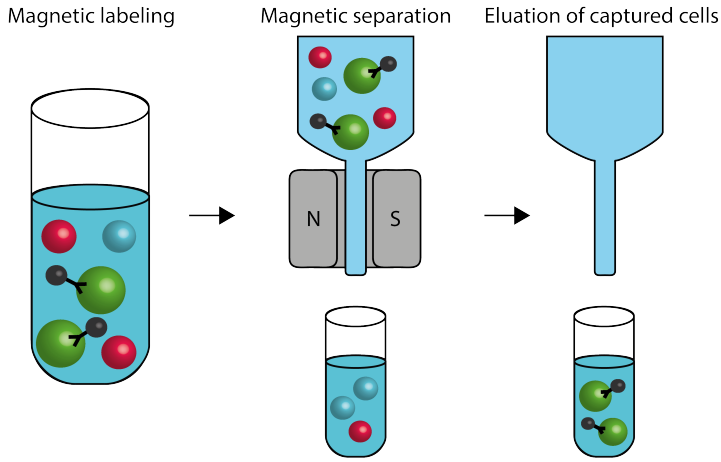

Figure 3.2: Schematic illustration of positive selection using MACS.

selection in combination with different biomarkers has been use, it is evident that not one of the methods is finding all of the rare cells of target.

CellSearch

A more specific example that relies on magnetic forces to isolate cells is the CellSearch system. This semi-automated system has been specifically designed for isolating and detecting circulating tumor cells and is the only system that has been approved by the FDA to do so[3,39]. Circulating tumor cells are separated from blood by anti-EpCAM antibody-coated magnetic beads and subsequently identified with the use of fluorescently labeled antibodies against cytokeratins and nuclear stains, while contaminating white blood cells are stained for CD45 expression.[5] To be able to identify and enumerate the cells they are magnetically aligned in a single focal depth where they can easily be observed.

The system has reliably been used to identify CTCs from all major carcinomas[3–5,40] but as the system relies on isolation of the CTCs through targeting the EpCAM it cannot be used to detect CTCs from other forms of cancers. Nevertheless, it is a useful tool as carcinomas make up about 80% of all diagnosed cancer forms. Another worry is, however, that the system will fail to detect all CTCs originating from carcinomas as well, as the epithelial-mesenchymal transition may lead to the loss of epithelial cell markers[9].

The recovery of cancer cells from patient samples can obviously not be determined as the true number of cancer cells per mL blood is unknown. To study the recovery of CTCs Swennenhius *et al.*[31] spiked 7.5 mL blood sample with 500, 50, or 5 SKBR-3 cells before performing CellSearch isolation. The experiments showed a recovery of approximately 75%.

The CellSearch system has also been used to isolate circulating endothelial cells. Ilie

et al.[41] showed elevated levels of CECs in blood drawn from patients suffering from non-small cell lung cancer, compared to patients suffering from small cell lung cancer, chronic obstructive pulmonary disease, and healthy individuals, through the use of anti-CD146 coated magnetic beads.

3.3 Centrifugation

If left alone, all particles having a higher density than their suspending medium will eventually settle on the bottom of their container or within their density equilibrium, with the help of gravity alone, where larger or denser particles will settle faster. This process can be sped up considerably using a centrifuge.

Differential centrifugation

Differential centrifugation separates cells and particles based on their density and size. Larger and denser particles will travel through the suspending medium faster and, thus, settle at the bottom of a centrifuge tube in a shorter time. The method can for example be used to separate different subcellular organelles from each other[42], or wash or concentrate settled cells through discarding the supernatant and resuspending them in smaller liquid volumes. To separate cells and particles using a centrifuge the cut-off size is changed by changing the centrifugation speed and time.

Although the method is very easy to apply, each sample can only be separated into two fractions at the same time. To differentiate the sample further, the sample has to be centrifuged again. The smaller particles to be separated, the longer and faster the centrifugation has to be done in order to get them to settle on the centrifuge tube bottom. Handling smaller liquid volumes or low cell numbers through centrifugation also has its drawbacks[43]. For example when using centrifugation to concentrate low cell numbers, small resuspension volumes may be needed that are not practically possible to handle in ordinary centrifugation systems. The centrifugation of low cell numbers also increases the risk of substantial sample losses, if the sample forms a pellet too small to be seen or fails to form a pellet at all.

Density gradient centrifugation

Cells can also be separated solely based on their density, using density gradient centrifugation. To separate cells using this method the cell suspension of interest is carefully layered on top of a solution having a density gradient. Centrifuging the sample then allows the different components to reach their equilibrium positions from where they gently can be recovered after the centrifugation is terminated[42,44] (Figure 3.3).

Nucleated cells from blood, including rare cells such as CTCs, endothelial cells, or nRBCs, can be isolated using gradient centrifugation. Along with these cells, tough, some leukocytes are also isolated so further isolation will be needed. Frequent loss of rare cells is also a problem as they migrate into the plasma fraction[45].

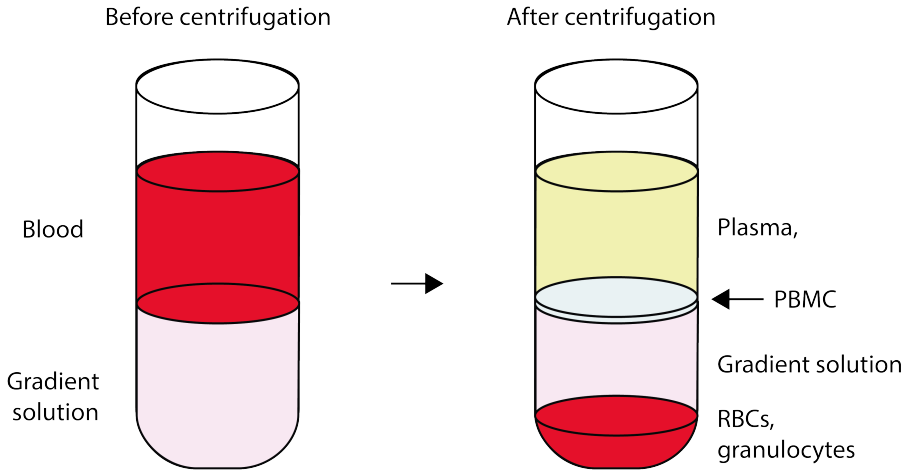

Figure 3.3: Schematic illustration of the gradient centrifugation process.

A form of density gradient centrifugation that can be used for rare cell isolation of CTCs is the Rosettesep^{TM} technique. While still using a density gradient for the isolation the sample is also treated with an antibody cocktail that will crosslink unwanted cells, for example CD45+ cells, to red blood cells and form rosettes. These crosslinked cell complexes will then be denser than the single rare cells and will then be pelleted together with the free RBCs.

Using a density gradient, compared to differential centrifugation, more than two fractions can be separated at the time. A disadvantage, however, is that a new density gradient has to be prepared for each new separation application and the densities of the different cell populations have to be known[44].

Centrifugation methods do not require any other instrumentation than a centrifuge and relatively large samples can be processed at a time. The purity and recovery of both methods are largely dependent on the post-centrifugation collection of the sample but also the size and density difference, and concentration of the different components to be separated. Centrifugation may also have an effect on the viability[46] or function[47] of the processed cells that in the end can bias readouts.

3.4 Culture

Cells can be concentrated through culture, where the cells simply are allowed to proliferate and expand. This is a technique often used for bacteria. The method is very effective, but time consuming and dependent on the growth rate and initial concentration of the

cells of interest. In theory this method can be used to amplify a single viable organism to detectable levels. When many microorganisms are present at the same time rare organisms might be outgrown by more abundant species. By using a selective enrichment medium that promotes the growth of one type of organism while suppressing the growth of others, rarer microorganisms can also be isolated.

3.5 Filtration

Filtration methods can be used both to separated and concentrate cells. The sample is simply run through a filter with a certain cut-off size, letting everything smaller than this size run through and collecting everything that is larger. The target cells can either be collected on the filter or in the filtrated fraction. Filtration is for example used for leukocyte depletion from whole blood before blood transfusion[48].

As many CTCs are larger than white and red blood cells they have been isolated using polycarbonate membrane filters, which allows for further analysis and characterization of the cells. However, CTCs may not always be larger than the blood cells, which may lead to unwanted cell losses[45]. Xu *et al.* fabricated a filter in parylene-C with an optimal slot size of 6 µm where they could filter 1 mL blood in less than 5 minutes (Figure 3.4). When spiking a blood sample with 10 PC3 cells per mL they could achieve a capture efficiency of 90%, a cell viability of 90%, and a 200-fold enrichment of the cancer cells relative to the peripheral blood mononuclear cells (PBMCs). After pre-processing a 7.5 mL blood sample through density gradient centrifugation, to pre-concentrate the sample and eliminate RBCs, an 1500-fold enrichment could be achieved, although at the expense of a reduction in the capture efficiency to ~70%[49]. Although filters can be effective they are prone to be clogged. Finding the right cut-off size may also be difficult due to the variations in deformability between different cell types. After sorting the captured cells can also sometimes be hard to retrieve.

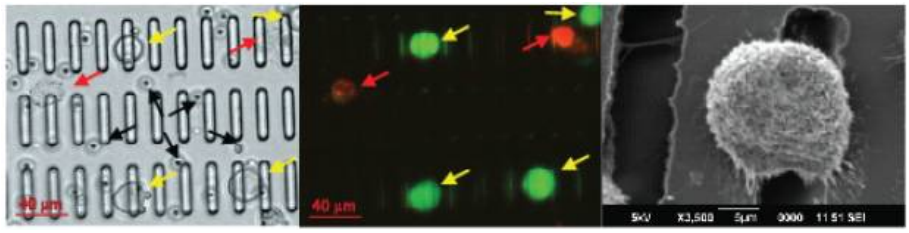

Figure 3.4: Cancer cells captured on the microfilter and imaged under bright-field (left) and fluorescence (center) of the same field; yellow arrows, live captured cancer cells; red arrows, dead cancer cells; black arrows, PBMCs. Right, scanning electron microscopy of captured cancer cell. Reprinted by permission from the American Association for Cancer Research: Xu et al. A cancer detection platform which measures telomerase activity from live circulating tumor cells captured on a microfilter, 2010 Aug 15, Cancer Research, 70(16), 6420-6426[49].

4

Microfluidic methods for rare cell sample preparation

Microfluidic methods have been extensively used for cell separation, where the scaling effects present in microsystems offers possibilities not present in macroscale systems. As opposed to the conventional methods the microfluidic methods also often rely on more non-traditional biomarkers and intrinsic cell properties[50]. The microfluidic methods can be further divided into passive and active cell processing methods, where active methods rely on externally applied force fields while passive methods do not. Furthermore, the methods can also be divided into continuous flow or batch methods.

4.1 Passive microfluidic methods

The simplest microfluidic devices that have been used for rare cell processing are the passive microfluidic devices that are not reliant on any externally applied force fields. The methods are more or less complex and include filters, microstructures, biomimetic, deterministic lateral displacement, affinity chromatography, and inertia.

Filters

A commonly employed separation criterion in microfluidic cell separation devices is size. Perhaps the simplest devices that discriminate based on size are the filters (Figure 4.1). In addition some filters also use deformability as an exclusion criterion. Four types of microfilters have been reported, weir, pillar, cross-flow and membranes, and the use of filters has been reported for rare cell processing[11,51,52]. When used to isolate WBCs from RBCs the cross-flow filter was found superior in terms of capture efficiency as well as whole blood handling capacity, before clogging the filter.[53]. The result is somewhat intuitive as the cross flow filter, as opposed to the other filter types which uses obstructed flows, is arranged perpendicular to the primary channel flow, which allows larger particles to continue in the direction of the primary flow without clogging the filter, although the problem is not entirely eliminated.

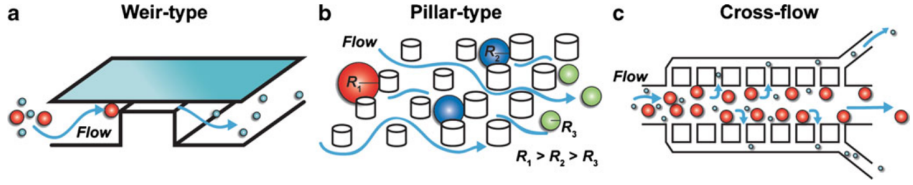

Figure 4.1: Microfluidic filter designs. a) Weir-type filter. b) Pillar filter. c) Cross-flow filter. Reprinted from: Gossett, D. R., Weaver, W. M., Mach, A. J., Hur, S. C., Tse, H. T. K., Lee, W., Amini, H., & Di Carlo, D. (2010). Label-free cell separation and sorting in microfluidic systems. Analytical and Bioanalytical Chemistry, 397(8), 3249-67[50]. Reprinted with kind permission from Springer Science and Business Media.

Even so, Mohamed *et al.*[11] used a pillar filter to separate nRBCs from WBCs despite the fact that the populations are overlapping in size, where the nRBCs are 9 µm to 12 µm in diameter while WBCs range from 7 µm to 14 µm (Coulter counter data). To successfully separate the two populations they took advantage of the fact that nRBCs are both asymmetric and deformable as opposed to WBCs that cannot deform as much. Because of this the nRBCs could pass through the channels smallest dimension that was 2.5 µm wide and 5 µm deep while the WBCs were retained. The device was operated at a flow rate of 0.35 mL/h. Zheng *et al.*[52] developed a three-dimensional microfilter of membrane type for the isolation of spiked CTCs from 10 times diluted whole blood. The three-dimensional design ensured that the trapped cells were kept viable in order to allow further functional studies of the captured cells. They showed a capture efficiency of 86.5 $\pm$ 5.3% but the sample volume throughput of the device was limited to about 1 mL of whole blood in order to not clog the device.

The simple design of filters and their relative flexibility of use is a clear advantage and usually the filtration process can be done within minutes. Furthermore, the method does not rely on biomarkers, making them interesting in hopes of finding subpopulations or populations with no known biomarkers. A drawback is, however, that they are prone to clog after handling a large enough number of cells. Cell populations also tend to have a

heterogeneous size distribution making the decision of choosing the filter cut-off size difficult. Different cell populations also are more or less deformable and, thus, able to squeeze through smaller filter pores than their diameter indicates. As rare cells are by definition found in small numbers and in a large population of background cells, a relatively large sample volume will have to be processed to isolate enough cells for analysis purposes. In light of this, filters may not always be a suitable choice for the processing of these samples.

Microstructures

Microstructure protrusions planar and lateral to the flow such as grooves, chevrons, herringbones, or microwells have been explored for cell separation purposes based on size, density, or deformability[50].

Tan *et al.* used microwells to isolate spiked cancer cells from diluted blood with a capture efficiency of 80%[54]. The device used a pre-filter to ensure that no cell clumps entered the microwell area (Figure 4.2). Furthermore, the cells could also be recovered and were shown to be viable after the isolation.

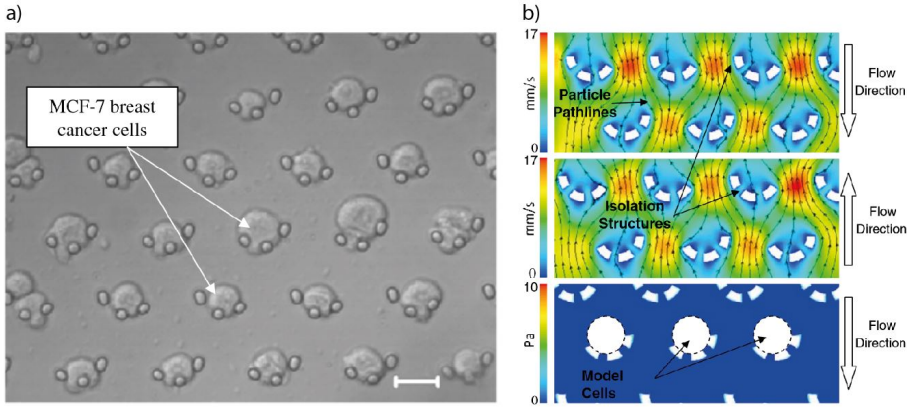

Figure 4.2: Microdevice based on microstructures for cancer cell isolation and enumeration. a) Captured cancer cells. b) Simulations showing the velocity profile when isolating and retreiving cells, and the shear stress acting on a spherical cell model when the cells are arrested in the microstructure. Reprinted from: Tan, S. J., Yobas, L., Lee, G. Y. H., Ong, C. N., & Lim, C. T. (2009). Microdevice for the isolation and enumeration of cancer cells from blood. Biomedical Microdevices, 11(4), 883-92[54]. Reprinted with kind permission from Springer Science and Business Media.

Most microstructure chips have been used in combination with other techniques such as immunoaffinity capture and are readily integrated with these. The use of microstructures can, however, make the fabrication process of the device more complicated. Dependent on the microstructure the device may also be more or less prone to clog.

Biomimetic

Biomimetic devices utilize the intrinsic properties of blood and the microvasculature to achieve the desired separation. Their exact separation mechanisms have not been described but, nevertheless, the biomimetic effects have been observed and replicated in microfluidic systems. Biomimetic phenomena that have been used to separate cells include plasma skimming, leukocyte margination, and the Zweifach-Fung effect, also known as the bifurcation law[50].

Hou *et al.*[55] used a device inspired by the phenomenon of leukocyte margination to separate malaria-infected RBCs from blood (Figure 4.3). The leukocyte margination phenomenon occurs in smaller blood vessels where RBCs, which are smaller in size and more deformable than WBCs, tend to migrate to the axial centre of the vessel while the WBCs tend to end up in the plasma rich layer along the vessel walls.

Malaria-infected cells are less deformable than uninfected RBCs and will, thus, migrate to the channel walls instead of the centre as the uninfected RBCs. By using this biomimetic technique 80% of the malaria-infected RBCs were collected in the side outlets. As the same phenomenon also displaces the WBCs to the channel walls 80% of these were, however, simultaneously collected in the side outlets indicating a need for an additional separation step. The separation process was performed at a flow rate of 5 µL/min, which may be considered low, but as opposed to many other separation techniques it could be performed on whole blood. It could, in fact, only be performed on blood with a hematocrit of more than 40%.

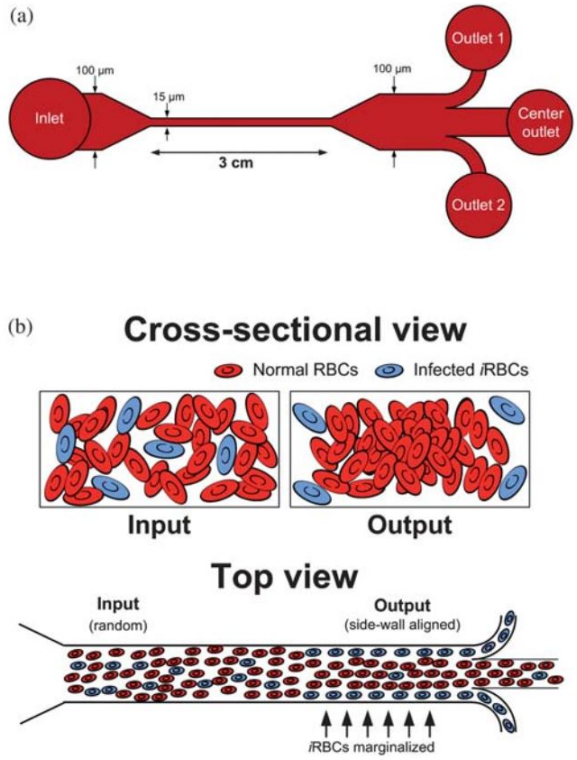

Figure 4.3: Biomimetic microchannel design and separation principle. a) Schematic illustration of the device design. b) Cross-sectional and top view before and after the separation. The initially randomly distributed cells are separated where the normal RBCs are distributed in the channel center while the infected RBCs are distributed in along the channel side walls. Reproduced from Ref.[55] with permission from The Royal Society of Chemistry.

Deterministic lateral displacement

Using deterministic lateral displacement (DLD) cell can be separated based on size, and sometimes shape and deformability, trough utilizing micropost arrays arranged in rows, where each row has a lateral offset from the previous[56]. Particles below a critical size will follow the streamlines through the device between the array gaps without experiencing any lateral displacement. Larger particles, however, will move laterally as they cross into neighbouring streamlines[57].

Huang *et al.*[58] relied on DLD to separate nRBCs from whole blood. nRBCs and WBCs were first separated from the maternal adult RBCs in the device where 99.99% of the maternal RBCs could be depleted at a flow rate of 0.35 mL/h. The sample was then treated to render the nRBCs paramagnetic after which the sample was run through a magnetic column to separate the WBCs from the nRBCs. The final contamination of WBCs was found to be 0.01-0.1%. Cells were then visually detected and nRBCs could be identified in 58/58 samples.

Using a combination of DLD, inertia, and magnetophoresis in an integrated device, termed "'CTC-iChip"', Ozkumur *et al.*[59] showed that they could sort CTCs from whole blood at a sorting rate of 10^7 cells/s and 8 mL/h. The device first used DLD to sort the RBCs from the WBCs and CTCs, the WBCs and CTCs were then focused using inertia, after which they were separated using magnetophoresis (Figure 4.4). An advantage of the device was that it could be used to separate the CTCs both through positive selection, where the CTCs are affinity-bound to the magnetic particles relying on specific surface markers of these cells, or through negative selection where the WBCs are instead depleted by the magnetophoresis. In the positive selection mode it was possible to detect CTCs in 90% of the clinical samples analysed, while the CellSearch system only detected CTCs in 57% of the samples. Although more cells could be found using the CTC-iChip it cannot be excluded that a subpopulation of cancer cells that are similar in size to the RBCs are lost together with the depleting of these cells. The size of the CTCs will likely vary for different types of cancers and the detection efficiency of this system will then vary more than the one of the CellSearch system that does not discriminate on cell size.

DLD has been shown to have a very good size resolution,[56] and DLD devices are capable of processing whole blood even if it is most times diluted[50]. As the separation is based on the position of the microposts in the array, a new device has to be fabricated for each new separation type considered. A solution to this problem has, however, been proposed by Beech *et al.* through a tuneable DLD device where the size between the microposts could be changed through stretching the device[60]. Cell separation using DLD is mostly done with relatively low flow rates, making the processing slow when there is a need to separate several mL of sample[57]. In light of this, Loutherback *et al.*,[61] presented a device that was capable of separating spiked cancer cells from dilute blood at a flow rate of 10 mL/min without compromising the viability of the cells. With the device they showed an ~85% recovery. The purity was, however, only 16.7% (with an input value of 4.9% cancer cells). The high variability in operating flow rates is mostly dependent on the fabrication mode. DLD microchannels fabricated in PDMS cannot be made as deep as channels fabricated using silicon. Using silicon the fabrication process is, however, much more complicated and

special equipment is needed as deep reactive ion etching (DRIE) has to be performed, also making these devices more expensive to produce. Another restricting factor using PDMS-based devices are that the microposts can deform, or the bonding between the PDMS and glass lid can be destroyed if the pressure in the device is too high. A high pressure will make the PDMS microposts deform into an hourglass shape leading to different critical particle separation sizes along the channel depth.

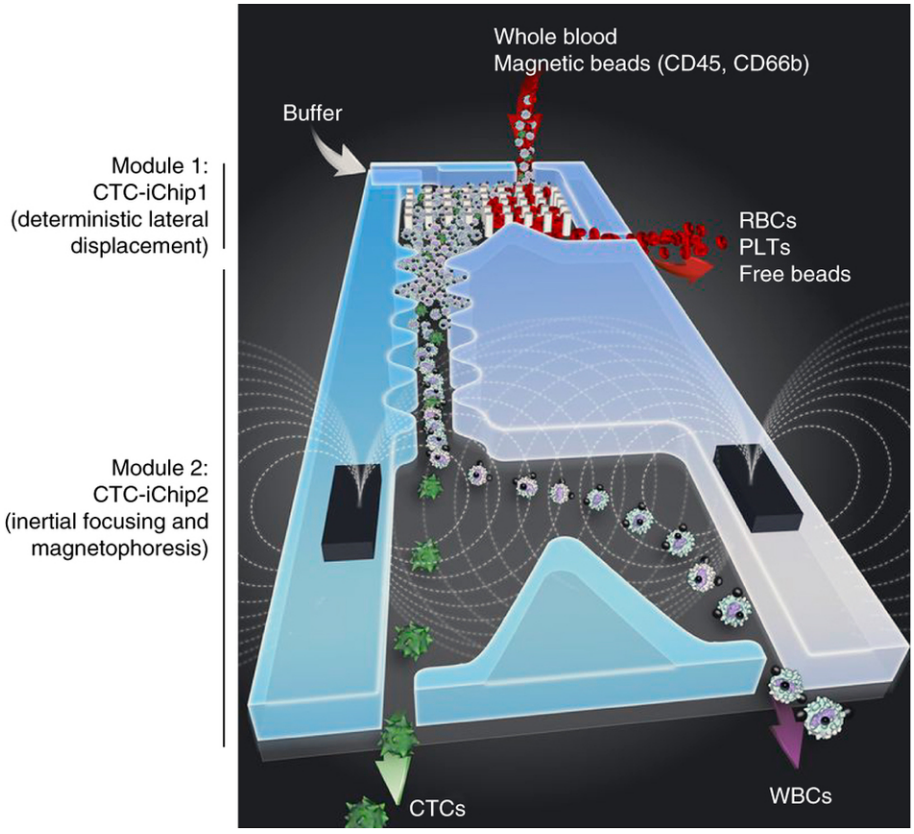

Figure 4.4: The CTC-iChip is first using a DLD device to remove the RBCs and platelets from the nucleated cells, inertial focusing is then used to prefocus the cells before the magnetophoresis where bead-labeled WBCs are separated from unlabeled CTCs. Reprinted by permission from Macmillan Publishers Ltd: Nature Protocols, Karabacak, N. M., Spuhler, P. S., Fachin, F., Lim, E. J., Pai, V., Ozkumur, E., Martel, J. M., Kojic, N., Smith, K., Chen, P., Yang, J., Hwang, H., Morgan, B., Trautwein, J., Barber, T. A., Stott, S. L., Maheswaran, S., Kapur, R., Haber, D. A., & Toner, M. (2014). Microfluidic, marker-free isolation of circulating tumor cells from blood samples. Nature Protocols, 9(3), 694-710[62].

Affinity chromatography

The possibility to isolate rare cells using affinity isolation trough the interaction between solid surfaces and cells has been extensively explored[63–68]. The large surface to volume ratio of microfluidic channels has been proven especially useful for this as it increases the possibility of cell-surface interactions, which leads to better isolation efficiencies. The method can be used both in a positive and negative selection mode, where either the target cells or the background cells are captured on the surface. Despite the larger surface to volume ratio in microchannels the cell-surface interactions often has to be further facilitated. For example, a nanoscale hydrodynamic lubrication layer exists close to the surface, in laminar flows, which can hinder the cell access to the antibody-coated surface.[39]

Adams *et al.*[69] showed that they could process 1 mL of blood in less than 40 minutes in a PMMA device using immobilized anti-EpCAM antibodies covering the surface of the microdevice. Furthermore, CTCs spiked in whole blood could be captured with an efficiency of more than 97%, subsequently released and counted on-device. Nagrath *et al.*[70] used anti-EpCAM antibody coated microposts to further increase the cell-surface interaction. Using the chip they could successfully identify CTCs in whole blood of patients with metastatic lung, prostate, pancreatic, breast, and colon cancer in 115 of 116 samples and a 50% purity. Stott *et al.*[71] used a combination of a herringbone chip and immunoaffinity capture to isolate CTCs from blood (Figure 4.5). The herringbone was used to generate microvortices in order to increase the interaction between the cells and the antibody covered chip surface. The capture could then be visually analysed, trough on-chip staining, and CTCs were detected in 14 of 15 samples from patients with metastatic prostate cancer where a median of 63 CTCs/mL and mean of 386 ± 238 CTCs/mL were found.

Compared to several other isolation techniques, affinity isolation requires fewer or no sample preparation steps as the labelling occurs on the surface of the device instead of beforehand on the cells. This advantage results in a shorter isolation time and makes the overall procedure simpler. Fewer sample preparation steps further minimises the risks of cell loss during processing. It can be complicated to find an optimum processing flow rate where a balance between the separation efficiency and the purity must be taken into account. It is in reality hard to find settings where both of these requirements are optimal. At a lower flow rate the interaction between the cells and the surface is higher and this will, thus, result in a higher recovery of target cells. At the same time this also gives the background cells more time to unspecifically bind to the surface while the low flow velocity is not sufficient to wash them away. At a higher flow rate the purity will, thus, be higher as the unspecifically bound background cells can be washed away more efficiently. This will, however, also result in a lower recovery when the target cells do not get enough time to specifically bind to the surface. For rare cell isolation, finding the rare cells can to some extent be considered more important, whereas the recovery is more important than the purity and thus a lower flow rate is favoured[26, 39]. As affinity chromatography-based methods rely on the availability of specific biomarkers on the cells they have the same inherent shortcomings as *e.g.* the CellSearch method where subpopulations negative for the biomarker expression may be lost.

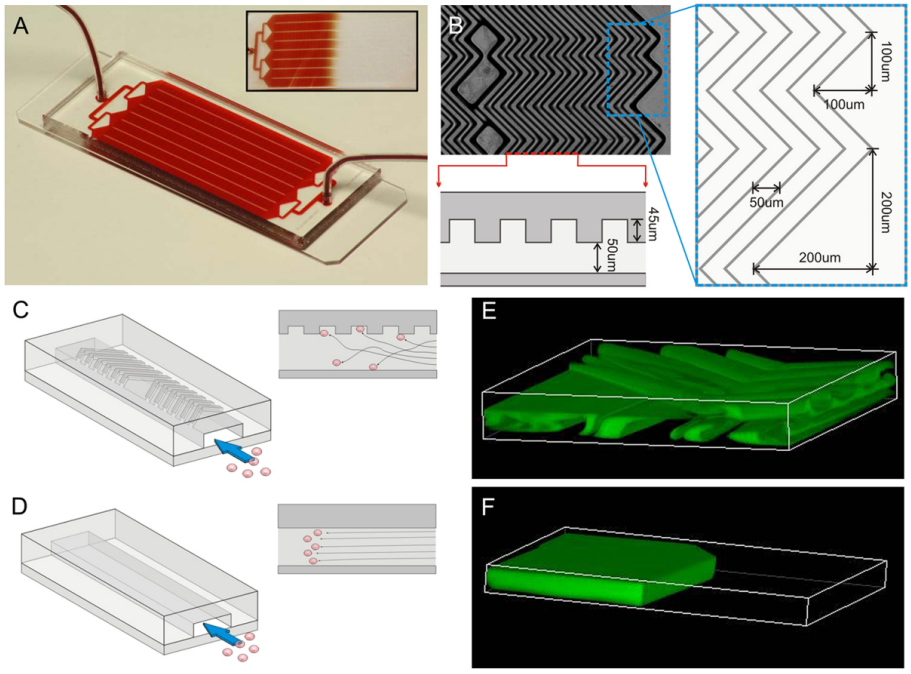

Figure 4.5: A) The herringbone chip consists of a microfluidic device with an array of channels with a single inlet and outlet. Inset illustrates the uniform blood flow through the device. B) A micrograph of the grooved surface illustrates the asymmetry and periodicity of the herringbone grooves. C) Illustration of the cell-surface interactions in the herringbone chip and D) a traditional flat-walled microfluidic device. E) Flow visualization using two paired streams of the same viscosity demonstrated the chaotic microvortices generated by the herringbone grooves, and the lack of mixing in F) the traditional flat-walled device. Reprinted from: Stott, S. L., Hsu, C.-H., Tsukrov, D. I., Yu, M., Miyamoto, D. T., Waltman, B. A., Rothenberg, S. M., Shah, A. M., Smas, M. E., Korir, G. K., Floyd, F. P., Gilman, A. J., Lord, J. B., Winokur, D., Springer, S., Irimia, D., Nagrath, S., Sequist, L. V, Lee, R. J., Isselbacher, K. J., Maheswaran, S., Haber, D. A., & Toner, M. (2010). Isolation of circulating tumor cells using a microvortex-generating herringbone-chip. Proceedings of the National Academy of Sciences of the United States of America, 107(43), 18392-7[71].

Inertia

In flow rates where the Reynolds number is in the range of 1-100 inertial effects become significant. Inertia can be used to separate particles based on size, shape, and deformability[72–75] and is dependent on the balance between the two inertial lift forces; the shear gradient lift force and the wall effect lift force. By changing the channel dimensions the number of equilibrium focusing positions can be manipulated[50].

Inertial systems with many different geometries have been applied to rare cell separation.[75–78] Mach and Di Carlo[79] used a gradually expanding channel to separate blood from bacteria. They showed that after running the sample two times through their device 80% of the bacteria could be cleared from the sample. The processing, however, demanded a dilution of the blood to 0.5% hematocrit, making the processing time extensive. To solve this problem they also presented a massively parallel system that could process 240 mL/h with a throughput of 400 million cells/min. It was proposed that the device could be used for neonatal sepsis and that the processing time could be further shortened by stacking several devices in parallel. In order to reuse this blood it, however, have to be reconcentrated and have the rest of the bacteria removed as well. In another attempt to separated blood from bacteria Wu *et al.*[80] used inertia in combination with a sheath flow and showed a recovery of 62% and a purity of 99.87% of the bacteria when processing 57400 cells/s with a flow rate of 18 µL/min. Hur, Mach and Di Carlo[81] proposed a parallel system for isolation of CTCs from blood through trapping them in microscale vortices (Figure 4.6). The proposed system could process 7.5 million cells/s of diluted whole blood (1% hematocrit) and with a capture efficiency as high as 43% depending on the initial cell concentration. Although processing dilute blood the system was capable of concentrating rare cells from 1 mL blood into 860nl of processed sample.

In curved channels an additional inertial effect can be observed. As the fluid is driven around a curve the fluid is set in motion perpendicular to the primary fluid flow, resulting in two counter-rotating vortices, termed Dean flow, which may also influence the particle focusing position[73].

Khoo *et al.*[82] used three stacked spiral microchannels to separate CTCs from RBC-lysed, two times concentrated blood. In the devices, through the use of sheath flow, the larger CTCs were focused on the inner side of the spiral while the smaller white and red blood cells remained un-focused and just completed one Dean cycle in the device to end up on the outer side of the spiral (Figure 4.7). A 7.5 mL blood sample could be processed in 5 min, and when benchmarked against the CellSearch system significantly more CTCs were found using the spiral system. In a similar approach Warkiani *et al.*[83] used a slanted spiral microchannel which effectively eliminated the need for the sheath flow. The device could process a 7.5 mL blood sample in 8 min. While using two times diluted RBC-lysed blood 85% of spiked cancer cells could be recovered with a contamination of only 500 WBCs per mL. CTCs could also be isolated from 10/10 patient samples from patients suffering from advanced stages of metastatic breast and lung cancer.

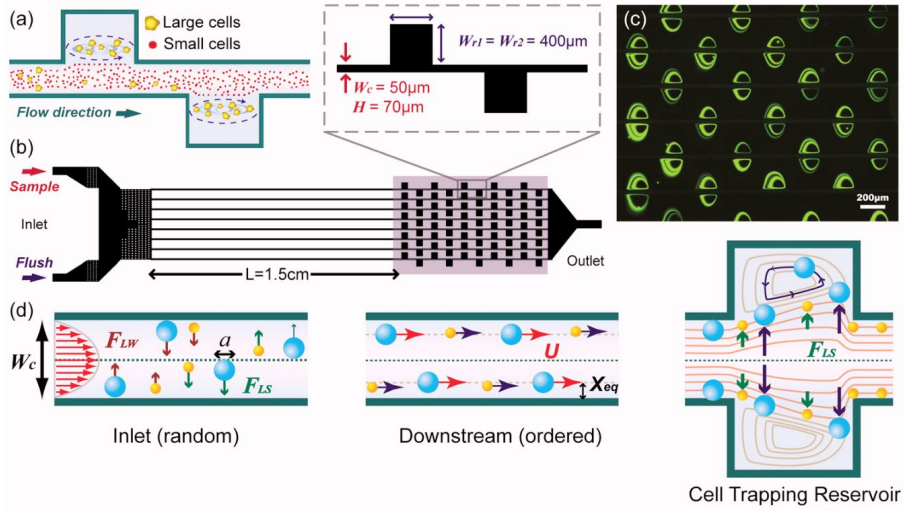

Figure 4.6: Device design and working principle. a) Larger cells are trapped in the reservoir while smaller cells freely pass through due to difference in the lift force that cells encounter. b) The device consists of eight parallel high aspect ratio straight channels (50x70 μm) with ten cell trapping reservoirs (400x400x70 μm) in each channel. c) Parallel trapping of 10 μm fluorescent particles in microscale vortices. d) A particle with a diameter a experiences wall effect lift F_{LW} and shear-gradient lift force F_{LS}, in straight channels, resulting in a dynamic lateral equilibrium position X_{eq} and uniform particle velocity U. Here, X_{eq} is defined as the distance between the center of particles and the channel walls. At the reservoir, larger particles experiencing larger F_{LS} are pushed towards the vortex center and trapped, whereas smaller particles are flushed out of the region. Reprinted with permission from Hur, S. C., Mach, A. J., & Di Carlo, D. (2011). High-throughput size-based rare cell enrichment using microscale vortices. Biomicrofluidics, 5(2), 22206[74]. Copyright 2011, AIP Publishing LLC.

Advantages of inertial systems are that they are not reliant on any external field to process samples. This makes the laboratory setup less complicated. This, however, also means that a new device has to be fabricated for each new application as the inertial forces are dependent on the channel inner dimensions. Compared to most other microfluidic devices, inertial devices are able to process samples under relatively high flow rates. There is, however, a limitation in particle concentration before steric interaction between particles hinders the focusing. This critical concentration is dependent on the particle diameter[73].

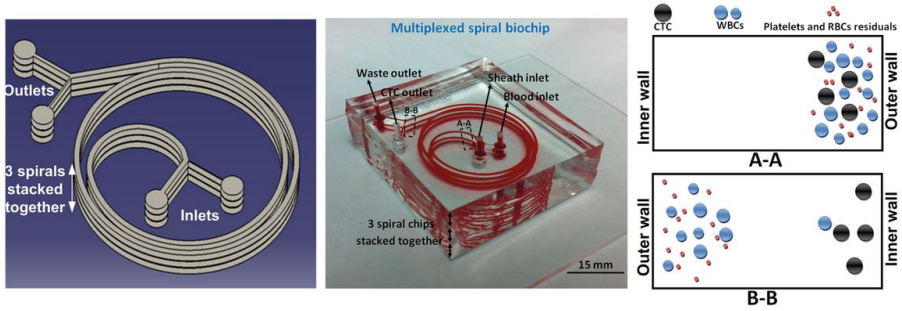

Figure 4.7: Illustration of the device (left), photograph of the device (middle) and cross-section of the device near the inlet and outlet, respectively. CTCs focus near the inner wall while WBCs and platelets go through one Dean cycle and migrates back towards the outer wall[82].

4.2 Active microfluidic methods

Active microfluidic methods rely on external fields to separate and handle cells and particles. This makes the laboratory setups more complicated but the active forces can be manipulated more easily, which eliminates the need to make a new device for every new application as is the case for several of the passive methods.

Field-flow-fractionation

Field flow fractionation (FFF) comprises several batch-based techniques that relies on an external field perpendicular to the primary channel flow for separation and can, thus, not always be classified as an active method depending on which external force field that is used. The external field can *e.g.* be electrically, thermally, gravitationally, or centrifugally induced and the particles are separated, based on small differences in biophysical properties such as size, shape, density, rigidity, or subcellular structures. Particles can be separated using FFF because the external field moves them into different laminar flow regimes and, thus, their retention time in the channel will differ[84].

The techniques generally generate high recovery rates; however, as they usually are operated in batch mode the throughput is currently low. Although FFF systems are capable of making a relatively fine discrimination between particles the batch mode operation makes them rather inconvenient to use for cell separation as only about 10^6 cells can be processed in one batch. In order to avoid these shortcomings of FFF operated in batch mode Shim *et al.*[85] developed a DEP-FFF system that could be run continuously. Using this system they could isolate spiked CTCs from peripheral blood mononuclear cells (PBMCs) with a recovery of 75%, and isolation of cancer cells from patient samples was also shown. The method was capable of processing a 10 mL patient sample in less than one hour. As for all systems relying on DEP to separate cells a specific conducting buffer is needed, introducing sample preparation steps where rare cells might be lost. Dean flow fractionation has also

been used to separate CTCs from blood in a two-stage system.[86] The device was able to process samples with at 20% hematocrit and CTCs were identified in samples collected from 20/20 metastatic lung cancer patients. The device had a processing speed of 3mL/h.

Magnetophoresis and magnetic trapping

Magnetophoresis usually uses affinity-coated magnetic particles to sort or concentrate cells based on surface markers, but intracellular nanoparticles[87] or marker-free sorting of RBCs,[88] through their intrinsic paramagnetic properties, have also been shown. The combination of magnetics and microfluidics has meant that magnetic selection can be made in continuous flow, even though magnetic trapping in microfluidic devices also has been employed to isolate CTCs[89] or concentrate *E. coli*[90]. The separation process is dependent on a non-uniform magnetic field directed perpendicular to the primary fluid flow. By deflecting magnetic particles in this field the magnetic particles can be separated from each other and from non-magnetic particles. The sorting is further dependent on the magnetic susceptibility and size of the particles[91].

Xia *et al.*[92] showed that they could separate *E. coli* from two times diluted RBCs with a recovery of 78% of the bacteria with less than 1% contamination of RBCs (Figure 4.8). The device was operated at a flow rate of 25 µL/h, and 10000 processed cells/s. This very low processing flow rate can be said not to be relevant for clinical applications. The same group, however, later reported on a device for cleansing whole blood from the fungi *C. albicans*, which was able to remove 80% of the contaminating fungi at a flow rate of 20 mL/h[93].

Plouffe *et al.*[94] reported on a device that could separate spiked MCF-7 cells (50 cells/mL) from whole blood with a recovery of over 85-95% and a purity of 80-55%. The group also showed that the device could be used to simultaneously separate hematopoietic stem cells and endothelial progenitor cells from whole blood using anti-CD133-antibody-functionalized magnetic beads. For this experiment they showed a recovery of 96% as compared to measurements on the original samples performed by flow cytometry. The experiments could be performed at a flow rate of 14 mL/h.

Compared to previously described macroscale systems such as MACS, microfluidic systems relying on magnetic forces to sort cells have the advantage to be able to process samples continuously. More than one cell type can also be isolated at the same time.[95] As target cells are selected through specific markers the selectivity for magnetophoresis is relatively high, and the method is not as dependent on specific microstructures or channel dimensions or particle-particle interactions. The marker-specific selection, however, means that specific markers of the target cells have to be known to process them. This may for example cause a loss of subpopulations not harbouring the specific marker or making the isolation of an unknown bacterial species from blood complicated. Another challenge for the magnetic-based systems is the fact that the magnetic force field is increasing exponentially when approaching the magnet. This leads to the risk of having particles get stuck to the device wall if the flow rates are not adjusted properly.

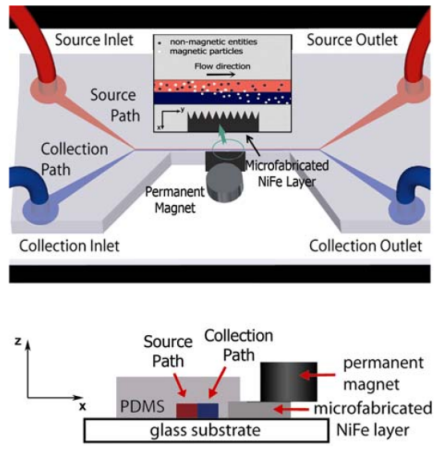

Figure 4.8: Schematic depiction of the magnetophoresis device that contains a microfabricated layer of soft magnetic NiFe material adjacent to a microfluidic channel with two inlets and outlets. The inset shows how magnetic beads flowing in the upper source paths are pulled across the laminar streamline boundary into the lower collection path when subjected to a magnetic field gradient produced by the microfabricated NiFe layer located along the lower side of the channel. Reprinted from: Xia, N., Hunt, T. P., Mayers, B. T., Alsberg, E., Whitesides, G. M., Westervelt, R. M., & Ingber, D. E. (2006). Combined microfluidic-micromagnetic separation of living cells in continuous flow. Biomedical Microdevices, 8(4), 299-308[92]. Reprinted with kind permission from Springer Science and Business Media.

Acoustophoresis and acoustic trapping

Acoustophoresis uses ultrasound to process rare cells in either continuous flow, through the use of bulk acoustic waves (BAW) or standing surface acoustic waves (SSAW), or in batch mode trough acoustic trapping. The methods all rely on the formation of standing acoustic waves to manipulate the cells based on their size, density, or compressibility.

Bulk acoustic waves have been used to manipulate rare cells in the papers included in this thesis, which will be further discussed below. In addition to this Augustsson *et al.*[96] separated spiked CTCs from WBCs. With the introduction of two-dimensional pre-alignment the device was used to recover 85.4% of the cancer cells with a contamination of 0.7% of WBCs and a flow rate of 70 µL/min. In an attempt to take the sample preparation further Iranmanesh *et al.*[97] presented an integrated system that simultaneously separated spiked CTCs from RBCs, trapped and concentrated the recovered cancer cells and allowed for on chip fluorescence image analysis of the trapped cells (Figure 4.9). 85.5% of the cancer cells could be recovered with a purity of 100%, and the cells were concentrated 130 times in the trap. The sample processing flow rate was, however, only 4.5 µL/min making rare cell processing time consuming.

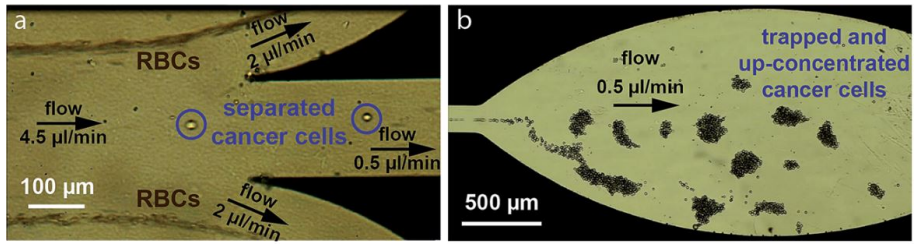

Figure 4.9: Microscopic view of the acoustophoresis chip. a) Separation of A549 lung cancer cell line from RBCs. b) Trapping and concentration of the separated cancer cells. Reprinted from Ref.[97] with permission from The Royal Society of Chemistry.

BAW has also been used to concentrate cells. Hawkes and Coakley[98] used acoustophoresis-enhanced sedimentation, where yeast cells were focused into aggregates which eventually made them sediment when heavy enough, to concentrate *S. cerevisiae* 5-fold with a recovery of 98.5% of the cells. The experiments were run at a flow rate of 4.8 mL/min. Jakobsson *et al.*[99] used a recirculating acoustophoresis device and showed that RBCs could be concentrated 1166 $\pm$ 110 times with a 98.7% recovery, and DU145 cells and MCF-7 cells could be concentrated 817 $\pm$ 125 times with a recovery of 90.2%, and 519 $\pm$ 115.7 times with a recovery of 81.7%, respectively.

Standing surface acoustic waves have also been used for rare cell processing. Ai, Sanders and Marrone[100] used SSAW to separate *E. coli* spiked with pre-isolated PBMCs. In the target outlet 95.65% bacteria and 3.92% WBCs could be found, while 7.24% of the cells collected in the waste outlet were found to be bacteria and 91.48% were WBCs. The sample was processed with a flow rate of 0.5 µL/min. Li *et al.*[101] used a tilted-angle SSAW device to separate spiked CTCs from WBCs at a sample processing flow rate of 20 µL/min (Figure 4.10). While removing 99% of the WBCs 60-80% of the cancer cells could be recovered. The device was also used to isolate CTCs from three patients with metastatic breast cancer.

Standing acoustic waves can also be used to trap cells and particles in order *e.g.* concentrate of wash them. Using seed particles Hammarström, Laurell, and Nilsson showed that they could trap bacteria with a capture efficiency of 95%[102].

Acoustophoresis is a label-free method which is advantageous when isolating rare cells with no known specific markers. Devices depending on BAW can also be operated at relatively high flow rates compared to other microfluidic methods, although SSAW devices have not shown the same throughput. SSAW devices, however, can be fabricated in softer materials such as PDMS, while BAW devices generally rely on more rigid materials in order to efficiently form the standing waves. The reliant on an external force field to process the cells also makes the instrumental set-up more complicated, but in turn enables one device to be used for many different applications as the applied force can be externally adjusted.

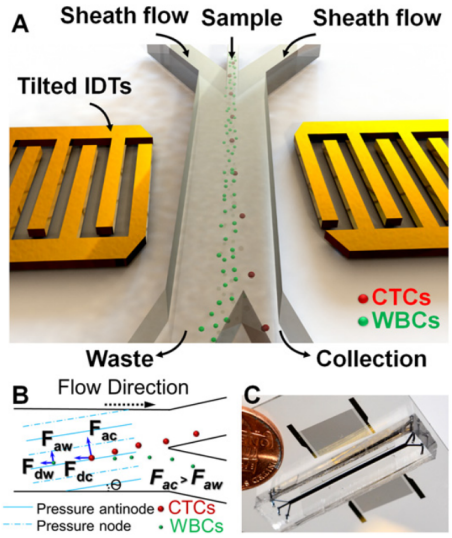

Figure 4.10: SSAW device for cancer cell separation. a) Illustration of the device. b) Schematic of the working mechanism behind the tilted-angle SSAW-based device. The direction of the pressure nodes and pressure antinodes were established at an angle of inclination (θ) to the fluid flow direction inside a microfluidic channel. Larger CTCs experience a larger acoustic radiation force (F_{ac}) than WBCs (F_{aw}). F_{dc} and F_{dw} are the drag force experienced by CTCs and WBCs, respectively. c) A photograph of the device. Reprinted from: Li, P., Mao, Z., Peng, Z., Zhou, L., Chen, Y., Huang, P.-H., Truica, C. I., Drabick, J. J., El-Deiry, W. S., Dao, M., Suresh, S., & Huang, T. J. (2015). Acoustic separation of circulating tumor cells. Proceedings of the National Academy of Sciences of the United States of America, 112(16), 4970-4975[101]. Copyright 2015 National Academy of Sciences, USA.

Dielectrophoresis

Dielectrophoresis (DEP) is a label-free method that has been widely used in microfluidics, including rare cell applications[103]. Using DEP, cells are processed based on size and variations in the dielectric properties of different cell populations. The non-uniform electric DEP force field induces a force on the particles due to an induced or permanent dipole. DEP systems harbour many factors that can be manipulated that contribute to the resultant DEP force field. Among these factors are driving current, AC or DC, electrode geometry, and frequency. Particles either feel a force directed towards the field maximum, denoted positive DEP (pDEP), or away from the field maximum, denoted negative DEP (nDEP)[104].

Braschler *et al.*[105] used a continuous flow pDEP device to separated *B. bovis* (cattle pathogen) infected RBCs from uninfected RBCs. It was shown that the infection changed the dielectric response of the cells and the infected cells could be enriched seven times to

a purity of 50%. Becker *et al.*[106] proposed a DEP device that selectively trapped human breast cancer cells (cell line MDA213) over RBCs and T-cells using the device as an affinity column. The device could sort 10^3 cells/s.

Mancada-Hernández and Lapizco-Encinas[107] used an insulator-based DEP device, where the compression of the electrical field lines between the insulator posts was utilized, to trap both *S. cerevisiae* and *E. coli* in order to concentrate them (Figure 4.11). When lowering the applied voltage first the bacteria and then the yeast cells could be selectively released. The yeast cells were concentrated 23.41-fold and the bacteria were concentrated 88.1-fold as measured in the trap.

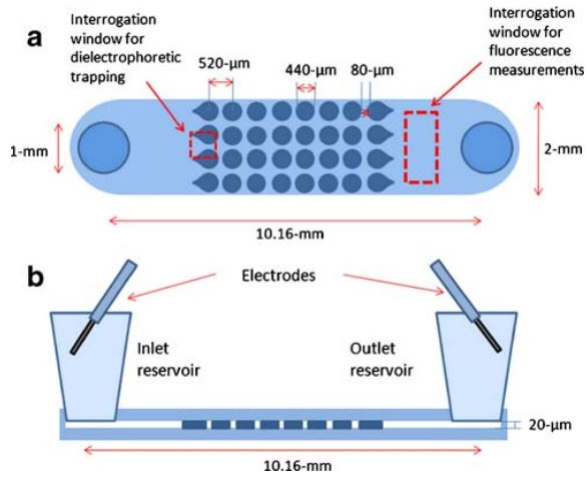

Figure 4.11: a) Schematic representation of the DEP device top view showing channel dimensions and insulating structures geometry. b) Schematic representation of microchannel side view showing reservoirs and electrodes. Reprinted from: Moncada-HernÃ¡ndez, H., & Lapizco-Encinas, B. H. (2010). Simultaneous concentration and separation of microorganisms: insulator-based dielectrophoretic approach. Analytical and Bioanalytical Chemistry, 396(5), 1805-16[107]. Reprinted with kind permission from Springer Science and Business Media.

An advantage of DEP is that it is conducted in a label-free manner, which can be useful especially when isolating rare cells with no known specific markers. Compared to other label-free methods, DEP devices also process small cells and particles, such as bacteria, with more ease. Disadvantages of DEP systems are the reliance of a specific buffer to be able to process cells. Most DEP devices are also applied at relatively low flow rates, in the order of 1-10 µL/min, making them less applicable for rare cell separation or concentration.

4.3 Summary and conclusion of microfluidic methods

Both passive and active microfluidic methods, described above, have been used to process rare cells. Generally, passive methods, not reliant on an external force field to process cells, will enable a less complicated instrumental set-up. This on the other hand means that the processing results are reliant on internal forces generated in the devices, which means that a new device has to be fabricated for each new application. Most active methods can also be used to process higher cell concentrations than passive methods as their performance is not as dependent on cell-cell interactions. Methods operated in batch mode, compared to continuous flow, can more easily be used to concentrate samples and generate higher concentration factors. The batch operation mode, however, puts constrains on the amounts of cells or sample volume that can be processed in one run. Label-free techniques have the advantage to not be reliant on specific markers, which is especially useful when dealing with rare cells with no known specific markers. Label-dependent techniques on the other hand can offer a higher specificity when used to separate or process specific cell types. One method might not be superior to the others for all applications. Rather the pros and cons for each method should be reviewed before applying it in order to find the most suitable one.

5

Acoustofluidics

Acoustofluidics is the combination of acoustics and microfluidics, wherein the study of sound and its interaction with particles or cells is combined with the study of fluid behaviour in micrometer channels. This section will focus on describing the theory developed for acoustofluidic devices utilizing bulk acoustic waves as is used in papers I-V included in this thesis.

5.1 Microfluidics

Microfluidics encompasses the science and technology of the behaviour of fluids, in micrometer channels. Microfluidics has been applied to cell processing and bioanalysis *e.g.* to carry out separation and detection with high resolution and sensitivity, where the small sample and reagent consumption has proven to be an advantage which lowers costs and shortens analysis times[108]. With shrinking dimensions the surface to volume ratio increases creating specific phenomena not normally encountered in macroscale systems. This section will cover characteristic microfluidic phenomena that are relevant to the work presented in papers I-V included in this thesis. The implications of these phenomena for acoustofluidic applications will be covered in the sections below.

Laminar flow

For most flows in microfluidic channels viscosity dominates over inertia, which leads to the absence of turbulence, most often seen in macroscale flows, and the establishment of laminar flow streams (Figure 5.1). The laminar flow behaviour can easily be realized and is utilized to spatially and temporally control the flow of solutes as well as particles suspended therein[109]. This behaviour occurs when the Reynolds number (Re), which gives the ratio of viscous to inertial forces, is small (Re $\ll$ 2300).

$$Re = \frac{\rho U H}{\mu}$$

where U is the average velocity of the fluid, H is the channel dimension, and ρ and μ are the fluid density and dynamic viscosity, respectively[72]. In laminar flows phenomen such as diffusion also becomes increasingly important and is the only way in which mixing between solutions occur.[110] A sufficiently large particle, to not be affected by diffusion, suspended in the fluid will, thus, travel through the whole microchannel in the same laminar flow stream that it was positioned in when it entered the channel.

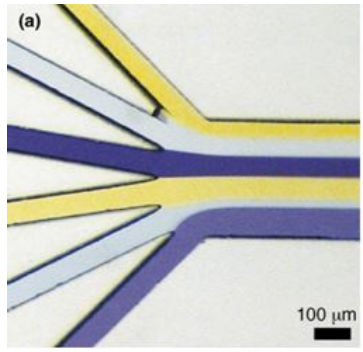

Figure 5.1: Laminar flow. Reprinted with permission from Weibel, D. B., Kruithof, M., Potenta, S., Sia, S. K., Lee, A., & Whitesides, G. M. (2005). Torque-actuated valves for microfluidics. Analytical Chemistry, 77(15), 4726-33[111]. Copyright 2005 American Chemical Society.

Poiseuille flow

A Poiseuille flow has a parabolic flow profile, where the fluid velocity is highest in the channel center and then gradually decreases as it approaches zero at the channel walls (Figure 5.2). This flow profile exists because of the non-slip boundary condition at the walls stating that the fluid velocity there will be zero. The effect of this will transfer, through the viscosity, to the bulk fluid and, thus, creating the parabolic flow profile. For a particle suspended in the fluid this means that it will have an increasingly longer retention time in the channel the closer to the walls, or top or bottom of the channel it is positioned[109] .

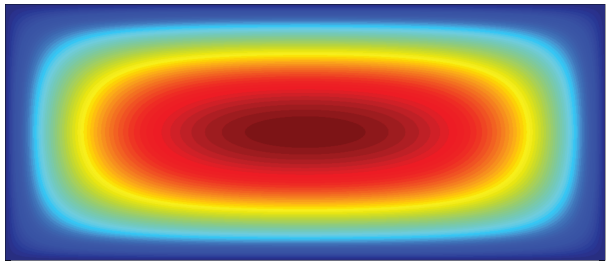

Figure 5.2: Flow velocity profile in a ~375 µm x 150 µm cross section microchannel. The colours indicate the fluid velocity, where blue indicates the lowest and red the highest flow velocities.

Stokes' drag

When a particle is dragged through a fluid, the particle experiences a viscous drag, a frictional force known as Stokes' drag (F_{drag}) during laminar flow conditions. This occurs for example when a particle is pushed through a fluid by an externally generated force. This drag force is directed opposite to the external force and the velocity of the particle.

$$F_{\text{drag}} = 6\pi\mu a u$$

where μ is the dynamic viscosity, a is the particle radius, and u is the velocity of the particle.

5.2 Acoustics

In the field of acoustofluidics, sound, in the form of ultrasound standing waves, is used to move particles to specific positions in microfluidic channels. When a particle is suspended in an ultrasound standing wave field, the induced force on the particle is a result of both the primary and secondary radiation forces, as well as the Stokes' drag force from the acoustic streaming. The primary acoustic radiation force originates from scattering of the standing wave on a particle and affects the particles position relative to the resonant cavity. The secondary acoustic radiation force is due to interactions of the scattered waves from two particles and affects the particles relative positions. This force is commonly orders of magnitude smaller and is only significant on very short particle-particle distances, *i.e.* at very high particle concentrations. In the papers I-V included in this thesis the particle concentration has deliberately been kept below 10^9/mL to minimize the effect of the acoustic and hydrodynamic interactions between particles and, thus, it will not be discussed further herein. The fundamental theory on acoustic standing wave forces on particles has earlier been described by King[112], Yosioka and Kawasima[113], Gorkov[114] and Nyborg[115], among others.

Primary acoustic radiation force

The primary acoustic radiation force (F_{rad}) is the force responsible for moving particles, suspended in an acoustic standing wave field, to the node or anti-node of the standing wave (Figure 5.3). When considering the case of a plane standing acoustic wave, an expression for the axial primary acoustic radiation force on a spherical particle with a radius much smaller than the wavelength can be derived.

$$F_{\mathrm{rad}} = 4\pi a^3 \Phi k_y E_{ac} \sin(2k_y y)$$

$$\Phi = \frac{\kappa_o - \kappa_p}{3k_o} + \frac{\rho_p - \rho_o}{2\rho_p + \rho_o}$$

where Φ is the acoustic contrast factor, a is the particle radius, k_y= $2\pi/\lambda$ is the wave number, E_{ac} is the acoustic energy density, y is the distance from the wall, κ_p is the isothermal compressibility of the particle, κ_o is the isothermal compressibility of the suspending fluid, ρ_p is the particle density, and ρ_o is the suspending fluid density[116].

It should be noted that the magnitude of the primary acoustic radiation force is strongly dependent on the particle volume such that larger particles will experience a larger force than smaller particles and will thus be moved faster towards the node or anti-node in the acoustic radiation force field.

When a particle is moved by the primary acoustic radiation force it is retarded by the Stokes' drag such that $F_{\mathrm{rad}} = F_{\mathrm{drag}}$. By balancing these forces the velocity, u_{rad}, of the particle can be derived.

$$u_{\mathrm{rad}} = \frac{2\Phi}{3\mu} a^2 k_y E_{\mathrm{ac}} \sin(2k_y y)$$

The particle velocity is dependent on the square of the particle radius. The two times velocity difference between 5 µm and 7 µm particles is the smallest difference that has been shown to be separable so far *e.g.* in paper III and IV.

The sign of the acoustic contrast factor, Φ, based on the density and compressibility of the particles in relation to the suspending medium, determines if the particle will move towards the standing wave node or anti-node. This factor is typically positive for cells suspended in physiological liquids such as plasma, phosphate buffered saline (PBS), or cell culture medium, and negative for particles such as air bubbles or oil particles.

Most successful acoustophoresis separation experiments are dependent mostly on the particle size differences, but the effect of the density and compressibility can also be seen for example when Grenvall *et al.*[117] managed to separate monocytes from granulocytes even though they are very similar in size.

Two-dimensional focusing

Early acoustophoresis particle separation experiments relied on focusing the particles in one dimension[118,119].

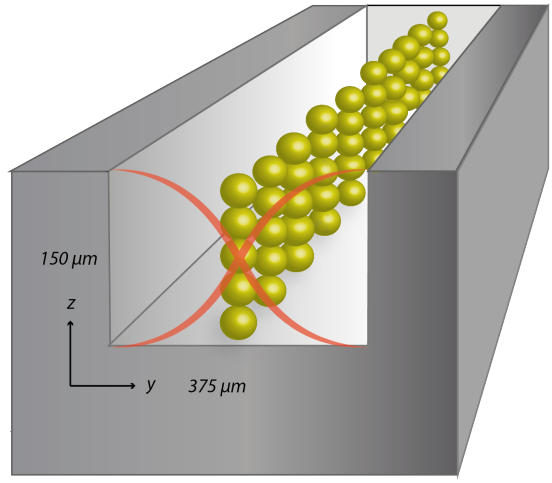

Figure 5.3: Particles acoustically focused in the ultrasound standing wave node in a microchannel with commonly used dimensions operated at a frequency of 2 MHz.

The parabolic flow profile in the microchannels will, however, have an impact on the separation efficiency when operated in this mode. This is due to the fact that particles suspended in different parts of the channel will have different retention time in the device and, thus, experience the acoustic standing wave field increasingly longer the nearer the walls or top and bottom of the channel the particles are positioned. A smaller particle initially positioned closer to the wall and especially top and bottom of the channel may, thus, be able to move to the same final position as a larger particle initially positioned closer to the channel centre. As the retention time in the force field for the smaller particle will be longer it will make up for the fact that this particle will experience a smaller acoustic radiation force and, thus, move slower.

In order to improve the separation resolution the particles can be prealigned in two dimensions, both horizontally and vertically, to ensure that they all are positioned in the same fluid velocity regime and all have the same retention time in the microchannel before sorting. Figure 5.4 shows confocal images where one-dimensional and two-dimensional focusing is compared.

Two-dimensional prealignment has also been used for sorting purposes in papers III and IV. In papers I and V, where acoustophoresis is used to concentrate cells and particles, these were two-dimensionally focused in order to position them in the fastest moving fluid regime when passing the outlet region. In the outlet region where the channel widens, the channel width no longer matches the wavelength of the ultrasound. In this region resonances occur in several directions, creating an unknown acoustic standing wave field that may divert the particles from their original trajectories to end up in the waste outlet.

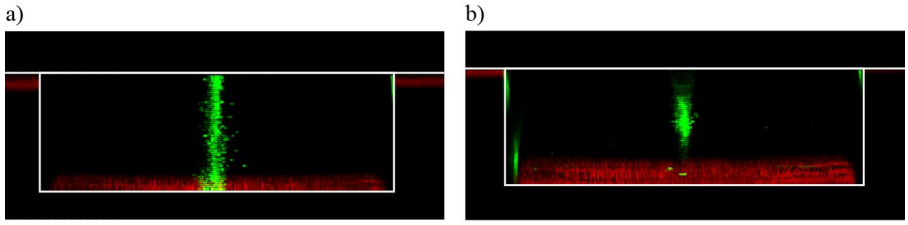

Figure 5.4: Confocal images showing a cross-section of the microchannel as indicated by the white lines. a) Particles focused (green) in one dimension vertically. The channel bottom is viewed in red. b) Particles focused in two dimensions. The focused cluster appears longer in the height direction because of the confocal depth of about 20 µm caused by the thick cover glass of the device. This is illustrated by the elongated image of a stationary particle in the lower left corner of the flow channel. Adapted from Ref.[120] with permission from The Royal Society of Chemistry.

If the particles move in the slower moving fluid regime past this region they will spend enough time there to be diverted. If they are, however, two-dimensionally focused to be positioned in the faster moving fluid regime they will pass this region faster and will not become diverted from their original trajectories. The complexity of the acoustic standing wave field in this region is shown in Figure 5.5 where the amplitude has been increased to exaggerate this phenomenon. The one-dimensionally focused particles are divided into several bands located at different channel depths. Particles closer to the top and bottom of the channel are escaping to the sides and will eventually, with increased amplitude even get trapped in local vortex-surrounded acoustic hot spots.

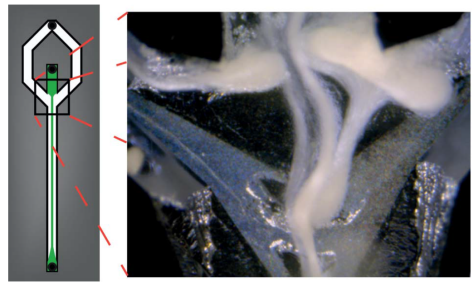

Figure 5.5: The effect of the undesired standing wave node pattern, in the outlet region, on particles focused in one dimension. The acoustic field divides the focused particle-band into several bands located at different channel depths, where the particles moving closer to the bottom and top of the channel become diverted to the side outlets or temporarily trapped in local hot spots surrounded by vortices.

In paper II two-dimensional focusing was shown to change the acoustic streaming pattern to not counteract the focusing of submicrometer particles in the way that one-dimensional-induced acoustic streaming does.

Acoustic streaming

An acoustic standing wave in a microchannel will not only assert a primary radiation force on particles suspended in the acoustic standing wave field, it will also induce the acoustic streaming driven by the shear stress near rigid walls in the acoustic boundary layers of the standing wave (Figure 5.6)[121]. This phenomenon was originally described by, and named after, Lord Rayleigh to Rayleigh streaming[122]. Later, the theory has been extended by Schlichting[123], Nyborg[124], Hamilton[125], and Muller[126], among others.

The Rayleigh streaming seen in acoustofluidic devices is driven by the viscous dissipation of acoustic energy into the boundary layer of the fluid along the channel walls. The dissipation in the boundary layer next to the wall is relatively large in comparison with the bulk dissipation because of the steep velocity gradient that is formed perpendicular to the channel wall because of the non-slip boundary condition dictating that the velocity by the wall decreases to zero. The boundary layer δ_v in the acoustofluidic devices presented in this thesis is less than 1 µm thick, harbouring the steep velocity gradient. The viscous dissipation results in a momentum flux close to the channel wall, which in turn results in the formation of boundary layer vortices called Schlichting streaming. This boundary layer streaming will in turn generate the large streaming vortices seen in the bulk of the fluid, the Rayleigh streaming. The acoustic streaming is particularly pronounced when $\lambda \gg h \gg \delta_v$, where λ is the ultrasound wavelength and h is the microchannel height (perpendicular to the direction of propagation of the standing wave)[121].

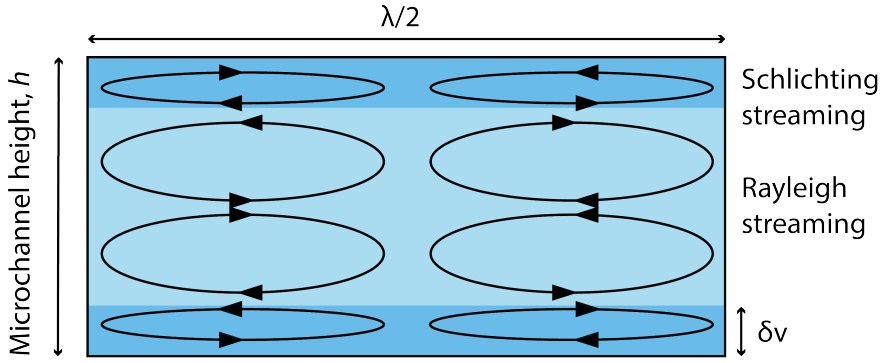

Figure 5.6: One-dimensionally induced acoustic streaming. The size of the viscous boundary layer where the Schlichting streaming takes place is highly exaggerated.

Acoustic streaming induced by a single standing wave

In devices similar to the ones presented in this thesis, the motion in the acoustic force field of particles (with properties similar to polystyrene) larger than the critical particles diameter of ~2µm is dominated by the acoustic radiation force. The motion of smaller

particles is, however, dominated by the Stokes' drag-induced acoustic streaming (Figure 5.7)[127,128]. At some positions in the microchannel the resulting motion of the Stokes' drag-induced acoustic streaming counteracts the motion induced by the primary acoustic radiation force. For larger particles this presents no problem as the primary acoustic radiation force is larger which keeps the focused particles in the nodal plane of the acoustic standing wave. For smaller particles, however, this disables focusing of the particles when the acoustic streaming-induced drag force drags the particles away from the nodal plane at the channel top and bottom. The transition from acoustic radiation force-induced to acoustic streaming-induced drag force motion is easily understood when considering that the primary acoustic radiation force scales with the cube of the particle radius while the acoustic streaming-induced drag force scales with the radius. Thus, as the particle radius decreases the primary radiation force decreases faster than the streaming-induced drag force.

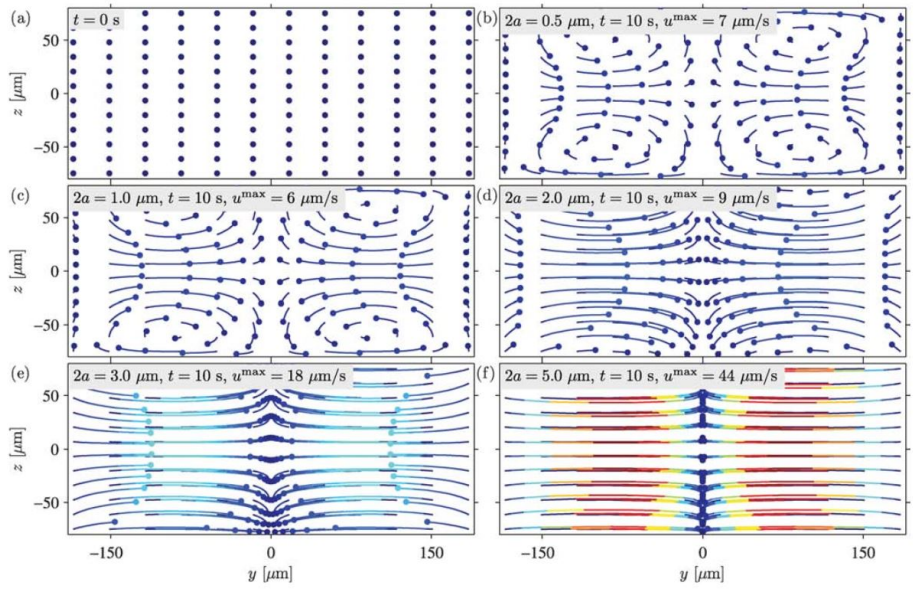

Figure 5.7: a) The starting position (dots) of 144 evenly distributed particles at t=0 s. The trajectories (coloured lines) and positions (dots) that the particles have reached by acoustophoresis a t=10 s for five different particle diameters: b) 0.5 µm c) 1 µm d) 2 µm e) 3 µm, and f) 5 µm. The colours indicate the instantaneous particle velocity u ranging from 0 µm/s (dark blue) to 44 µm/s (dark red). The lengths of the trajectories indicate the distance covered by the particles in 10 s. Reproduced from Ref.[128] with permission from The Royal Society of Chemistry.

Acoustic streaming induced by two orthogonal standing waves

When actuating the microchannel in two dimensions by two orthogonal resonances the generated acoustic streaming velocity field is fundamentally different compared to a single standing wave actuation[129]. The two-dimensionally actuated streaming velocity field does not counteract the primary radiation force in the same way as the classic Rayleigh streaming does. In paper II it was discovered that the critical particle diameter, where the crossover from radiation force-dominated to acoustic streaming-induced drag force-dominated particle motion takes place, could be reduced below 0.5 µm in diameter (for polystyrene-like particles) when actuating the microchannel in two dimensions. Figure 5.8 shows a comparison between a one-dimensionally and two-dimensionally actuated nearly-square microchannel and the corresponding particles trajectories for 0.5 µm particles. Figure 5.8 a shows that the submicrometer particles are caught in the characteristic quadrupolar structure of the streaming flow when actuated in only one dimension, while figure b and c show the corresponding streaming velocity fields for two different phase shifts between the oscillations of the walls when actuating the channel in two dimensions. As the experimental results in paper II shows that 0.5 µm particles can be focused it indicated that the used device is dominated by a streaming velocity field similar to the one showed in figure 5.8 c rather than 5.8 b. This streaming pattern has also been observed in parts of the microchannel, although the phase shift between the oscillations of the walls presumably varies along the channel length.

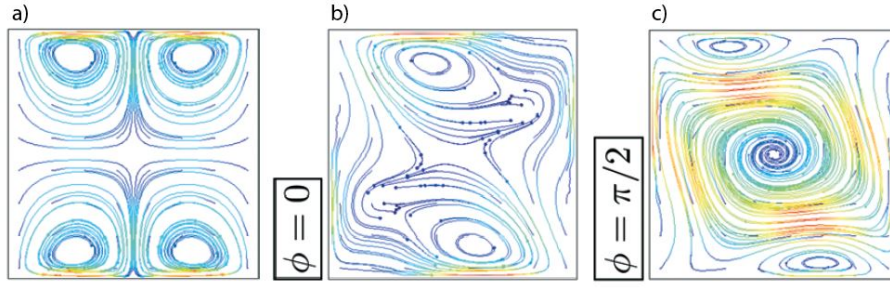

Figure 5.8: Acoustophoretic motion trajectories, as driven by the combination of primary acoustic radiation force and streaming-induced drag, of 0.5 µm particles in a nearly-square microchannel cross section. a) Shows the resulting trajectories of a one-dimensionally actuated channel, and b) and c) shows the trajectories for two different phase shifts between the oscillation of the walls in a two-dimensionally actuated channel. Adapted from Ref.[129] with permission from The Royal Society of Chemistry.

6

Microfabrication

The acoustophoresis devices utilized in papers I-V included in this thesis were fabricated through wet etching of silicon. Silicon is a rigid material that has an acoustic impedance significantly different from that of water or water-based biofluids. This, together with the straight channel walls produced by anisotropic wet etching along crystal planes, allows for an effective generation of acoustic standing waves. In addition to silicon, glass has been used to fabricate acoustofluidic devices[130]. An advantage of fabricating devices from wet-etched glass instead of wet-etched silicon, in addition to reduced fabrication costs, is that the device design is not bound by following crystal planes and can be fabricated in any design desirable where the width is at least two times the depth of the channel. The slightly rounded side walls of the glass channel can, however, cause some unwanted acoustic resonances not seen in wet-etched silicon devices. To decrease the fabrication costs and facilitate the fabrication process further plastics or polymers such as PDMS is often used in microfluidic devices. Even though a few attempts have been made to use these also for acoustofluidic devices,[131] these softer materials have an acoustic impedance closer to water which makes it harder to establish the standing wave as the reflection of the sound in the channel is less efficient. Even though a reflector in another material can be used, the softer material also severely dampens the actuation.

In papers I and III-V (100)-oriented silicon was used, and in paper II (110)-oriented silicon was used to produce a square channel. The microfabrication process for a (100)-oriented silicon wafer is explained in Figure 6.1.

Oxidization

In order to protect the silicon wafer and etch the desired pattern the wafer is first oxidized to produce a thin protective masking layer of silicon dioxide on the surface of the wafer. The silicon dioxide layer is formed by thermal oxidation for 6-8 h, where the wafer is exposed to oxygen or water vapour in a high temperature furnace (~1100°C). This results in an oxide layer that is approximately 1 µm thick.

Mask

To produce the desired channel first a mask is needed. The channel is first drawn in a CAD program, and then transferred to a positive photoresist and chromium-covered glass slide, by using a UV-laser only exposing the channel structure. The mask is then developed where the UV-exposed photoresist is stripped from the glass slide uncovering the chromium underneath. The chromium is then etched away to finally expose the glass.

Photoresist patterning

When the wafer is oxidized and the mask is fabricated the mask pattern can be transferred to the wafer. First the wafer is coated with a layer of positive photoresist. The resist-covered wafer is baked in an oven to solidify the photoresist making it non-sticky after which it is exposed to UV-light through the mask, exposing only the desired area of the wafer. The wafer can then be developed uncovering the silicon dioxide in the UV-light exposed areas. Finally the wafer is baked again in an oven to crosslink the polymer to make it resistant to the oxide etchant, after which it is no longer photo sensitive.

Oxide etching

The bare silicon dioxide can then be etched away, using hydrofluoric acid (HF) exposing the silicon underneath. The rest of the photoresist can also be removed exposing the silicon dioxide that protects the covered areas of the wafer from being etched in the next step.

Silicon etching

The exposed silicon is etched, using potassium hydroxide (KOH) heated to 80°C. Etching channels aligned with the <100> direction in a (100)-oriented silicon wafer will always produce a channel geometry wider than deep as the wafer will be etched with the same rate in both lateral and vertical directions, while etching channels aligned with the <111> direction in a (110)-oriented silicon wafer will only etch the wafer in the vertical direction making square or deeper than wide channel geometries possible.

Bonding

Before bonding the silicon to the glass lid the single channels are diced out from the wafer. Holes are then drilled through the single silicon channels to produce the inlets and outlets of the chips. Before bonding the silicon dioxide also have to be striped, by once again exposing the chips to HF. The chips can then be anodically bonded to borosilicate glass lids to seal the channels. After cleaning the silicon chip and glass lid thoroughly, the bonding is performed by placing the silicon-covered glass on a hot plate heated to 450°C, placing one electrode on the glass-covered silicon and having the hot plate work as the other electrode. When applying a voltage of 1000 V an electrostatic bond will be created between the silicon and the glass plate permanently bonding them together.

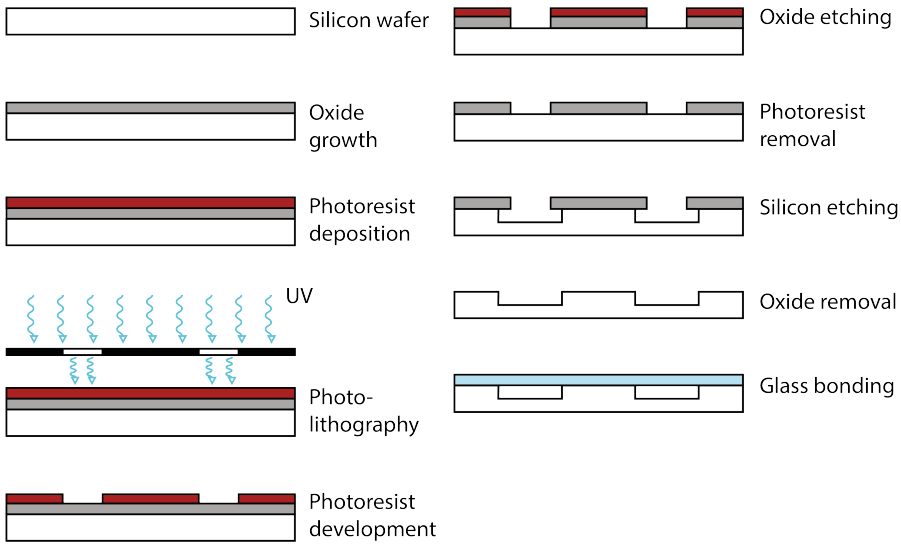

Figure 6.1: The microfabrication process of a (100)-oriented silicon wafer to produce an acoustofluidic device.

7

Technical advancements

The foundation of this thesis is comprised of the five included papers. This section intends to introduce each paper and the aim and motivation for the work. The overall aim has been to develop microfluidic devices that are useful for rare cell handling. The methods can be used as stand-alone devices, but also as integrated parts of a more complex system including other sample preparation or analysis units, towards a true μTAS (as partly shown in papers III-V and illustrated in Figure 7.1).

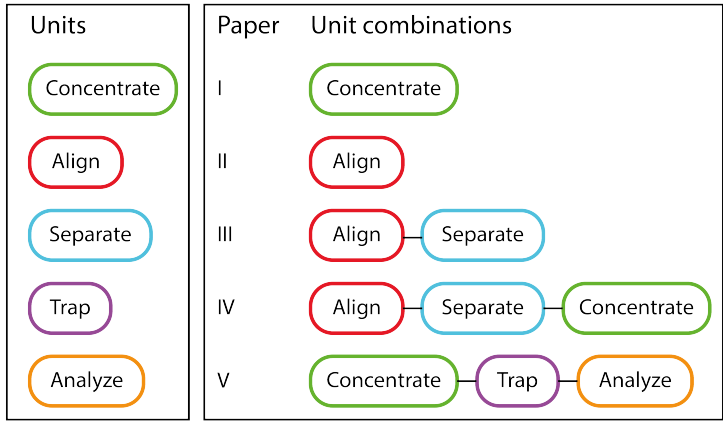

Figure 7.1: Operation units used or combined in the different papers included in this thesis.

Paper I - Two-hundredfold volume concentration of dilute cell and particle suspensions using chip integrated multistage acoustophoresis

Rare cells, after isolation, are often dilute since they originate from large volumes of sample. When handling dilute cell suspensions containing few cells, or small sample volumes produced by microfluidic processing, ordinary concentration techniques such as centrifugation might not be practically usable. To these ends, in the first paper, acoustophoresis was used to concentrate cells and particles in order to facilitate subsequent analysis. In the paper it was shown that sequential concentration steps and two-dimensional focusing was crucial to achieving the highest concentration factors. The sequential concentration steps were used to multiply a modest concentration factor achieved in each step to a high overall concentration factor. The two-dimensional focusing allowed the particles to all be positioned in the flow regime with the highest flow rate which reduced the time spent in the acoustically chaotic trifurcation regions to a minimum, preventing them from being deflected from their established flow trajectories (Figure 7.2). Using these findings dilute cancer cell suspensions could be concentrated 195.7 ± 36.2-fold with a recovery of 97.2 ± 3.3 %. The chip was further envisioned to be an integrable unit of a larger Lab-on-a-Chip system.

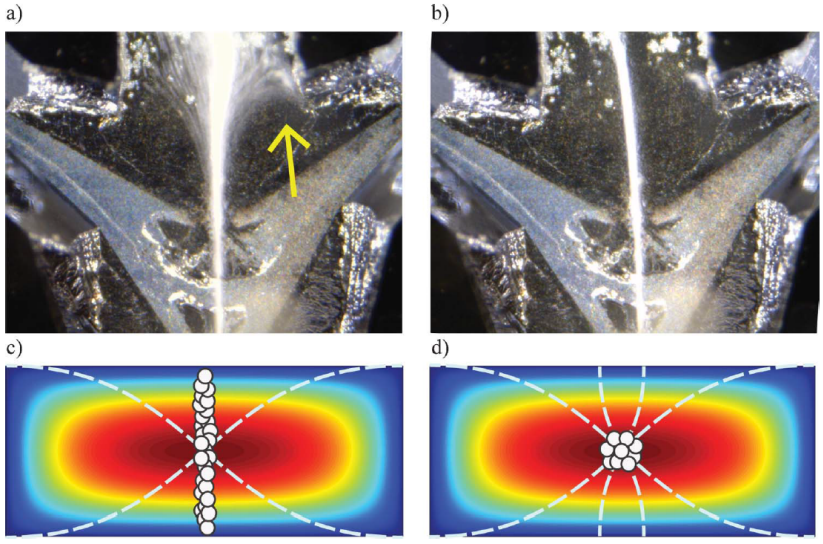

Figure 7.2: a) Particles focused in one dimension in the last outlet region. The yellow arrow indicates escape of particles to the side outlet. b) Particles focused in two dimensions in the last outlet region. c) and d) Schematic cross-section of the micro-channel showing particles focused in one and two dimension and their position within the flow velocity profile. Red represents the fastest and blue the slowest moving fluid regime. The dashed lines indicate the ultrasound standing waves. Reproduced from Ref.[120] with permission from The Royal Society of Chemistry.

Paper II - Focusing of sub-micrometer particles and bacteria enabled by two-dimensional acoustophoresis

Acoustophoresis devices that focus particles in one dimension and are operated at a frequency of around 2 MHz handles larger cells efficiently. They can, however, not be efficiently used to handle particles and rare cells smaller than about 2 µm in diameter, practically meaning that most bacteria cannot be acoustophoretically processed. While the acoustophoresis-induced motion of larger particles is dominated by the acoustic radiation force, the motion of smaller particles is instead dominated by the acoustic streaming-induced drag force. Larger particles can, thus, be focused while smaller particles instead are trapped in the streaming vortices inherent with the acoustic field. It was found that while simultaneously exciting two orthogonal resonances an acoustic streaming velocity field was formed that did no longer counteract the primary radiation force which allowed submicrometer particles to be focused. Further it was showed that the critical particles diameter, where the crossover from radiation force-dominated to acoustic streaming-induced drag force-dominated particle motion, was decreased below 0.5 µm (for polystyrene-like particles), a four-fold size reduction (Figure 7.3). The device was also used to focus *E. coli* with a focusability of 0.95 ± 0.35. Simulations and experiment showed that the streaming velocity field was dominated by a large centred flow roll instead of the four characteristic Rayleigh vortices seen when actuating the channel in one dimension. It was envisioned that the results would open the field of acoustophoresis to new applications in microbiology for biomedical, environmental, or food purposes.

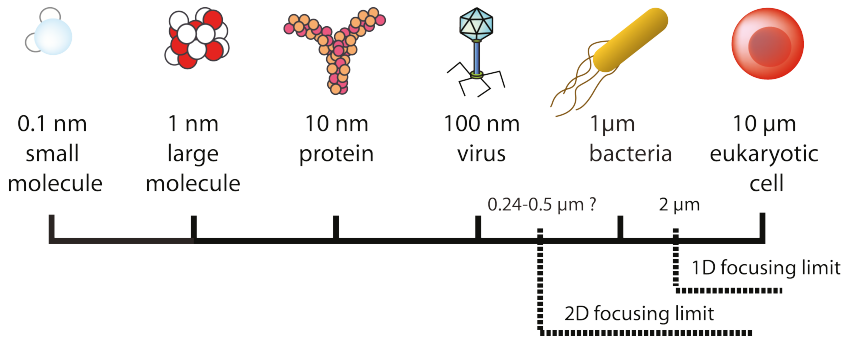

Figure 7.3: Comparative illustration of bioparticles sizes in relation to the acoustophoresis focusing limits for one-dimensional and two-dimensional focusing.

Paper III - A single inlet two-stage acoustophoresis chip enabling tumor cell enrichment from white blood cells

In the third paper the focus was again turned to the handling of larger rare cells presenting a device that enabled a simplified fluidic setup for cancer cell separation from WBCs (Figure 7.4). This was achieved by removing the centre fluid inlet when performing the separation. The simplified fluidic setup has three obvious advantages. It will facilitate the control of the flow in the device making it easier to keep it stabile, which in turn will generate better recoveries and less contamination of target cells. It will also easier lend itself to integration with other operation units keeping the fluidic connections to a minimum. Furthermore, the need to match the acoustic impedances of fluids when using multiple inlet streams is eliminated. When removing the centre fluid stream the prealignment becomes crucial for the separation ability. Without the centre stream, which hydrodynamically laminates the particles to the channel walls, particles that were not peraligned would be randomly distributed in the whole channel not allowing them to be separated. It was also shown that it was important to control the ratio of the flow through the centre outlet compared to the side outlets, to generate the highest separation efficiency. Using this device, spiked cancer cells could be separated from WBCs with at recovery of 86.5 $\pm$ 6.7% of the cancer cells with 1.1 $\pm$ 0.2% contamination of WBCs. In addition to the mentioned advantages this device also made it possible to concentrate the recovered cells about 2,5-fold instead of diluting them as devices relying on hydrodynamic pre-positioning often do, important especially for rare cell processing.

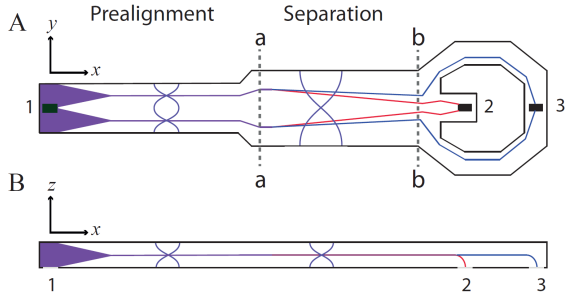

Figure 7.4: Illustration of the chip and particle trajectories from (A) the top and (B) the side. Cells and particles are infused at (1) and are acoustically prealigned in two dimensions to two positions along the width (y-axis) of the chip and are at the same time levitated to mid-height (z-axis) of the channel (purple lines). The prealigned cells then enter the wider separation channel at (a-a), where the larger, denser, or less compressible cells are focused faster towards the center of the channel (red line). Thus, these cells or particles are separated from smaller, less dense, or more compressible cells (blue line) and the two different fractions can be collected in the two outlets (2) and (3). Adapted from Ref.[132] with permission from The Royal Society of Chemistry.

Paper IV - Acoustofluidic, label-free separation and simultaneous concentration of rare tumor cells from white blood cells

After demonstrating that acoustophoresis can be used to either concentrate or separate cells an obvious next step was to integrate the two operation units. Many cell separators dilute the target cells in the process, something that is a clear disadvantage when processing rare cells. As the rare cells are, after isolation, often dilute the subsequent analysis of the separated cells will be facilitated by concentrating the cells. Ordinary concentration methods such as centrifugation might not be practically useful to handle these microfluidically generated samples with small volumes and low cell numbers. The integration of a separation and a concentration unit will therefore provide a useful tool for the processing of rare cells in microfluidic systems. In Paper IV such an integrated device to simultaneously separate and concentrate spiked cancer cells from WBCs was used (Figure 7.5). It was found that MCF-7 cells could be separated from WBCs with a recovery of $91.8 \pm 1.0\%$ and a contamination of $0.6 \pm 0.1\%$ WBCs with a simultaneous 23.8 ± 1.3-fold concentration of the cancer cells, and DU145 cells could be recovered with an efficiency of $84.1 \pm 2.1\%$ with $0.2 \pm 0.04\%$ contamination of WBCs while concentrating the cancer cells 9.6 ± 0.4-fold. Integrated with an analysis unit this device has the potential to contribute to the clinical monitoring of cancer patients as well as the development of personalized medicine with targeted therapies specific to an individual patient's tumor biology.

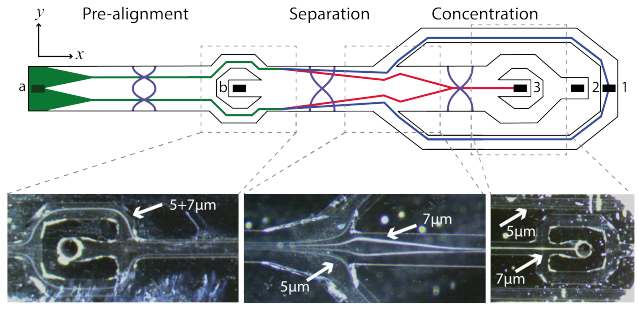

Figure 7.5: Illustration of the chip from the top showing particle trajectories and inset photographs, showing the separation of 5 and 7 µm polystyrene particles. Particles were infused through inlet (a) and prealigned in two dimensions, horizontally and vertically (y- and z-directions). A cell-free liquid was infused through inlet (b) where the cells of interest were isolated in the separation channel. Waste cells were discarded through outlet (1) as the target cells were refocused in the concentration channel. Concentrated cells were then collected through outlet (3), and cell-free liquid was discarded through outlet (2). Reprinted with permission from Antfolk, M., Magnusson, C., Augustsson, P., Lilja, H., & Laurell, T. (2015). Acoustofluidic, label-free separation and simultaneous concentration of rare tumor cells from white blood cells. Analytical Chemistry, 87(18), 9322-8[133]. Copyright 2015 American Chemical Society

Paper V - Highly efficient single cell arraying by integrating acoustophoretic cell pre-concentration and dielectrophoretic cell trapping

Finally, in paper V it was shown that the acoustophoresis device can be integrated with an analysis device, composed of an electroactive microwell array (EMA) based on dielectrophoresis trapping, enabling simultaneous concentration, trapping and subsequent analysis of target cells (Figure 7.6). In this work, the method, presented in paper I was used, to concentrate cells by focusing them in two dimensions. Most importantly, as a consequence of the cell concentration step, the device also translates a flow of a higher flow rate into a lower one. This was especially beneficial for the EMA trapping chip that was reliant on a low flow rate to efficiently trap cells. The low flow rate meant that the processing of samples would be very time consuming and in principle non applicable to clinical samples. When integrating the two devices a higher sample input flow rate could be used. The integrated system could process samples with a ~10-fold higher flow rate as compared to the EMA trapping chip alone while still recovering over 90% of the cells. This proof-of-concept work can be further extended by additional functions, such as cell sorting, by integration with the device presented in paper IV, or extended analysis after cell trapping, as has been previously performed in a similar EMA trap.

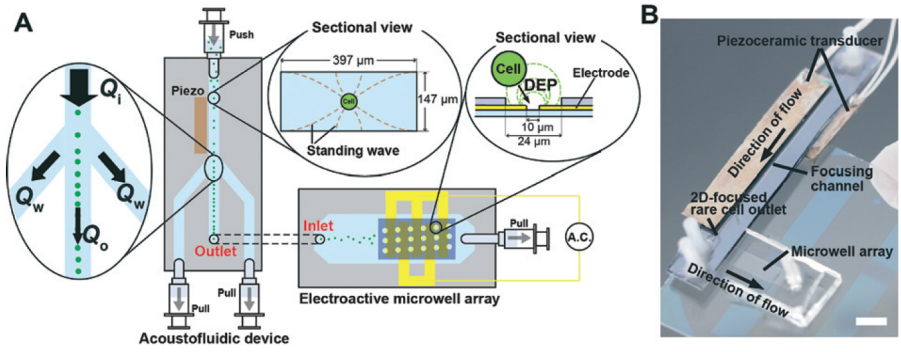

Figure 7.6: Integration of the acoustofluidic chip and the EMA chip. (A) Schematic image of integration. The target cells introduced from the inlet of the acoustofluidic chip are focused at the center of the channel using ultrasound standing waves. The central stream of the chip with the focused cells flows into the EMA chip. The cells are trapped into the microwell array using DEP in the EMA chip. (B) Photo of the integrated device. The outlet of the acoustofluidic device is directly interfaced to the inlet of the EMA chip. Scale bar is 4mm. Reproduced from Ref.[134] with permission from The Royal Society of Chemistry.

8

Concluding remarks

This thesis has presented new acoustophoresis-based methods for rare cell processing. It has been shown that acoustophoresis can be used to concentrate or separate cancer cells from white blood cells, either in stand-alone devices or integrated on the same device. This thesis also showed the possibility to alter the acoustic streaming velocity field as to allow focusing of submicrometer particles. Finally, it was shown that an acoustophoresis device can be integrated with other functionalities.

As opposed to many other microfluidic techniques for cell handling, acoustophoresis is already used in a commercial flow cytometer instrument, the Attune^{TM}. To some extent this proves the usefulness of the technique. Nevertheless, there is a lot of research still to be done before the technology will reach its full potential. For example the possibility to integrate many sequential unit operations, as shown in this thesis, may be further explored.

Through a close collaboration with the Technical University of Denmark, DTU, much light has been shed on the fundamentals and the physics behind the area of acoustofluidics. Several newly published papers have for instance addressed acoustic streaming, but there is a lot of more ground to cover. Advances in theoretical understanding as well as measurements of the acoustic properties of cells, will also lead to a more fundamental understanding where it will be possible to fully determine the motion of cells in acoustic fields.

As the technical understanding advances, new application areas should also be sought for. By closer interactions between engineers, physicians, and biologists, new projects can, no doubt, be born.

Furthermore, as the research field of microfluidics is maturing more, many research groups are striving towards building true μTAS devices where several different microfluidic methods are combined. Acoustophoresis has been used to perform many different operations such as cell sorting and separation, concentration, washing and trapping where their usefulness would increase even further by integrating them with other sample preparation, or detection and analysis units. There is always more to discover that could ever be envisioned.

9

Populärvetenskaplig sammanfattning

Under min doktorandtid har jag forskat kring en metod kallad akustofores, där ultraljud används tillsammans med mikrofluidik, det vill säga vätskeflöden i mikroskopiska kanaler. Allt för att bidra till att besvara olika medicinska frågeställningar. Det slutliga målet är att konstruera en medicinskteknisk apparat som kan användas inom sjukvården, som hjälp för att diagnostisera eller övervaka olika sjukdomstillstånd.

Mer specifikt har jag fokuserat på att koncentrera eller sorterar ut det som kallas sällsynta celler från blodprov. Sällsynta celler finns bara i små mängder i en mycket större population av andra celler. Antalet sällsynta celler är oftast färre än 1000 per milliliter i ett blodprov medan det t.ex. samtidigt finns ca 5 miljarder röda blodceller. Att leta efter dessa celler kan därför liknas vid att leta efter en nål i en höstack.

Ett exempel på sällsynta celler är cirkulerande tumörceller, vilket är celler som ger sig iväg från en cancertumör, via blodomloppet, till en ny vävnad och där bildar metastaser (sekundära tumörer). Det är när cancercellerna befinner sig i blodomloppet som de benämns cirkulerande tumörceller. Om det är möjligt att leta upp och bestämma antalet celler, så går det att övervaka hur aggressiv cancern är och om det är troligt att metastaser kommer att bildas. Genom att hitta cirkulerande tumörceller i ett blodprov återfinns en bit av tumören, som det är möjligt att använda för att t.ex. testa mediciner, utan att behöva ta mer invasiva biopsier. I avhandlingen visar jag att det är möjligt att använda akustofores till att sortera ut och koncentrera cancerceller från blodprov.

Ett annat exempel på sällsynta celler som kan finnas i blodet är bakterier. Om bakterier lyckas ta sig in i blomloppet så kan det leda till blodförgiftning eller sepsis, vilket är ett sjukdomstillstånd som snabbt utvecklas negativt om inte rätt behandling ges i form av antibiotika. Eftersom det finns många varierande typer av antibiotika som verkar mot olika bakterier, så är det viktigt att patienten behandlas med lämpligast variant. Vid misstänkta fall av sepsis så finns det inte tid att avvakta med behandling innan bakteriearten som

infekterat patienten hunnit fastställas, så behandlande läkare är tvingad att ge en cocktail av olika antibiotika och hoppas att någon av dessa verkar. Samtidigt tas ett blodprov från patienten som skickas på odling och analys, men där det kan dröja allt från en till fyra dagar innan besked kan lämnas om vilken bakterie som orsakat infektionen. Allt är beroende av tillräcklig snabb bakterietillväxt så att mängden gör det möjligt att bestämma vilken typ av bakterie det är fråga om, och om den är resistent mot någon antibiotika. Om snabbare sortering och koncentrering kan ske av bakterier så att renheten och antalet är tillräcklig för analys, så kan fler patienter botas samtidigt som det är möjligt att förebygga onödig antibiotikaanvändande.

Samtidigt som mina kollegor i laboratoriet arbetar med att försöka sortera ut bakterier från blod, så har jag arbetat med en metod för att försöka koncentrera dem. Vid tidigare försök har akustofores inte kunna användas för så små celler som bakterier, då dessa är mycket mindre än mänskliga celler. I avhandlingen har jag visat en metod som gör att det nu också är möjligt.

För att kunna processa dessa prover med sällsynta celler så flödar jag dem genom mikroskopiska kanaler, som är ungefär en tredjedels millimeter breda. Vid flöden av vätskor igenom mikrokanaler, så uppstår fenomen som vanligtvis inte uppstår vid vätskeflöden igenom större kanaler. Ett av dessa benämns laminära flöden, och yttrar sig i att vätskan inte blandas utan flödar genom kanalen på samma sätt som den anbringades. Anta att det finns en kanal med tre inlopp och att röd vätska tillförs genom det mittersta inloppet och blå vätska genom sidoinloppen. De kommer då att fortsätta flöda parallellt som tre separata strömmar genom mikrokanalen (se Figur 9.1b). Om samma tillvägagångssätt tillämpats i en större kanal så skulle vätskorna blanda sig och anta en lila färg (se Figur 9.1a). Om jag istället för olikfärgade vätskor tillför blod i sidoinloppen och en ren vätska, utan celler, i andra inloppet så är det möjlig att kontrollera var i kanalen blodet kommer att vara lokaliserat. I kombination med det använder jag också ultraljud i form av stående vågor, där ljudet studsar fram och tillbaka mellan kanalväggarna. Ultraljudet gör att jag kan flytta celler i sidled i kanalen in i den cellfria vätskan, på ett sätt som de annars inte skulle röra sig på grund av det laminära flödet. Större celler påverkas mer av ultraljud och flyttar sig snabbare i sidled (se Figur 9.1c). Det kan utnyttjas för att t.ex. sortera ut cancerceller från blodet eftersom dessa vanligen är större än blodceller. När olika celler har separerats till differentierade positioner i kanalen så kan de pumpas ut i olika utlopp, samlas upp, räknas eller analyseras vidare.

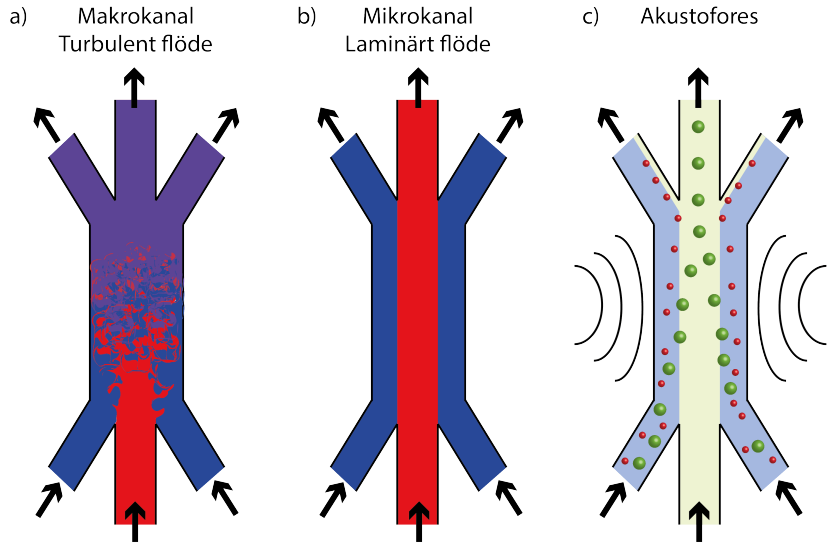

Figure 9.1: a) Turbulent flöde i en makrokanal. b) Laminärt flöde i en mikrokanal lik de som använts i avhandlingen. c) Akustofores. De större gröna cellerna flyttas snabbare i sidled av ultraljudet och kan därför separeras från de mindre röda cellerna. De svarta konvexa linjerna visar ultraljudet. Pilarna visar riktningen på flödet.

10

Acknowledgements

Finally, I am approaching the end of a dream that started somewhere in the basement of the Infectious Disease Clinic in Lund where I was having a position during the summer. More specifically, the story about my work at the Department of Biomedical Engineering started when I was looking out of the window from my previous work position at Ideon. Every day I watched Björn and co-workers passing by on their way to have lunch, thinking that they looked so friendly and happy towards each other. Little did I know that after six month of constant nagging on Thomas I would be included in that group. For this I would like to express my deepest and most sincere gratitude towards my supervisor Thomas Laurell for taking a chance on me and letting me become a part of your research group, and towards my supervisors Per Augstusson and Andreas Lenshof. Thanks to my collaborators in Denmark, Henrik Bruus and Peter Muller Tribler for many interesting discussion and contributing to this thesis, and in Japan, Teruo Fujii, Soo Hyeon Kim, Shohei Kaneda and Marina Kobayashi for welcoming me to your lab and contributing to this thesis. Thanks Cecilia Magnusson for great collaboration, conference company, and all cell biology advice and Hans Lilja for contributing with a much needed clinical perspective. Thanks also to Stefan Scheding for letting me use your cell lab.

I would also like to thank all the people at Elmät in no particular order. Johan Nilsson for heading the department and letting me work here. Per Augustsson for great collaboration and supervision throughout my whole time as a PhD student but most for great rums-AW, spotting all suspicious querulant activity, and teaching me how to turn on a computer. Ola Jakobsson for great collaborations, for living life on the edge by eating before asking, and for always lightening up the mood. Carl Grenvall for winning the best Christmas decoration-award and for always helping me when I get stuck in the vinkelvolt. Klara Petersson for starting out at the department and learning acoustophoresis together with me and for listening enthusiastically when I had my Neanderthal phase. Björn Hammarström for PCR experiments and for winning the least complex lab-bench award. Maria Tenje for being an awesome mentor, role model, and friend. Belinda Lyddby for great conference

company and always having a good spirit. Kevin Cushing for being very hard-working in the lab without being negative as your particles. Fredrik Ejserholm for great computer support, winning the oldest reference in PhD thesis-award and teaching me all about the complexity of the parental benefit system. Simon Ekström for nice allotment hang outs. Mikael Evander for always having fabrication advice and for lending me the secret good glass cutter. Anna Fornell for making use of my old glass chips and not being a bubble. Fabio Garofalo for great enthusiasm over high-throughput channels. Kishore Jagadeesan for contributing to the Asian food party. Sameer Deshmukh for good AW company and lightening up the mood in the lab. Linus Jonsson for trying to save my badly bonded chips and for offering me your oxidized wafers. Andreas Lenshof for supervision and secret plans on taking over the world with SAW. Maybe I was not supposed to tell. Pelle Ohlsson for sharing the nightly bus ride through Finland-experience. Eva Undvall for making a great addition to the "'CTC-group"'. Anke Urbansky for good advice on gradient centrifugation and great company in the BMC lab. Pamela Svensson for tolerating all baby or postdoc talk. Anette Wolff for introducing some color to the office and not being a bad wolf. Hong Yan for being my department bestie and showing me that I am not alone in remembering everything that happens. Martin Bengtsson for introducing me to the clean room and always being helpful whenever I run into problems. Lars Wallman for not telling on me even though I once promised you I would never use an oscilloscope ever again. Magnus Cinthio, Tomas Jansson, Hans Persson and Monica Almqvist for an interesting course on biomedical ultrasound. John Albinsson, Maria Evertsson and Tobias Erlöv for being great statistics course buddies. Désirée Jarebrant, Ulrika Westerdahl, and Malgorzata Luczak for keeping track on the more complicated things in life. Last but not least, the Sol-group for secret meetings. Also thanks to whomever I have forgotten.

Most of all, thanks to my family for always being motivating and supportive and to my dear Christian for supporting me throughout this whole experience and for taking such good care of Ellen.

References

[1] T.R. Ashworth. A case of cancer in which cells similar to those in the tumours were seen in the blood after death. *Australian Med J*, 14:146–149, 1869.

[2] W. Y. Lin, Y. Wang, S. Wang, and H. R. Tseng. Integrated Microfluidic Reactors. *Nano Today*, 4(6):470–481, Dec 2009.

[3] W. J. Allard, J. Matera, M. C. Miller, M. Repollet, M. C. Connelly, C. Rao, A. G. Tibbe, J. W. Uhr, and L. W. Terstappen. Tumor cells circulate in the peripheral blood of all major carcinomas but not in healthy subjects or patients with nonmalignant diseases. *Clin Cancer Res*, 10(20):6897–6904, Oct 2004.

[4] S. J. Cohen, C. J. Punt, N. Iannotti, B. H. Saidman, K. D. Sabbath, N. Y. Gabrail, J. Picus, M. Morse, E. Mitchell, M. C. Miller, G. V. Doyle, H. Tissing, L. W. Terstappen, and N. J. Meropol. Relationship of circulating tumor cells to tumor response, progression-free survival, and overall survival in patients with metastatic colorectal cancer. *J Clin Oncol*, 26(19):3213–3221, Jul 2008.

[5] M. Cristofanilli, G. T. Budd, M. J. Ellis, A. Stopeck, J. Matera, M. C. Miller, J. M. Reuben, G. V. Doyle, W. J. Allard, L. W. Terstappen, and D. F. Hayes. Circulating tumor cells, disease progression, and survival in metastatic breast cancer. *N Engl J Med*, 351(8):781–791, Aug 2004.

[6] R. A. Ghossein, H. I. Scher, W. L. Gerald, W. K. Kelly, T. Curley, A. Amsterdam, Z. F. Zhang, and J. Rosai. Detection of circulating tumor cells in patients with localized and metastatic prostatic carcinoma: clinical implications. *J Clin Oncol*, 13(5):1195–1200, May 1995.

[7] R. Ran, L. Li, M. Wang, S. Wang, Z. Zheng, and P. P. Lin. Determination of EGFR mutations in single cells microdissected from enriched lung tumor cells in peripheral blood. *Anal Bioanal Chem*, 405(23):7377–7382, Sep 2013.

[8] A. Satelli, A. Mitra, J. J. Cutrera, M. Devarie, X. Xia, D. R. Ingram, D. Dibra, N. Somaiah, K. E. Torres, V. Ravi, J. A. Ludwig, E. S. Kleinerman, and S. Li. Universal marker and detection tool for human sarcoma circulating tumor cells. *Cancer Res*, 74(6):1645–1650, Mar 2014.

[9] B. Aktas, M. Tewes, T. Fehm, S. Hauch, R. Kimmig, and S. Kasimir-Bauer. Stem cell and epithelial-mesenchymal transition markers are frequently overexpressed in circulating tumor cells of metastatic breast cancer patients. *Breast Cancer Res*, 11(4):R46, 2009.

[10] S. S. Wachtel, L. P. Shulman, and D. Sammons. Fetal cells in maternal blood. *Clin Genet*, 59(2):74–79, Feb 2001.

[11] H. Mohamed, J. N. Turner, and M. Caggana. Biochip for separating fetal cells from maternal circulation. *J Chromatogr A*, 1162(2):187–192, Aug 2007.

[12] R. Akolekar, J. Beta, G. Picciarelli, C. Ogilvie, and F. D'Antonio. Procedure-related risk of miscarriage following amniocentesis and chorionic villus sampling: a systematic review and meta-analysis. *Ultrasound Obstet Gynecol*, 45(1):16–26, Jan 2015.

[13] S. Ponnusamy, H. Zhang, P. Kadam, Q. Lin, T. K. Lim, J. S. Sandhu, N. Kothandaraman, A. P. Mahyuddin, A. Biswas, A. Venkat, C. L. Hew, S. B. Joshi, M. C. Chung, and M. Choolani. Membrane proteins of human fetal primitive nucleated red blood cells. *J Proteomics*, 75(18):5762–5773, Oct 2012.

[14] L. Hatt, M. Brinch, R. Singh, K. M?ller, R. H. Lauridsen, J. M. Schlutter, N. Uldbjerg, B. Christensen, and S. K?lvraa. A new marker set that identifies fetal cells in maternal circulation with high specificity. *Prenat Diagn*, 34(11):1066–1072, Nov 2014.

[15] E. Guetta, L. Gutstein-Abo, and G. Barkai. Trophoblasts isolated from the maternal circulation: in vitro expansion and potential application in non-invasive prenatal diagnosis. *J Histochem Cytochem*, 53(3):337–339, Mar 2005.

[16] J. Cohen. The immunopathogenesis of sepsis. *Nature*, 420(6917):885–891, 2002.

[17] S. Shafazand and A. B. Weinacker. Blood cultures in the critical care unit: improving utilization and yield. *Chest*, 122(5):1727–1736, Nov 2002.

[18] M. Hristov, W. Erl, and P. C. Weber. Endothelial progenitor cells: isolation and characterization. *Trends Cardiovasc Med*, 13(5):201–206, Jul 2003.

[19] C. J. Boos, G. Y. Lip, and A. D. Blann. Circulating endothelial cells in cardiovascular disease. *J Am Coll Cardiol*, 48(8):1538–1547, Oct 2006.

[20] D. A. Ingram, L. E. Mead, H. Tanaka, V. Meade, A. Fenoglio, K. Mortell, K. Pollok, M. J. Ferkowicz, D. Gilley, and M. C. Yoder. Identification of a novel hierarchy of endothelial progenitor cells using human peripheral and umbilical cord blood. *Blood*, 104(9):2752–2760, Nov 2004.

[21] M. Zborowski and J. J. Chalmers. Rare cell separation and analysis by magnetic sorting. *Anal Chem*, 83(21):8050–8056, Nov 2011.

[22] J. Seligman, S. Slavin, and I. Fabian. A method for isolating pluripotent/multipotent stem cells from blood by using the pluripotent and germ-line DAZL gene as a marker. *Stem Cells Devs*, 18(9):1263–1271, Nov 2009.

[23] O. K. Lee, T. K. Kuo, W. M. Chen, K. D. Lee, S. L. Hsieh, and T. H. Chen. Isolation of multipotent mesenchymal stem cells from umbilical cord blood. *Blood*, 103(5):1669–1675, Mar 2004.

[24] F. Notta, S. Doulatov, E. Laurenti, A. Poeppl, I. Jurisica, and J. E. Dick. Isolation of single human hematopoietic stem cells capable of long-term multilineage engraftment. *Science*, 333(6039):218–221, Jul 2011.

[25] W. K. Peng, T. F. Kong, C. S. Ng, L. Chen, Y. Huang, A. A. Bhagat, N. T. Nguyen, P. R. Preiser, and J. Han. Micromagnetic resonance relaxometry for rapid label-free malaria diagnosis. *Nat Med*, 20(9):1069–1073, Sep 2014.

[26] Y. Chen, P. Li, P. H. Huang, Y. Xie, J. D. Mai, L. Wang, N. T. Nguyen, and T. J. Huang. Rare cell isolation and analysis in microfluidics. *Lab Chip*, 14(4):626–645, Feb 2014.

[27] W. Zhang, K. Kai, D. S. Choi, T. Iwamoto, Y. H. Nguyen, H. Wong, M. D. Landis, N. T. Ueno, J. Chang, and L. Qin. Microfluidics separation reveals the stem-cell-like deformability of tumor-initiating cells. *Proc Natl Acad Sci USA*, 109(46):18707–18712, Nov 2012.

[28] M. Brown and C. Wittwer. Flow cytometry: principles and clinical applications in hematology. *Clin Chem*, 46(8 Pt 2):1221–1229, Aug 2000.

[29] L. W. Arnold and J. Lannigan. Practical issues in high-speed cell sorting. *Curr Protoc Cytom*, Chapter 1:1–30, Jan 2010.

[30] D. W. Bianchi, A. F. Flint, M. F. Pizzimenti, J. H. Knoll, and S. A. Latt. Isolation of fetal DNA from nucleated erythrocytes in maternal blood. *Proc Natl Acad Sci USA*, 87(9):3279–3283, May 1990.

[31] J. F. Swennenhuis, J. Reumers, K. Thys, J. Aerssens, and L. W. Terstappen. Efficiency of whole genome amplification of single circulating tumor cells enriched by CellSearch and sorted by FACS. *Genome Med*, 5(11):106, 2013.

[32] S. Miltenyi, W. Muller, W. Weichel, and A. Radbruch. High gradient magnetic cell separation with MACS. *Cytometry*, 11(2):231–238, 1990.

[33] I. Šafařík and M. Šafaříková. Use of magnetic techniques for the isolation of cells. *J Chromatogr B Biomed Sci Appl*, 722(1-2):33–53, feb 1999.

[34] K. Bluemke, U. Bilkenroth, A. Meye, S. Fuessel, C. Lautenschlaeger, S. Goebel, A. Melchior, H. Heynemann, P. Fornara, and H. Taubert. Detection of circulating tumor cells in peripheral blood of patients with renal cell carcinoma correlates with prognosis. *Cancer Epidemiol Biomarkers Prev*, 18(8):2190–2194, Aug 2009.

[35] T. J. Molloy, A. J. Bosma, and L. J. van't Veer. Towards an optimized platform for the detection, enrichment, and semi-quantitation circulating tumor cells. *Breast Cancer Res Treat*, 112(2):297–307, Nov 2008.

[36] A. Ulmer, O. Schmidt-Kittler, J. Fischer, U. Ellwanger, G. Rassner, G. Riethmuller, G. Fierlbeck, and C. A. Klein. Immunomagnetic enrichment, genomic characterization, and prognostic impact of circulating melanoma cells. *Proc Natl Acad Sci USA*, 10(2):531–537, Jan 2004.

[37] T. E. Witzig, B. Bossy, T. Kimlinger, P. C. Roche, J. N. Ingle, C. Grant, J. Donohue, V. J. Suman, D. Harrington, J. Torre-Bueno, and K. D. Bauer. Detection of circulating cytokeratin-positive cells in the blood of breast cancer patients using immunomagnetic enrichment and digital microscopy. *Clin Cancer Res*, 8(5):1085–1091, May 2002.

[38] Y. L. Zheng, N. P. Carter, C. M. Price, S. M. Colman, P. J. Milton, G. A. Hackett, M. F. Greaves, and M. A. Ferguson-Smith. Prenatal diagnosis from maternal blood: simultaneous immunophenotyping and FISH of fetal nucleated erythrocytes isolated by negative magnetic cell sorting. *J Med Genet*, 30(12):1051–1056, Dec 1993.

[39] Y. Dong, A. M. Skelley, K. D. Merdek, K. M. Sprott, C. Jiang, W. E. Pierceall, J. Lin, M. Stocum, W. P. Carney, and D. A. Smirnov. Microfluidics and circulating tumor cells. *J Mol Diagn*, 15(2):149–157, Mar 2013.

[40] S. Riethdorf, H. Fritsche, V. Muller, T. Rau, C. Schindlbeck, B. Rack, W. Janni, C. Coith, K. Beck, F. Janicke, S. Jackson, T. Gornet, M. Cristofanilli, and K. Pantel. Detection of circulating tumor cells in peripheral blood of patients with metastatic breast cancer: a validation study of the CellSearch system. *Clin Cancer Res*, 13(3):920–928, Feb 2007.

[41] M. Ilie, E. Long, V. Hofman, E. Selva, C. Bonnetaud, J. Boyer, N. Venissac, C. Sanfiorenzo, B. Ferrua, C. H. Marquette, J. Mouroux, and P. Hofman. Clinical value of circulating endothelial cells and of soluble CD146 levels in patients undergoing surgery for non-small cell lung cancer. *Br J Cancer*, 110(5):1236–1243, Mar 2014.

[42] H. Lodish, A. Berk, S.L. Zipursky, P. Matsudaira, D.d Baltimore, and J. Darnell. Purification of Cells and Their Parts. In *Molecular Cell Biology*, chapter 5. W. H. Freeman, New York, 4 edition, 2000.

[43] J. Warrick, B. Casavant, M. Frisk, and D. Beebe. A microfluidic cell concentrator. *Anal Chem*, 82(19):8320–8326, Oct 2010.

[44] M.K. Brakke. Density Gradient Centrifugation: A New Separation Technique. *J Am Chem Soc*, 73(4):1847–1848, apr 1951.

[45] N. Gerges, J. Rak, and N. Jabado. New technologies for the detection of circulating tumour cells. *Br Med Bull*, 94:49–64, 2010.

[46] D.I.C. Wang, T.J. Sinskey, R.E. Gerner, and R.P. De Filippi. Effect of centrifugation on the viability of Burkitt lymphoma cells. *Biotechnol Bioeng*, 10(5):641–649, sep 1968.

[47] J. Yang, W. C. Hooper, D. J. Phillips, M. L. Tondella, and D. F. Talkington. Centrifugation of human lung epithelial carcinoma a549 cells up-regulates interleukin-1beta gene expression. *Clin Diagn Lab Immunol*, 9(5):1142–1143, Sep 2002.

[48] S. T. Wortham, G. A. Ortolano, and B. Wenz. A brief history of blood filtration: clot screens, microaggregate removal, and leukocyte reduction. *Transfus Med Rev*, 17(3):216–222, Jul 2003.

[49] T. Xu, B. Lu, Y. C. Tai, and A. Goldkorn. A cancer detection platform which measures telomerase activity from live circulating tumor cells captured on a microfilter. *Cancer Res*, 70(16):6420–6426, Aug 2010.

[50] D. R. Gossett, W. M. Weaver, A. J. Mach, S. C. Hur, H. T. Tse, W. Lee, H. Amini, and D. Di Carlo. Label-free cell separation and sorting in microfluidic systems. *Anal Bioanal Chem*, 397(8):3249–3267, Aug 2010.

[51] D. Lee, P. Sukumar, A. Mahyuddin, M. Choolani, and G. Xu. Separation of model mixtures of epsilon-globin positive fetal nucleated red blood cells and anucleate erythrocytes using a microfluidic device. *J Chromatogr A*, 1217(11):1862–1866, Mar 2010.

[52] S. Zheng, H. K. Lin, B. Lu, A. Williams, R. Datar, R. J. Cote, and Y. C. Tai. 3D microfilter device for viable circulating tumor cell (CTC) enrichment from blood. *Biomed Microdevices*, 13(1):203–213, Feb 2011.

[53] H. M. Ji, V. Samper, Y. Chen, C. K. Heng, T. M. Lim, and L. Yobas. Silicon-based microfilters for whole blood cell separation. *Biomed Microdevices*, 10(2):251–257, Apr 2008.

[54] S. J. Tan, L. Yobas, G. Y. Lee, C. N. Ong, and C. T. Lim. Microdevice for the isolation and enumeration of cancer cells from blood. *Biomed Microdevices*, 11(4):883–892, Aug 2009.

[55] H. W. Hou, A. A. Bhagat, A. G. Chong, P. Mao, K. S. Tan, J. Han, and C. T. Lim. Deformability based cell margination–a simple microfluidic design for malaria-infected erythrocyte separation. *Lab Chip*, 10(19):2605–2613, Oct 2010.

[56] L. R. Huang, E. C. Cox, R. H. Austin, and J. C. Sturm. Continuous particle separation through deterministic lateral displacement. *Science*, 304(5673):987–990, May 2004.

[57] J. McGrath, M. Jimenez, and H. Bridle. Deterministic lateral displacement for particle separation: a review. *Lab Chip*, 14(21):4139–4158, Nov 2014.

[58] R. Huang, T. A. Barber, M. A. Schmidt, R. G. Tompkins, M. Toner, D. W. Bianchi, R. Kapur, and W. L. Flejter. A microfluidics approach for the isolation of nucleated red blood cells (NRBCs) from the peripheral blood of pregnant women. *Prenat Diagn*, 28(10):892–899, Oct 2008.

[59] E. Ozkumur, A. M. Shah, J. C. Ciciliano, B. L. Emmink, D. T. Miyamoto, E. Brachtel, M. Yu, P. I. Chen, B. Morgan, J. Trautwein, A. Kimura, S. Sengupta, S. L. Stott, N. M. Karabacak, T. A. Barber, J. R. Walsh, K. Smith, P. S. Spuhler, J. P. Sullivan, R. J. Lee, D. T. Ting, X. Luo, A. T. Shaw, A. Bardia, L. V. Sequist, D. N. Louis, S. Maheswaran, R. Kapur, D. A. Haber, and M. Toner. Inertial focusing for tumor antigen-dependent and -independent sorting of rare circulating tumor cells. *Sci Transl Med*, 5(179):179ra47, Apr 2013.

[60] J. P. Beech and J. O. Tegenfeldt. Tuneable separation in elastomeric microfluidics devices. *Lab Chip*, 8(5):657–659, May 2008.

[61] K. Loutherback, J. D'Silva, L. Liu, A. Wu, R. H. Austin, and J. C. Sturm. Deterministic separation of cancer cells from blood at 10 mL/min. *AIP Adv*, 2(4):42107, Dec 2012.

[62] N. M. Karabacak, P. S. Spuhler, F. Fachin, E. J. Lim, V. Pai, E. Ozkumur, J. M. Martel, N. Kojic, K. Smith, P. I. Chen, J. Yang, H. Hwang, B. Morgan, J. Trautwein, T. A. Barber, S. L. Stott, S. Maheswaran, R. Kapur, D. A. Haber, and M. Toner. Microfluidic, marker-free isolation of circulating tumor cells from blood samples. *Nat Protoc*, 9(3):694–710, Mar 2014.

[63] U. Dharmasiri, S. Balamurugan, A. A. Adams, P. I. Okagbare, A. Obubuafo, and S. A. Soper. Highly efficient capture and enumeration of low abundance prostate cancer cells using prostate-specific membrane antigen aptamers immobilized to a polymeric microfluidic device. *Electrophoresis*, 30(18):3289–3300, Sep 2009.

[64] J. P. Gleghorn, E. D. Pratt, D. Denning, H. Liu, N. H. Bander, S. T. Tagawa, D. M. Nanus, P. A. Giannakakou, and B. J. Kirby. Capture of circulating tumor cells from whole blood of prostate cancer patients using geometrically enhanced differential immunocapture (GEDI) and a prostate-specific antibody. *Lab Chip*, 10(1):27–29, Jan 2010.

[65] A. D. Hughes and M. R. King. Use of naturally occurring halloysite nanotubes for enhanced capture of flowing cells. *Langmuir*, 26(14):12155–12164, Jul 2010.

[66] S. Mittal, I. Y. Wong, W. M. Deen, and M. Toner. Antibody-functionalized fluid-permeable surfaces for rolling cell capture at high flow rates. *Biophys J*, 102(4):721–730, Feb 2012.

[67] S. Wang, K. Liu, J. Liu, Z. T. Yu, X. Xu, L. Zhao, T. Lee, E. K. Lee, J. Reiss, Y. K. Lee, L. W. Chung, J. Huang, M. Rettig, D. Seligson, K. N. Duraiswamy, C. K. Shen, and H. R. Tseng. Highly efficient capture of circulating tumor cells by using nanostructured silicon substrates with integrated chaotic micromixers. *Angew Chem Int Ed Engl*, 50(13):3084–3088, Mar 2011.

[68] Y. Xu, J. A. Phillips, J. Yan, Q. Li, Z. H. Fan, and W. Tan. Aptamer-based microfluidic device for enrichment, sorting, and detection of multiple cancer cells. *Anal Chem*, 81(17):7436–7442, Sep 2009.

[69] A. A. Adams, P. I. Okagbare, J. Feng, M. L. Hupert, D. Patterson, J. Gottert, R. L. McCarley, D. Nikitopoulos, M. C. Murphy, and S. A. Soper. Highly efficient circulating tumor cell isolation from whole blood and label-free enumeration using polymer-based microfluidics with an integrated conductivity sensor. *J Am Chem Soc*, 130(27):8633–8641, Jul 2008.

[70] S. Nagrath, L. V. Sequist, S. Maheswaran, D. W. Bell, D. Irimia, L. Ulkus, M. R. Smith, E. L. Kwak, S. Digumarthy, A. Muzikansky, P. Ryan, U. J. Balis, R. G. Tompkins, D. A. Haber, and M. Toner. Isolation of rare circulating tumour cells in cancer patients by microchip technology. *Nature*, 450(7173):1235–1239, Dec 2007.

[71] S. L. Stott, C. H. Hsu, D. I. Tsukrov, M. Yu, D. T. Miyamoto, B. A. Waltman, S. M. Rothenberg, A. M. Shah, M. E. Smas, G. K. Korir, F. P. Floyd, A. J. Gilman, J. B. Lord, D. Winokur, S. Springer, D. Irimia, S. Nagrath, L. V. Sequist, R. J. Lee, K. J. Isselbacher, S. Maheswaran, D. A. Haber, and M. Toner. Isolation of circulating tumor cells using a microvortex-generating herringbone-chip. *Proc Natl Acad Sci USA*, 107(43):18392–18397, Oct 2010.

[72] H. Amini, W. Lee, and D. Di Carlo. Inertial microfluidic physics. *Lab Chip*, 14(15):2739–2761, Aug 2014.

[73] D. Di Carlo. Inertial microfluidics. *Lab Chip*, 9(21):3038–3046, Nov 2009.

[74] S.C Hur, S-E. Choi, S Kwon, and D. Di Carlo. Inertial focusing of non-spherical microparticles. *Appl Phys Lett*, 99(4):044101, jul 2011.

[75] S. C. Hur, N. K. Henderson-MacLennan, E. R. McCabe, and D. Di Carlo. Deformability-based cell classification and enrichment using inertial microfluidics. *Lab Chip*, 11(5):912–920, Mar 2011.

[76] A. A. Bhagat, H. W. Hou, L. D. Li, C. T. Lim, and J. Han. Pinched flow coupled shear-modulated inertial microfluidics for high-throughput rare blood cell separation. *Lab Chip*, 11(11):1870–1878, Jun 2011.

[77] A. J. Mach, J. H. Kim, A. Arshi, S. C. Hur, and D. Di Carlo. Automated cellular sample preparation using a Centrifuge-on-a-Chip. *Lab Chip*, 11(17):2827–2834, Sep 2011.

[78] V. Parichehreh, K. Medepallai, K. Babbarwal, and P. Sethu. Microfluidic inertia enhanced phase partitioning for enriching nucleated cell populations in blood. *Lab Chip*, 13(5):892–900, Mar 2013.

[79] A. J. Mach and D. Di Carlo. Continuous scalable blood filtration device using inertial microfluidics. *Biotechnol Bioeng*, 107(2):302–311, Oct 2010.

[80] Z. Wu, B. Willing, J. Bjerketorp, J. K. Jansson, and K. Hjort. Soft inertial microfluidics for high throughput separation of bacteria from human blood cells. *Lab Chip*, 9(9):1193–1199, May 2009.

[81] S. C. Hur, A. J. Mach, and D. Di Carlo. High-throughput size-based rare cell enrichment using microscale vortices. *Biomicrofluidics*, 5(2):22206, Jun 2011.

[82] B. L. Khoo, M. E. Warkiani, D. S. Tan, A. A. Bhagat, D. Irwin, D. P. Lau, A. S. Lim, K. H. Lim, S. S. Krisna, W. T. Lim, Y. S. Yap, S. C. Lee, R. A. Soo, J. Han, and C. T. Lim. Clinical validation of an ultra high-throughput spiral microfluidics for the detection and enrichment of viable circulating tumor cells. *PLoS ONE*, 9(7):e99409, 2014.

[83] M. E. Warkiani, G. Guan, K. B. Luan, W. C. Lee, A. A. Bhagat, P. K. Chaudhuri, D. S. Tan, W. T. Lim, S. C. Lee, P. C. Chen, C. T. Lim, and J. Han. Slanted spiral microfluidics for the ultra-fast, label-free isolation of circulating tumor cells. *Lab Chip*, 14(1):128–137, Jan 2014.

[84] B. Roda, A. Zattoni, P. Reschiglian, M. H. Moon, M. Mirasoli, E. Michelini, and A. Roda. Field-flow fractionation in bioanalysis: A review of recent trends. *Anal Chim Acta*, 635(2):132–143, Mar 2009.

[85] S. Shim, K. Stemke-Hale, A. M. Tsimberidou, J. Noshari, T. E. Anderson, and P. R. Gascoyne. Antibody-independent isolation of circulating tumor cells by continuous-flow dielectrophoresis. *Biomicrofluidics*, 7(1):11807, 2013.

[86] H. W. Hou, M. E. Warkiani, B. L. Khoo, Z. R. Li, R. A. Soo, D. S. Tan, W. T. Lim, J. Han, A. A. Bhagat, and C. T. Lim. Isolation and retrieval of circulating tumor cells using centrifugal forces. *Sci Rep*, 3:1259, 2013.

[87] N. Pamme and C. Wilhelm. Continuous sorting of magnetic cells via on-chip free-flow magnetophoresis. *Lab Chip*, 6(8):974–980, Aug 2006.

[88] M. Zborowski, G. R. Ostera, L. R. Moore, S. Milliron, J. J. Chalmers, and A. N. Schechter. Red blood cell magnetophoresis. *Biophys J*, 84(4):2638–2645, Apr 2003.

[89] K. Hoshino, Y. Y. Huang, N. Lane, M. Huebschman, J. W. Uhr, E. P. Frenkel, and X. Zhang. Microchip-based immunomagnetic detection of circulating tumor cells. *Lab Chip*, 11(20):3449–3457, Oct 2011.

[90] P. Grodzinski, J. Yang, R.H. Liu, and M. D. Ward. A modular microfluidic system for cell pre-concentration and genetic sample preparation. *Biomed Microdevices*, 5(4):303–310, 2003.

[91] N. Pamme and A. Manz. On-chip free-flow magnetophoresis: continuous flow separation of magnetic particles and agglomerates. *Anal Chem*, 76(24):7250–7256, Dec 2004.

[92] N. Xia, T. P. Hunt, B. T. Mayers, E. Alsberg, G. M. Whitesides, R. M. Westervelt, and D. E. Ingber. Combined microfluidic-micromagnetic separation of living cells in continuous flow. *Biomed Microdevices*, 8(4):299–308, Dec 2006.

[93] C. W. Yung, J. Fiering, A. J. Mueller, and D. E. Ingber. Micromagnetic-microfluidic blood cleansing device. *Lab Chip*, 9(9):1171–1177, May 2009.

[94] B. D. Plouffe, M. Mahalanabis, L. H. Lewis, C. M. Klapperich, and S. K. Murthy. Clinically relevant microfluidic magnetophoretic isolation of rare-cell populations for diagnostic and therapeutic monitoring applications. *Anal Chem*, 84(3):1336–1344, Feb 2012.

[95] J. D. Adams, U. Kim, and H. T. Soh. Multitarget magnetic activated cell sorter. *Proc Natl Acad Sci USA*, 105(47):18165–18170, Nov 2008.

[96] P. Augustsson, C. Magnusson, M. Nordin, H. Lilja, and T. Laurell. Microfluidic, label-free enrichment of prostate cancer cells in blood based on acoustophoresis. *Anal Chem*, 84(18):7954–7962, Sep 2012.

[97] I. Iranmanesh, A. Ramachandraiah, H.and Russom, and M. Wiklund. On-chip ultrasonic sample preparation for cell based assays. *RSC Adv*, 5(91):74304–74311, sep 2015.

[98] J.J. Hawkes and W.T Coakley. A continuous flow ultrasonic cell-filtering method. *Enzyme Microb Technol*, 19(1):57–62, 1996.

[99] O. Jakobsson, S. S. Oh, M. Antfolk, M. Eisenstein, T. Laurell, and H. T. Soh. Thousand-fold volumetric concentration of live cells with a recirculating acoustofluidic device. *Anal Chem*, 87(16):8497–8502, Aug 2015.

[100] Y. Ai, C. K. Sanders, and B. L. Marrone. Separation of Escherichia coli bacteria from peripheral blood mononuclear cells using standing surface acoustic waves. *Anal Chem*, 85(19):9126–9134, Oct 2013.

[101] P. Li, Z. Mao, Z. Peng, L. Zhou, Y. Chen, P. H. Huang, C. I. Truica, J. J. Drabick, W. S. El-Deiry, M. Dao, S. Suresh, and T. J. Huang. Acoustic separation of circulating tumor cells. *Proc Natl Acad Sci USA*, 112(16):4970–4975, Apr 2015.

[102] B. Hammarström, T. Laurell, and J. Nilsson. Seed particle-enabled acoustic trapping of bacteria and nanoparticles in continuous flow systems. *Lab Chip*, 12(21):4296–4304, Nov 2012.

[103] Z. Gagnon and H. C. Chang. Aligning fast alternating current electroosmotic flow fields and characteristic frequencies with dielectrophoretic traps to achieve rapid bacteria detection. *Electrophoresis*, 26(19):3725–3737, Oct 2005.

[104] J. Voldman. Electrical forces for microscale cell manipulation. *Annu Rev Biomed Eng*, 8:425–454, 2006.

[105] T. Braschler, N. Demierre, E. Nascimento, T. Silva, A. G. Oliva, and P. Renaud. Continuous separation of cells by balanced dielectrophoretic forces at multiple frequencies. *Lab Chip*, 8(2):280–286, Feb 2008.

[106] F. F. Becker, X. B. Wang, Y. Huang, R. Pethig, J. Vykoukal, and P. R. Gascoyne. Separation of human breast cancer cells from blood by differential dielectric affinity. *Proc Natl Acad Sci USA*, 92(3):860–864, Jan 1995.

[107] H. Moncada-Hernández and B. H. Lapizco-Encinas. Simultaneous concentration and separation of microorganisms: insulator-based dielectrophoretic approach. *Anal Bioanal Chem*, 396(5):1805–1816, Mar 2010.

[108] G. M. Whitesides. The origins and the future of microfluidics. *Nature*, 442(7101):368–373, Jul 2006.

[109] H. Bruus. Acoustofluidics 1: Governing equations in microfluidics. *Lab Chip*, 11(22):3742–3751, Nov 2011.

[110] J. Atencia and D. J. Beebe. Controlled microfluidic interfaces. *Nature*, 437(7059):648–655, Sep 2005.

[111] D. B. Weibel, M. Kruithof, S. Potenta, S. K. Sia, A. Lee, and G. M. Whitesides. Torque-actuated valves for microfluidics. *Anal Chem*, 77(15):4726–4733, Aug 2005.

[112] L.V. King. On the Acoustic Radiation Pressure on Spheres.pdf.

[113] K. Yosioka and Y. Kawasima. Acoustic radiation pressure on a compressible sphere. *Acustica*, 5:167–173, 1955.

[114] L P Gor'kov. On the forces acting on a small particle in an acoustical field in an ideal fluid. *Soviet Physics Doklady*, 6(9):773–775, 1962.

[115] W. L. Nyborg. Radiation pressure on a small rigid sphere. *J Acoust Soc Am*, 42(5):947–952, 1967.

[116] P. Augustsson, R. Barnkob, S. T. Wereley, H. Bruus, and T. Laurell. Automated and temperature-controlled micro-PIV measurements enabling long-term-stable microchannel acoustophoresis characterization. *Lab Chip*, 11(24):4152–4164, Dec 2011.

[117] C. Grenvall, C. Magnusson, H. Lilja, and T. Laurell. Concurrent isolation of lymphocytes and granulocytes using prefocused free flow acoustophoresis. *Anal Chem*, 87(11):5596–5604, Jun 2015.

[118] T. Laurell, F. Petersson, and A. Nilsson. Chip integrated strategies for acoustic separation and manipulation of cells and particles. *Chem Soc Rev*, 36(3):492–506, Mar 2007.

[119] F. Petersson, L. Aberg, A. M. Sward-Nilsson, and T. Laurell. Free flow acoustophoresis: microfluidic-based mode of particle and cell separation. *Anal Chem*, 79(14):5117–5123, Jul 2007.

[120] M. Nordin and T. Laurell. Two-hundredfold volume concentration of dilute cell and particle suspensions using chip integrated multistage acoustophoresis. *Lab Chip*, 12(22):4610–4616, Nov 2012.

[121] M. Wiklund, R. Green, and M. Ohlin. Acoustofluidics 14: Applications of acoustic streaming in microfluidic devices. *Lab Chip*, 12(14):2438–2451, Jul 2012.

[122] Lord Rayleigh. On the circulation of air observed in Kundt's tubes, and on some allied acoustical problems. *Philos Trans R Soc Lond*, 175:1–21, jul 1884.

[123] H. Schlichting. Berechnung obener periodischer Grenzschichtströmungen. *Physik Z*, 33:327–335, 1932.

[124] W.L. Nyborg. Acoustic Streaming near a Boundary. *J Acoust Soc Am*, 30(4):329, jun 1958.

[125] M. F. Hamilton, Y. A. Ilinskii, and E. A. Zabolotskaya. Acoustic streaming generated by standing waves in two-dimensional channels of arbitrary width. *J Acoust Soc Am*, 113(1):153–160, Jan 2003.

[126] P. B. Muller, M. Rossi, A. G. Marin, R. Barnkob, P. Augustsson, T. Laurell, C. J. Kahler, and H. Bruus. Ultrasound-induced acoustophoretic motion of microparticles in three dimensions. *Phys Rev E Stat Nonlin Soft Matter Phys*, 88(2):023006, Aug 2013.

[127] R. Barnkob, P. Augustsson, T. Laurell, and H. Bruus. Acoustic radiation- and streaming-induced microparticle velocities determined by microparticle image velocimetry in an ultrasound symmetry plane. *Phys Rev E Stat Nonlin Soft Matter Phys*, 86(5 Pt 2):056307, Nov 2012.

[128] P. B. Muller, R. Barnkob, M. J. Jensen, and H. Bruus. A numerical study of microparticle acoustophoresis driven by acoustic radiation forces and streaming-induced drag forces. *Lab Chip*, 12(22):4617–4627, Nov 2012.

[129] M. Antfolk, P. B. Muller, P. Augustsson, H. Bruus, and T. Laurell. Focusing of sub-micrometer particles and bacteria enabled by two-dimensional acoustophoresis. *Lab Chip*, 14(15):2791–2799, Aug 2014.

[130] M. Evander, A. Lenshof, T. Laurell, and J. Nilsson. Acoustophoresis in wet-etched glass chips. *Anal Chem*, 80(13):5178–5185, Jul 2008.

[131] I. González, M. Tijero, A. Martin, V. Acosta, J. Berganzo, A. Castillejo, M. Bouali, and J. Soto. Optimizing Polymer Lab-on-Chip Platforms for Ultrasonic Manipulation: Influence of the Substrate. *Micromachines*, 6(5):574–591, may 2015.

[132] M. Antfolk, C. Antfolk, H. Lilja, T. Laurell, and P. Augustsson. A single inlet two-stage acoustophoresis chip enabling tumor cell enrichment from white blood cells. *Lab Chip*, 15(9):2102–2109, May 2015.

[133] M. Antfolk, C. Magnusson, P. Augustsson, H. Lilja, and T. Laurell. Acoustofluidic, Label-Free Separation and Simultaneous Concentration of Rare Tumor Cells from White Blood Cells. *Anal Chem*, 87(18):9322–9328, Sep 2015.

[134] S. H. Kim, M. Antfolk, M. Kobayashi, S. Kaneda, T. Laurell, and T. Fujii. Highly efficient single cell arraying by integrating acoustophoretic cell pre-concentration and dielectrophoretic cell trapping. *Lab Chip*, 15(22):4356–4363, Oct 2015.

Paper I

Two-hundredfold volume concentration of dilute cell and particles suspensions using chip integrated multistage acoustophoresis

Maria Nordin, and Thomas Laurell

Lab on a Chip, 2012, 12(22), 4610-4616.

Paper I

Lab on a Chip

Dynamic Article Links

Cite this: *Lab Chip*, 2012, **12**, 4610–4616

www.rsc.org/loc

PAPER

Two-hundredfold volume concentration of dilute cell and particle suspensions using chip integrated multistage acoustophoresis†

Maria Nordin*[a] and Thomas Laurell*[ab]

Received 31st May 2012, Accepted 9th August 2012
DOI: 10.1039/c2lc40629b

Concentrating cells is a frequently performed step in cell biological assays and medical diagnostics. The commonly used centrifuge exhibits limitations when dealing with rare cell events and small sample volumes. Here, we present an acoustophoresis microfluidic chip utilising ultrasound to concentrate particles and cells into a smaller volume. The method is label-free, continuous and independent of suspending fluid, allowing for low cost and minimal preparation of the samples. Sequential concentration regions and two-dimensional acoustic standing wave focusing of cells and particles were found critical to accomplish concentration factors beyond one hundred times. Microparticles (5 μm in diameter) used to characterize the system were concentrated up to 194.2 ± 9.6 times with a recovery of 97.1 ± 4.8%. Red blood cells and prostate cancer cells were concentrated 145.0 ± 5.0 times and 195.7 ± 36.2 times, respectively, with recoveries of 97.2 ± 3.3% and 97.9 ± 18.1%. The data demonstrate that acoustophoresis is an effective technique for continuous flow-based concentration of cells and particles, offering a much needed intermediate step between sorting and detection of rare cell samples in lab-on-a-chip systems.

Introduction

Concentrating rare cells or dilute cell samples is a critical step in bioanalysis and cell biology. Low concentration microorganisms or rare cells associated with various diseases, such as bacteria in bacteraemia[1] or circulating tumour cells[2] often require concentration before detection and identification. This crucial step can mean the difference between a positive or negative diagnostic readout. Assessment of water and food quality[3] can also pose challenges in terms of sample concentration, where contaminating cells often are low in numbers.

Centrifugation is the most widely used method for concentrating samples. However, this technique suffers from drawbacks, especially in combination with low cell numbers or small liquid volumes.[4] Concentration of low cell numbers will require small re-suspension volumes that are not practically possible to handle in ordinary centrifugation systems. Furthermore, centrifugation of low cell numbers will increase the risk of substantial sample losses if the sample forms a pellet that is too small to be seen or if no pellet forms at all. Centrifugation may also have an effect on cell viability[5] and function,[6] which in the end can bias readouts. When combined with lab-on-a-chip applications, where small volumes often are the end product, the centrifuge may not be a suitable option.

Microfluidic-based and lab-on-a-chip concentrating systems provide potential solutions to the problems inherent in the use of centrifugation. Microfluidic systems make it possible to handle samples in a continuous mode, without restricting sample volumes, as large volumes may have to be processed in order to collect a sufficient number of cells from highly dilute samples. As opposed to most macroscale systems, they also offer the possibility of handling samples in a closed environment. This allows for concentration of rare cells for transplantation or cell culture, without exposing them to the same contamination risks as *e.g.* ordinary centrifugation or FACS based cell processing would.

Possibilities for concentration in microfluidic systems have previously been studied. Reported methods include the use of gravity,[4] hydrodynamic forces,[7,8] electrical forces,[9–14] magnetic forces[15] and acoustophoresis-enhanced sedimentation.[16] The results obtained using these methods are summarised in Table 1. It can be seen that there is a lack of systems yielding high concentration factors while maintaining a high recovery and throughput.

This paper presents a high-throughput acoustophoresis microfluidic chip, capable of achieving concentration factors for cells and particles of up to two hundred times with minimal losses. The chip utilises ultrasound standing wave forces to focus cells and particles, in two dimensions, in a confined liquid volume in the micro-channel centre. Cells and particles are focused by the primary acoustic radiation force in two

[a]*Dept. Measurement Technology and Industrial Electrical Engineering, Div. Nanobiotechnology, Lund University, Lund, Sweden. E-mail: maria.nordin@elmat.lth.se*
[b]*Dept. Biomedical Engineering, Dongguk University, Seoul, South Korea. E-mail: thomas.laurell@elmat.lth.se*
† Electronic supplementary information (ESI) available. See DOI: 10.1039/c2lc40629b

Table 1 Summary of primary results obtained on concentration in microfluidic systems

Method	Particle/cell	Initial concentration (mL^{-1})	Sample inflow rate ($\mu L\ min^{-1}$)	Concentration factor	Recovery/ Efficiency (%)	Comment	Reference
Gravity	LNCaP	$5*10^5$	Max 8	9.7	98.9 ± 0.2		4
Microvortices	MCF-7	250	4400	20	20		7
Hydrodynamic	1–3 μm polymer bead	$1.8*10^7$, $4.7*10^6$ and $6.8*10^6$, respectively	0.5	63–80	67–90		8
Electrostatic trapping	*Salmonella*	10^6 CFU	100	14.2	85.2		9
Zone electrophoresis Isoelectric focusing	*E. herbicola*	NA	4.98	NA	NA	Needs specific buffer	10
Dielectrophoretic trapping	HeLa	$5*10^5$	0	NA	76	Needs specific buffer	11
Ion concentration polarization	RBC *E. coli*	200–500 times dilute of whole blood	Max 5	19 and 20, respectively	100	Needs specific buffer	12
Dielectrophoretic trapping	*E. coli* *S. Cerevisiae*	$6*10^8$ $6*10^6$	NA	88.1 and 23.14, respectively (in the trap)	NA	Needs specific buffer	13
Free flow electrophoresis	*E. coli*	$5*10^4$ CFU	15	53.57	87.06	Needs specific buffer	14
Immunomagnetic trapping	*E. coli*	$1*10^3$	200[a]	NA	82	Needs antibody-labeled magnetic beads	15
Acoustophoresis-enchanced sedimentation	*S. cerevisiae*	$7.2*10^9$	4800	5	98.5		16

[a] The input flow rate is not given, but rather the total flow rate of sample solution and capture solution.

dimensions, according to their intrinsic properties size, density and compressibility.[17–22] Acoustophoresis is a label-free method, allowing for low cost and minimal sample preparation. In addition, the ultrasound has previously been shown to be gentle to cells.[23–26] The continuous flow mode makes it possible to achieve concentration factors of several orders of magnitude of dilute samples, and the method can be used independently of suspending fluid. Furthermore, the continuous flow processing makes it suitable for integration with downstream unit operations, providing a much needed intermediate step, *e.g.* between sorting and detection of rare cell samples in microfluidic chips.

Material and methods

Microfabrication

The silicon chip was fabricated using photolithography and anisotropic wet etching in KOH (40 g/100 mL H_20, 80 °C). Holes for inlets and outlets were drilled in the silicon using a diamond drill. The chip was sealed by anodic bonding of a glass lid. For more detail on the chip fabrication see.[20]

Device design

The chip was composed of one inlet and one or two trifurcation outlet regions connected by a straight channel allowing cells and particles to become acoustically focused between each outlet region (Fig. 1). The focusing channel was 375 μm wide and 160 μm deep and the channel lengths between each outlet region were 30 and 5 mm, respectively. The channel width and height corresponded to half a wavelength of ultrasound at 1.99 MHz and 4.68 MHz. The chip was actuated using piezoceramic transducers (PZ26, Ferroperm piezoceramics, Kvistgaard, Denmark) resonant at 2 MHz and 5 MHz. The 2 MHz piezo was attached by cyanoacrylate glue (Loctite Super glue, Henkel Norden AB, Stockholm, Sweden) to the glass lid covering the entire length and a third of the width of the chip. The 5 MHz piezo was attached to the silicon back of the chip covering the space between the inlet and the first outlet region. In order to keep settings identical in the experiments with one and two trifurcated outlet regions, the same chip was used for both configurations. In the one outlet region configuration the unused outlets on the chip were sealed (Fig. 1a).

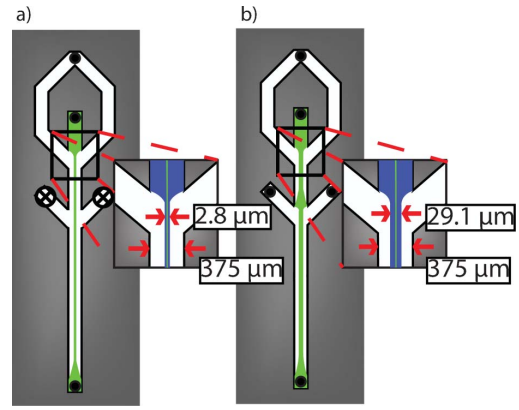

Fig. 1 Chip configurations. a) The one outlet region system. The unused, sealed outlets are indicated by a black cross. b) The two outlet regions system. The green lines illustrate particles focusing in the channel. In the two outlet regions system the particles will have to re-focus after the first outlet region. The insert drawings illustrate the maximum allowed width of the critical centre fraction of the input flow (blue) that must contain the focused particles for these to all be collected in the centre outlet. Insert numbers indicate the minimum allowed width of this fraction when doing 100 times concentration in both systems. The total channel width, 375 μm is also indicated.

Instrumental setup

The two transducers were actuated using power amplifiers (width actuation: Amplifier Research 75A250A, Souderton, PA, USA; depth actuation: an in-house built circuit board with a power amplifier: LT1012, Linear Technology Corp., Milpitas, CA, USA). Two function generators (Agilent 33120A, Agilent technologies Inc. Santa Clara, CA, USA) were used. The applied voltage was monitored using an oscilloscope (TDS 210, Tektronix, UK Ltd., Bracknell, UK). Microscopy pictures and videos were generated using a Dino-Lite digital microscope (AM413T5 Dino-Lite Pro, AnMo Electronics Corporation, Hsinchu, Taiwan).

Experimental setup

The flow rates in the chip were controlled by connecting all the inlets and outlets to glass syringes (Hamilton Bonaduz AG, Bonaduz, Switzerland) mounted on syringe pumps (Nemesys, Cetoni GmbH, Korbussen, Germany). The inflow rate was, unless otherwise stated, set to 100 μL min^{-1} and the centre output flow rates were varied between 1–20 μL min^{-1} to achieve different concentration factors. An overview of the combined flow rate settings along with the results can be found in Supplementary Table 1–3. Samples were collected using a 2-position 3-port valve (MV201-C360, LabSmith, Livermore, CA, USA) connected in series with the last centre outlet. The sample collection system is illustrated in more detail in Supplementary Fig. 2. The collected 10 μL sample volumes were subsequently diluted to an appropriate volume, and counted in a Bürker chamber (Marienfeld, Lauda-Königshofen, Germany). To minimise possible measurement errors from sedimentation in the syringes, concentration factors were obtained by comparing samples collected with the ultrasound either on or off. The recovery values were obtained as the ratio between measured particle concentration and theoretical concentration at 100% recovery.

Microparticles

For characterizing the system, polystyrene particles (5 μm in diameter) (Fluka/Sigma-Aldrich, Buchs, Switzerland) were suspended in MilliQ H_2O and 0.002% Triton-X100 to a particle concentration of 0.02 wt% or 0.005 wt%. Particle and cell concentrations were deliberately kept relatively high, in terms of rare cells, to facilitate enumeration in the analytical step.

Confocal microscopy

Confocal microscopy was used to depict the distribution of microparticles when performing one- and two-dimensional focusing. Yellow fluorescent particles (4.1 μm in diameter) (Kisker GmbH, Steinfurt, Germany), suspended in MilliQ H_2O to a concentration of $1*10^6$ mL^{-1}, were used to obtain confocal images with an Olympus microscope (BX51WI, Olympus Corporation, Tokyo, Japan) and the Fluoview 300 software was subsequently used to reconstruct cross section images.

Red blood cells

Red blood cells were used as a model cell to further characterize the system. Blood samples were obtained from healthy volunteers at Lund University Hospital (Lund, Sweden). Whole blood was diluted 5000 times in PBS prior to concentration experiments.

Prostate cancer cells

The human prostate cancer cell line, DU145, was used as a model of circulating tumour cells. The cells were obtained from the American Type Tissue Collection and cultured according to their recommendations. Briefly, RPMI-1640 medium (Sigma-Aldrich, St Louis, MO, USA) was supplemented with 10% fetal bovine serum (Sigma-Aldrich, St Louis, MO, USA), 55 IU mL^{-1} penicillin and 55 μg mL^{-1} streptomycin (Sigma-Aldrich, St Louis, MO, USA). Cells were cultured at 37 °C in a humidified atmosphere containing 5% CO_2. $1*10^6$ cells mL^{-1} were used to

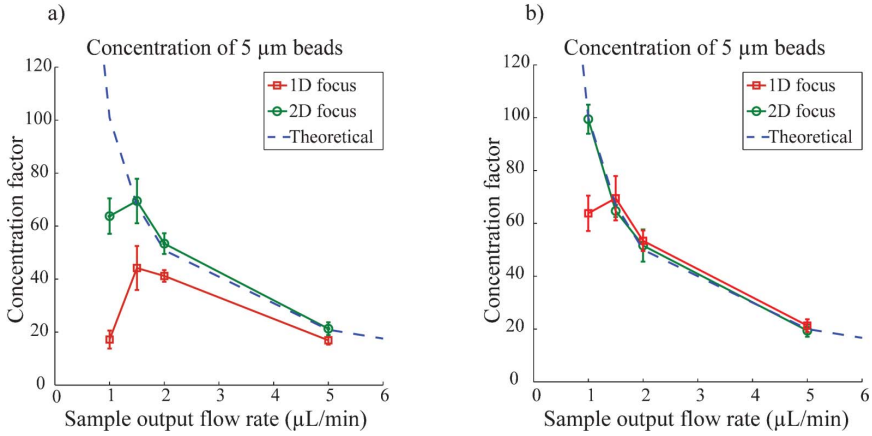

Fig. 2 Concentration of 5 μm diameter polystyrene particles for different sample output flow rates. a) Concentration using one trifurcation outlet region. b) Concentration using two trifurcation outlet regions. The error bars show the standard deviation, n = 3 (3 control and 3 concentrated samples). The input flow rate was maintained constant at 100 μL min^{-1}. The dashed line indicates the theoretical concentration factor at 100% recovery.

obtain the "ultrasound off" control samples. In the experiments assessing 100 and 200 times concentration, the cell input suspensions were diluted to $1*10^5$ cells mL^{-1} and $2.5*10^4$ cells mL^{-1}, respectively.

Results and discussion

In this paper we report on an acoustophoresis chip for several orders of magnitude concentration of cells and particles. The chip operates in a half wave length resonance mode and utilises ultrasonic standing wave forces, in two dimensions, to focus particles and cells in the acoustic pressure node located in the micro-channel centre.

Chip characterization

One-dimensional focusing. First, the concentration capacity using one trifurcation outlet region (Fig. 1a) was investigated, a design extensively used for acoustophoresis.[27] This set-up could concentrate 4.6 $\pm$ 1.1 and 9.0 $\pm$ 2.0 times with a recovery of 92 $\pm$ 22% and 90 $\pm$ 20%, respectively. However, when trying to achieve higher concentration factors, the recovery decreased rapidly. The highest concentration factor for this configuration, 44 $\pm$ 8.3 times with a recovery of 66 $\pm$ 12.4%, was obtained when trying to achieve a concentrate factor of 67 times. This corresponded to a sample output flow rate of 1.5 μL min^{-1} using a sample input flow rate of 100 μL min^{-1}. When trying to concentrate 100 times, *i.e.* lowering the sample output flow rate to 1 μL min^{-1}, a concentration factor of only 17.2 $\pm$ 3.4 was obtained, resulting in the corresponding recovery of 17.2 $\pm$ 3.4% (Fig. 2a).

There are two causes of the moderate performance of this set-up. The first is explained by the accuracy of the flow system. When trying to achieve high concentration factors, only a minute fraction of the total flow, containing all the particles, should be extracted *via* the centre outlet (*e.g.* 1% of the total flow for 100 times concentration). Given the Poiseuille flow profile, the width of this critical centre fraction that account for 1% of the total flow, is significantly smaller than 1% of the channel width, *i.e.* calculated to be 2.8 μm, when accounting for both the horizontal and the vertical contribution to the flow profile (Fig. 1.).

For the particles to enter the centre outlet they have to be focused within the critical centre fraction of the flow. The 5 μm diameter particles used are larger than the 2.8 μm critical centre fraction width, and consequently, a full recovery of particles under this condition was difficult to achieve. Not only would particles situated side by side in the channel be lost, but minor fluctuations in the flow moving the particle only about half a radius, 1.4 μm, to either side, would also contribute to reduced recovery. Likewise, when the critical centre fraction width was 5.7 μm wide, corresponding to 2% of the total flow, minor flow fluctuations would also have a large impact on the recovery. This partly explains the significantly reduced recovery seen for sample output flow rates between 1 and 2 μL min^{-1}, corresponding to 1 and 2% of the total flow using a total flow rate of 100 μL min^{-1} (Fig. 2a).

The second cause of the moderate performance, when trying to generate higher concentration factors, is found in a combination of the ultrasonic standing wave conditions and the flow system. In the outlet region, where the channel widens and the width no longer matches a single node ultrasound standing wave, an undefined acoustic field of undesired higher modes, not located in the channel centre, is present. As most of the particles pass in the rapid flow regime, there will not be sufficient time for the particles to be deflected from their original trajectory. However, particles positioned close to the top and bottom of the channel, where the flow velocity approaches zero, will spend much longer time in this undefined acoustic field and may thus be deflected from their original trajectory (Fig. 3a). Since the width of the critical centre fraction that exits through the centre outlet is narrow, a lateral displacement of a few micrometers will mean the difference between particles entering the centre outlet or escaping to the waste side outlets. Increasing the acoustic amplitude of the one-dimensional horizontal acoustic focus will not narrow the focused band further to allow the slow-moving particles to enter the centre outlet. In fact, this will counteract the purpose and rather increase the forces in the undefined acoustic field in the outlet region, causing even more particles to escape to the side outlets. The influence of the undesired standing wave node patterns in the outlet region is demonstrated in Fig. 4 and supplementary video 1, where the actuation amplitude was increased to emphasize the outlet region artefact. The undefined acoustic field separates the focused particles in several bands located at different channel depths. Particles closer to the top and bottom of the channel tend to escape to the sides and will eventually, with increased amplitude, also get temporarily trapped in local vortex-surrounded hot spots.

Two-dimensional focusing. The lateral particle migration caused by the undefined acoustic field in the outlet region can be prevented by applying a second vertical standing wave, orthogonal to the first one, resonating in the main focusing channel as well as the outlet regions. This will focus the particles in two dimensions. The two-dimensional focusing will position the particles in the faster moving flow regime in the channel centre (Fig. 3d), decreasing their retention time in the undefined acoustic field at the outlet region, and hence their lateral migration (Fig. 3b) (A comparison between one-dimensional and two-dimensional focusing can be seen in Fig. 3 and supplementary video 2.). With two-dimensional focusing, higher concentration factors could be achieved, and a concentration factor of 69 $\pm$ 8.4 times with the corresponding recovery of 103 $\pm$ 12.1% was obtained (Fig. 2a). However, it was still not possible to achieve a concentration factor of 100 times, as the critical centre fraction was too narrow to contain all the particles within the required 2.8 μm wide zone. The recovery values were obtained as the ratio between measured particle concentration and theoretical concentration at 100% recovery. Hence, a combination of a measurement inaccuracy and the fact that the concentration factors are dependent on an exact flow rate may yield mean recovery values above 100%.

Multiple outlet regions. In the single outlet region set-up, it is clear that the width of the critical centre fraction is the limiting factor for achieving high concentration factors. Collecting the sample from a wider centre fraction would, on the other hand, mean a lower concentration factor. A solution to this dilemma is to realise a system utilising sequential outlet regions, allowing a

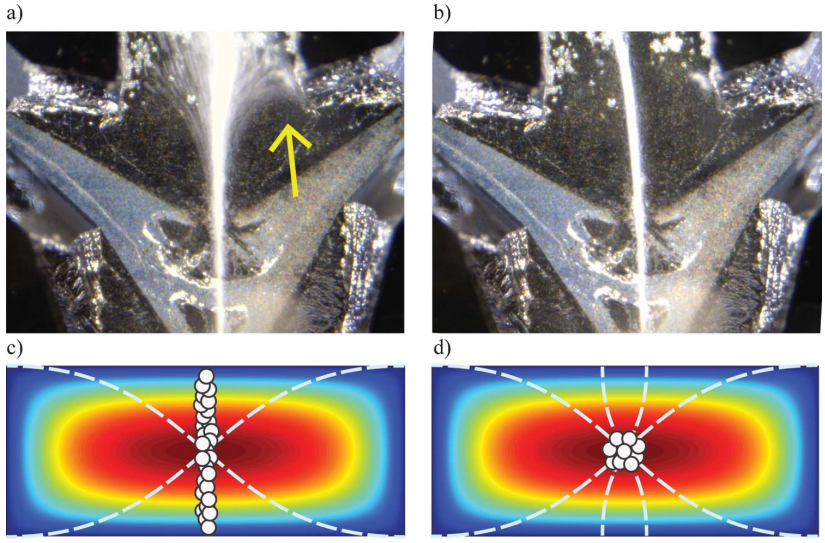

Fig. 3 a) Particles focused in one dimension in the last outlet region. The yellow arrow indicates escape of particles to the side outlet. b) Particles focused in two dimensions in the last outlet region. No escape of particles occurs. c) Schematic cross-section of the micro-channel showing particles focused in one dimension and their position within the Poiseuille flow profile. Red represents the fastest and blue the slowest moving fluid regime. The dashed lines indicate the ultrasound standing wave. d) Cross-section of the micro-channel showing particles focused in two dimensions and their position within the Poiseuille flow profile.

lower split flow rate ratio in each step. Although, each step only generates moderate concentration factors, in the end they will multiply to higher concentration factors. Importantly, the wider fluid fraction collected in the centre outlet allows for larger particle deviations from the original central flow trajectory, and hence a lower loss of cells or particles is ensured. For this reason a set-up with two sequential outlet regions was further studied.

Using the set-up with two sequential outlet regions substantially increased the obtainable concentration factors as predicted. The performances of both the one-dimensional and two-dimensional focusing systems displayed significant improvements. Using one-dimensional focusing and two outlet regions, a concentration factor of 67.4 ± 6.2 was obtained with a recovery of 100.6 ± 9.3% (Fig. 2b). The attempts of doing 100 times sample concentration resulted in a concentration factor of 52.7 ± 4.3 and a recovery of 52.7 ± 4.3%.

By using two-dimensional focusing in the multiple-outlet set-up, however, a sample concentration of 99.4 ± 5.5 times was accomplished with the corresponding recovery of 99.4 ± 5.5%. Based on these findings, the two-dimensional focusing system using two outlet regions was further investigated, and concentration factors up to 194.2 ± 9.6 times with a recovery of 97.1 ± 4.8% were obtained (Table 2).

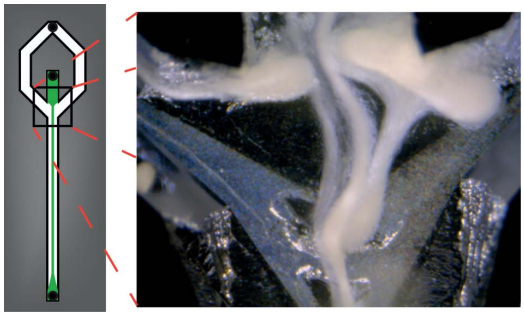

Fig. 4 The effect of the undesired standing wave node pattern, in the last outlet region, on particles focused in one dimension. The acoustic field separates the focused particle-band into several bands located at different channel depths, where the particles moving closer to the bottom and top of the channel become diverted to the side outlets or temporarily trapped in local hot spots surrounded by vortices.

Confocal microscopy

To demonstrate the effect of the two-dimensional acoustic focusing, confocal microscopy was used. The difference in one- and two-dimensional focusing can clearly be seen in Fig. 5. The magnification was limited to x20 in order to allow imaging of the entire channel cross section. This resulted in a confocal depth of

Table 2 Concentration of RBCs, DU145 and 5 μm diameter particles. Sample output flow rate was maintained constant at 1 μL min^{-1}. Errors indicate the standard deviation for n = 3 (3 control and 3 concentrated samples)

	Sample inflow rate (μL min^{-1})	Concentration factor	Recovery (%)
Red blood cells	100	100.7 ± 5.3	100.7 ± 5.3
	150	145.8 ± 5	97.2 ± 3.3
	200	181.1 ± 22.8	90.7 ± 11.4
DU145	100	98.9 ± 3.1	98.9 ± 3.1
	200	195.7 ± 36.2	97.9 ± 18.1
5 μm beads	200	194.2 ± 9.6	97.1 ± 4.8

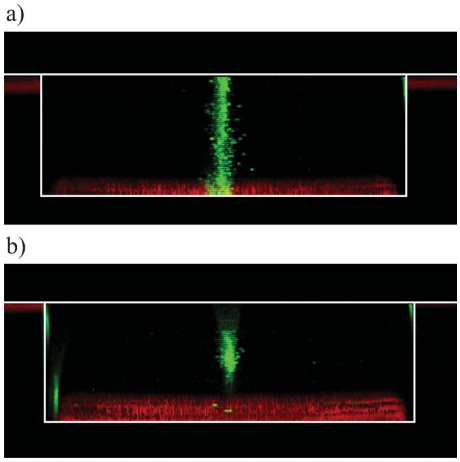

Fig. 5 Confocal images showing a cross-section of the micro-channel as indicated by the white square. a). Particles focused (green) in one dimension vertically. The channel bottom is viewed in red. b). Particles focused in two dimensions. The focused cluster appears longer in the height direction because of the confocal depth. This is illustrated by the elongated image of a stationary particle in the lower left corner of the flow channel. The confocal depth was about 20 μm.

about 20 μm, hence causing features in the images to appear longer, mostly in the vertical direction of the channel.[28] Consequently, the two-dimensionally focused particle cluster appeared more elongated than round (Fig. 5b and further illustrated in supplementary Fig. 1).

Red blood cell concentration

Highly diluted human red blood cells (RBCs) were used as a model system to study the abilities to concentrate live cells. A concentration factor of 145.8 ± 5.0 times with a recovery of 97.2 ± 3.3% (Table 2) was achieved when increasing the sample input flow rate to 150 μL min^{-1}, maintaining the sample output flow rate constant at 1 μL min^{-1}. Attempts to reach a concentration factor of 200 times by increasing the input flow rate to 200 μL min^{-1}, and maintaining the sample output flow rate of 1 μL min^{-1}, resulted in a reduced cell recovery of 90.7 ± 11.4% and a corresponding concentration factor of 181.1 ± 22.8. The reason for the increased loss of cells was visually confirmed to be attributed to an insufficient primary radiation force in the height direction of the channel. The reduced retention time in the channel caused by the increased total flow rate did thereby not allow all cells to focus vertically into the central acoustic pressure node, and thus some of the cells escaped to the side outlets in the region of the undefined acoustic field.

Prostate cancer cell concentration

The cell concentrator chip is intended for rare cell concentration, *e.g.* circulating tumour cells, as a step prior to on-chip analysis or cell culture. A prostate cancer cell line, DU145, was used as a model of circulating tumour cells. A maximum concentration factor of 195.7 ± 36.2 times with a recovery of 97.9 ± 18.1% was obtained (Table 2). The relatively large variations in these experiments were due to variations in the reference samples. Although relatively high concentration factors have been achieved with minute losses, the outlined cell concentrating strategy holds promise for further improvements.

Increasing the input flow rate and maintaining the sample output flow rate constant yields higher concentration factors. The current flow system is, however, limited by a difficulty in balancing a flow in the central outlet that is smaller than 0.5% of the total flow rate. Nevertheless, it can be anticipated that a fully integrated microfluidic solution will display improved performance, by a reduction in flow imbalance disturbances, which the current set-up with chip tubing connections to sample loops and syringe pumps may induce.

When using a 2 MHz transducer particles smaller than about 2 μm in diameter (density like polystyrene or cells) focus very slowly. Efficient focusing at smaller particle size is counteracted by acoustic streaming.[29] Smaller particles can, however, be focused by using *e.g.* a higher actuation frequency. Using the proposed chip design together with at higher frequency smaller cells or particles could be concentrated as well. A higher frequency will require a narrower channel width to satisfy the half wave length standing wave criteria and hence a decreased channel cross section. This in turn yields a shortened retention time in the acoustic focusing zone when operating at unchanged flow rates. We currently don't know if unchanged flow rates could be used in combination with a channel that is designed for a higher frequency and yet obtain efficient concentration factors for smaller species such as bacteria.

The variability of performance between devices is experienced to be low. However, no particular study in this respect has been performed. The only foreseen variability is minute variations in the optimal actuation frequency caused by small variations in channel width and height between fabrication batches and different particles suspension fluids.

Conclusions

This paper explores the use of acoustophoresis to concentrate dilute cell samples and particles. It is shown that two-dimensional acoustic standing wave focusing outperforms one-dimensional focusing and that the strategy of implementing several acoustic focusing regions and sequentially remove excess fluid opens the route to concentration factors in continuous flow mode beyond 100 times. Under high-throughput conditions up to 200 times of volume concentration with a minute loss of cells and particles was accomplished. On-going work will aim at further improved concentration factors and offer means to concentrate rare cell and small volume samples where regular centrifugation does not provide a satisfactory solution. The cell concentrator is currently developed to become an integral part of chip integrated cell separation and analysis units.

Acknowledgements

We thank Dr Per Augustsson for helpful discussions and Dr Cecilia Magnusson for the generous gift of the DU145 cells. The work was supported by the Swedish governmental agency for innovation systems, VINNOVA, CellCARE, grant no. 2009-00236, the Swedish Research Council, grant no.: 621-2010-4389, the Royal Physiographic Society, the Crafoord Foundation and the Carl Trygger Foundation.

References

1 S. Shafazand, *Chest*, 2002, **122**, 1727–1736.
2 W. J. Allard, J. Matera, M. C. Miller, M. Repollet, M. C. Connelly, C. Rao, A. G. J. Tibbe, J. W. Uhr and L. W. M. M. Terstappen, *Clin. Cancer Res.*, 2004, **10**, 6897–904.
3 K. A. Stevens and L.-A. Jaykus, *Crit. Rev. Microbiol.*, 2004, **30**, 7–24.
4 J. Warrick, B. Casavant, M. Frisk and D. Beebe, *Anal. Chem.*, 2010, **82**, 8320–6.
5 D. I. C. Wang, T. J. Sinskey, R. E. Gerner and R. P. De Filippi, *Biotechnol. Bioeng.*, 1968, **10**, 641–649.
6 J. Yang, W. C. Hooper, D. J. Phillips, M. L. Tondella and D. F. Talkington, *Clin. Vaccine Immunol.*, 2002, **9**, 1142–1143.
7 A. J. Mach, J. H. Kim, A. Arshi, S. C. Hur and D. DiCarlo, *Lab Chip*, 2011, **11**, 2827–3016.
8 M. Yamada and M. Seki, *Anal. Chem.*, 2006, **78**, 1357–1362.
9 A. K. Balasubramanian, K. a Soni, A. Beskok and S. D. Pillai, *Lab Chip*, 2007, **7**, 1315–21.
10 C. R. Cabrera and P. Yager, *Electrophoresis*, 2001, **22**, 355–62.
11 C.-P. Jen and H.-H. Chang, *Biomicrofluidics*, 2011, 5.
12 R. Kwak, S. J. Kim and J. Han, *Anal. Chem.*, 2011, **83**, 7348–55.
13 H. Moncada-Hernández and B. H. Lapizco-Encinas, *Anal. Bioanal. Chem.*, 2010, **396**, 1805–16.
14 D. Puchberger-Enengl, S. Podszun, H. Heinz, C. Hermann, P. Vulto and G. a. Urban, *Biomicrofluidics*, 2011, **5**, 44111.
15 P. Grodzinski, J. Yang, R. Liu and M. D. Ward, *Biomed. Microdevices*, 2003, **5**, 303–310.
16 J. J. Hawkes and W. T. Coakley, *Enzyme Microb. Technol.*, 1996, **19**, 57–62.
17 G. R. Goddard, J. C. Martin, S. W. Graves and G. Kaduchak, *Cytometry, Part A*, 2006, **69A**, 66–74.
18 J. J. Hawkes and W. T. Coakley, *Sens. Actuators, B*, 2001, **75**, 213–222.
19 O. Manneberg, J. Svennebring, H. M. Hertz and M. Wiklund, *J. Micromech. Microeng.*, 2008, **18**, 095025.
20 A. Nilsson, F. Petersson, H. Jönsson and T. Laurell, *Lab Chip*, 2004, **4**, 131–5.
21 F. Petersson, L. B. Åberg, A.-M. K. Swärd-Nilsson and T. Laurell, *Anal. Chem.*, 2007, **79**, 5117–23.
22 C. Grenvall, M. Carlsson, P. Augustsson and F. Petersson and T. Laurell, in *Proceedings of μTAS 2007*, ed. J.-L. Viovy, P. Tabeling, S. Cescroix, and L. Malaquin, Paris, 2007, pp. 1813–1815.
23 J. Hultström, O. Manneberg, K. Dopf, H. M. Hertz, H. Brismar and M. Wiklund, *Ultrasound Med. Biol.*, 2007, **33**, 145–51.
24 M. Evander, L. Johansson, T. Lilliehorn, J. Piskur, M. Lindvall, S. Johansson, M. Almqvist, T. Laurell and J. Nilsson, *Anal. Chem.*, 2007, **79**, 2984–2991.
25 J. Dykes, A. Lenshof, I.-B. Åstrand-Grundström, T. Laurell and S. Scheding, *PLoS One*, 2011, **6**, e23074.
26 M. Wiklund, *Lab Chip*, 2012, **12**, 2018–2028.
27 T. Laurell, F. Petersson and A. Nilsson, *Chem. Soc. Rev.*, 2007, **36**, 492–506.
28 R. W. Cole, T. Jinadasa and C. M. Brown, *Nat. Protoc.*, 2011, **6**, 1929–41.
29 P. Augustsson and T. Laurell, *Lab Chip*, 2012, **12**, 1742–1752.

Paper II

Focusing of sub-micrometer particles and bacteria enabled by two-dimensional acoustophoresis

Maria Antfolk, Peter B Muller, Per Augustsson, Henrik Bruus, and Thomas Laurell

Lab on a Chip, 2014, 14(15), 2791-2799.

Paper II

Lab on a Chip

PAPER

Focusing of sub-micrometer particles and bacteria enabled by two-dimensional acoustophoresis†

Cite this: *Lab Chip*, 2014, **14**, 2791

M. Antfolk,*[a] P. B. Muller,[b] P. Augustsson,[ac] H. Bruus[b] and T. Laurell*[a]

Handling of sub-micrometer bioparticles such as bacteria are becoming increasingly important in the biomedical field and in environmental and food analysis. As a result, there is an increased need for less labor-intensive and time-consuming handling methods. Here, an acoustophoresis-based microfluidic chip that uses ultrasound to focus sub-micrometer particles and bacteria, is presented. The ability to focus sub-micrometer bioparticles in a standing one-dimensional acoustic wave is generally limited by the acoustic-streaming-induced drag force, which becomes increasingly significant the smaller the particles are. By using two-dimensional acoustic focusing, *i.e.* focusing of the sub-micrometer particles both horizontally and vertically in the cross section of a microchannel, the acoustic streaming velocity field can be altered to allow focusing. Here, the focusability of *E. coli* and polystyrene particles as small as 0.5 μm in diameter in microchannels of square or rectangular cross sections, is demonstrated. Numerical analysis was used to determine generic transverse particle trajectories in the channels, which revealed spiral-shaped trajectories of the sub-micrometer particles towards the center of the microchannel; this was also confirmed by experimental observations. The ability to focus and enrich bacteria and other sub-micrometer bioparticles using acoustophoresis opens the research field to new microbiological applications.

Received 14th February 2014,
Accepted 20th May 2014

DOI: 10.1039/c4lc00202d

www.rsc.org/loc

Introduction

The ability to control and process sub-micrometer bioparticles, *e.g.* bacteria and subcellular organelles, is becoming increasingly important in biomedicine and in environmental and food analysis.[1,2] Methods such as blood culture of bacteria[1] and subcellular fractionation[3] are, however, labor-intensive, complicated, and time-consuming, and new technologies are being sought to redress these shortcomings.

Microfluidics offers a means of automated handling and analysis of sub-micrometer bioparticles with the associated advantage of a continuous mode of sample handling. Thus, considerations such as initial sample volume or batch volume are no longer relevant. Previously used methods for handling of sub-micrometer particles included filters,[4,5] dielectrophoresis,[6–8] inertia in combination with hydrodynamic forces,[9] magnetophoresis,[10,11] deterministic lateral displacement,[12] and surface acoustic waves (SAW).[13] These methods have been mainly used for handling of bacteria and particles of around 1 μm in diameter. Recently, SAW were used to separate 0.5 μm polystyrene particles from 0.3 μm particles,[14] Stoneley waves were used to focus 0.5 μm polystyrene particles at flow rates of 200 nL min^{-1},[15] and acoustic trapping has been used to successfully trap 0.1 μm particles using seeding particles.[16] Although acoustic seed trapping gives good recovery of sub-micrometer particles and bacteria, the system operates in batch mode, which is limited by the capacity of the acoustic trap. In spite of these developments, one common need is the ability to process sub-micrometer particles in continuous-flow mode together with the possibility of handling rare species in crude samples with high recovery rates without previous sample preparation.

In this regard, the use of acoustophoresis in microfluidic systems has attracted much attention in recent years as a continuous-flow and non-contact mode method of separating or enriching microparticles or cells while offering a reasonable degree of throughput. The method involves the use of ultrasound standing waves to focus cells or particles in the nodal (or anti-nodal) plane of the standing wave according to their intrinsic properties: size, density, and compressibility.[17] Furthermore, this label-free and gentle[18,19] method—which operates independently of the biochemical and electrical properties of the suspension medium—has been extensively explored to separate, wash, or concentrate various biological

[a] *Department of Biomedical Engineering, Lund University, Box 118, SE-221 00 Lund, Sweden. E-mail: thomas.laurell@bme.lth.se, maria.antfolk@bme.lth.se*
[b] *Department of Physics, Technical University of Denmark, DTU Physics Bldg 309, DK-2800 Kongens Lyngby, Denmark*
[c] *Department of Electrical Engineering and Computer Science, Massachusetts Institute of Technology, Cambridge, MA, USA*

† Electronic supplementary information (ESI) available. See DOI: 10.1039/c4lc00202d

samples including blood,[20–23] raw milk,[24] circulating tumor cells,[25,26] and yeast.[27]

For bulk acoustic waves (BAW) microchannel acoustophoresis is usually carried out in the 1–10 MHz frequency range and particles are focused along a single dimension. For larger particles, the acoustically induced particle motion is dominated by the primary acoustic radiation force, whereas the motion of smaller particles is instead dominated by the acoustic streaming-induced drag force of the suspending liquid.[28,29] Attempts have been made to address the need for bacterial or other sub-micrometer particle manipulation and enrichment in acoustic standing-wave systems. Bacteria have been processed with some success in batch mode using ultrasound to agglomerate them,[30,31] and a quarter-wavelength acoustic device was used to concentrate 1 μm particles in continuous flow.[32] However, no systems have yet emerged that enable continuous flow-based focusing of bacteria or other sub-micrometer particles at recovery rates above 90%, relevant when handling highly dilute suspensions.

This paper presents continuous flow-based sub-micrometer particle focusing using two-dimensional BAW-acoustophoresis. The use of two-dimensional focusing has previously only been explored for particles larger than 5 μm in diameter.[25,26,33–35] In contrast to the case with one-dimensional standing acoustic waves, the simultaneous excitation of two orthogonal resonances generates an acoustic streaming velocity field that does not counteract the primary radiation force. A numerical model that predicts a streaming field with essentially a single large vortex centered in the cross section of the channel, in agreement with experimental data, is also presented.

Theory

Particles in a standing-wave acoustophoresis system are primarily affected by two forces: the acoustic radiation force from scattering of the acoustic wave on the particles, and the drag force from the acoustic streaming velocity field of the fluid generated by viscous stresses in the acoustic boundary layers. The interplay between these two forces and the regimes in which they each dominate the particle motion in acoustophoresis systems have been studied extensively by Barnkob *et al.*[29] Through theoretical derivation and experimental verification, these authors have described how the motion of large particles is dominated by the acoustic radiation force while the motion of small particles is dominated by the drag force from the acoustic streaming.

To theoretically determine the critical particle diameter $2a_c$, where the crossover from radiation force-dominated particle motion to acoustic streaming-induced drag force-dominated particle motion occurs, the magnitudes of the two forces are equated, resulting in the following equation valid for single-particle motion in a half-wavelength resonance:[29]

$$2a_c = \sqrt{\frac{12s}{\pi}\frac{\nu}{\Phi f}} \approx 1.6\ \mu\text{m}, \qquad (1)$$

where s is a factor related to the channel geometry, ν is the kinematic viscosity of the medium, Φ is the acoustic contrast factor, and f is the frequency of the acoustic field. The numerical value is calculated for a polystyrene particle in water and a frequency of $f = 3.19$ MHz. The geometrical value used is $s = 0.47$ for a particle near the top or bottom walls, and includes thermal effects.[29] The critical particle size is independent of the applied peak-to-peak voltage U_{pp} driving the piezo-ceramic ultrasound transducer, because both the radiation force and the streaming depend linearly on the energy density of the standing acoustic wave. In contrast, it can be seen in eqn (1) that the critical particle size does depend on the material parameters ν of the fluid and Φ of the fluid and particles, and on the actuation frequency f. Increasing the frequency to achieve radiation force-dominated motion of smaller particles is a relatively straightforward solution, but such an increase often necessitates reduced channel dimensions, which drastically reduces the throughput of the device. In this paper we propose another solution, namely to change the whole acoustic resonance such that the acoustic radiation force and the acoustic streaming-induced drag work together in focusing the particles.

The acoustic streaming and acoustophoretic particle motion in a microchannel cross section have been studied numerically by Muller *et al.*[28] The method is valid for long, straight microchannels of constant rectangular cross section and employs a pertubation approach to the pressure, temperature and velocity fields. Briefly, the numerical scheme is as follows. The first-order acoustic fields are solved in the frequency domain for an oscillating velocity boundary condition on the walls of the rectangular channel domain. From the first-order fields, the acoustic radiation force is calculated from the expression given by Settnes and Bruus,[36] while the steady acoustic streaming velocity field is calculated numerically by solving the time-averaged second-order Navier–Stokes equation and continuity equation.[27] This method only considers actuation at a single frequency, but can readily be extended to consider actuation with two frequencies by superposition of the second-order streaming flows. For this superposition to be valid the separation of the two frequencies should be much larger than the width of the resonances, which is typically on the order of 10 kHz, such that the first-order fields of the two resonances do not couple in the time-averaged second-order source terms for the streaming velocity field.[28] However, if the two resonance frequencies are closely spaced, resulting in overlapping resonance curves, the two resonances can be excited simultaneously at a single frequency. In this case, the first-order fields of the two resonances couple in the time-averaged second-order source terms, and consequently the streaming velocity field cannot be calculated by superposition of second-order streaming flows. This case of close-lying overlapping resonances is the subject of the numerical analysis in the following section, where we show that the relative phases of the wall oscillations control the structure of the streaming flow, and that specific

values can lead to structures qualitatively different from the standard quadrupolar Rayleigh streaming flow observed for the half-wavelength resonance.[37]

Numerical analysis

The following numerical analysis is a generic investigation of the acoustophoretic motion of 0.5 μm-diameter particles in a nearly-square channel cross section. It is not intended to be a direct numerical simulation of the actual experiments presented in this paper; nevertheless, it predicts the existence of two fundamentally different acoustic streaming patterns relevant for the interpretation of the experiments. The numerical analysis employs the method presented by Muller *et al.*[28] and to avoid spurious effects of perfect square symmetry and to imitate the uncertainty in microchannel fabrication, the cross-sectional dimensions of the microchannel in the model was chosen to be 230.5 μm wide and 229.5 μm high. The parameters used in the model correspond to the biologically relevant temperature of 37 °C. The first-order velocity boundary condition applied to the walls was $u_{bc} = u_0 \cos(\omega t)\boldsymbol{e}_y$ on the left and right walls and $u_{bc} = u_0 \cos(\omega t + \phi)\boldsymbol{e}_z$ on the top and bottom walls, where u_0 is the amplitude, $\omega = 2\pi f$ is the angular frequency of the transducer, ϕ is a constant phase shift, and $\boldsymbol{e}_y$ and $\boldsymbol{e}_z$ are the unit vectors in the transverse horizontal and vertical directions, respectively. Because both the acoustic streaming-induced drag force and the acoustic radiation force depend non-linearly on the oscillating velocity boundary conditions, the consequences of changing the phase shift ϕ between the two wall pairs cannot easily be deduced analytically.

To characterize the resonances of the nearly-square channel, the average acoustic energy density,[38] denoted E_{ac}, was calculated numerically for a range of frequencies, shown in Fig. 1. This was done for several different actuations of the nearly-square channel. In each panel an inset shows a sketch of the channel geometry and which walls are actuated and by which phase factor $\cos(\omega t + \phi)$. In Fig. 1(a) the nearly-square channel was actuated in phase on the left/right walls to obtain the usual horizontal half-wavelength resonance, showing up as a Lorentzian peak centered around the resonance frequency $f_1 = 3.3032$ MHz. In Fig. 1(b) the nearly-square channel was actuated in phase on the top/bottom walls resulting in a peak at the slightly higher resonance frequency $f_2 = 3.3176$ MHz corresponding to the vertical half-wavelength resonance. f_2 is slightly higher than f_1 because the height of the nearly-square channel is slightly smaller than the width. In Fig. 1(c) the nearly-square channel was actuated in phase on all four walls ($\phi = 0$). Due to the finite width of the two resonance peaks, this actuation simultaneously excites both the horizontal and the vertical half-wavelength resonances, resulting in a resonance curve with two peaks and a plateau in between, in contrast to the previous single-peak resonance curves. As a guide to the eye, the single-peak resonance curves from Fig. 1(a–b) are included in Fig. 1(c) in grey. The frequency mid-way between the two resonance peaks is

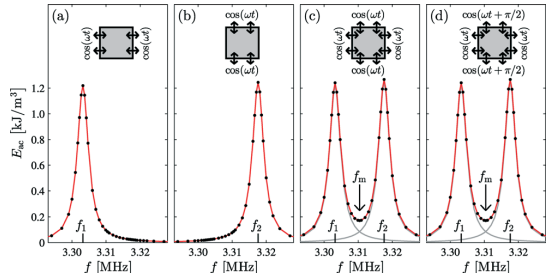

Fig. 1 Resonance curves, obtained by plotting the average acoustic energy density E_{ac} *vs.* the frequency $f = \omega/2\pi$ of the wall actuations. (a) A nearly-square channel, 230.5 μm by 229.5 μm cross section, with the left/right walls vibrating in phase. (b) The nearly-square channel with the top/bottom walls vibrating in phase. (c) The nearly-square channel with all walls vibrating in phase. The resonance curves from (a) and (b) are shown in grey. (d) Same as (c) except that the top/bottom wall pair vibrate with a phase shift of $\phi = \pi/2$ relative to the left/right wall pair. f_1 and f_2 are the two resonance frequencies corresponding to the horizontal and vertical half-wavelength resonance, respectively. f_m indicates the middle frequency between the two resonance peaks. All walls have the same oscillation amplitude u_0.

$f_m = (f_1 + f_2)/2 = 3.3104$ MHz. At this particular frequency, the amplitudes of the horizontal and the vertical resonances are the same, however much reduced relative to the two resonance maxima. In Fig. 1(d) the nearly-square channel was actuated on all four walls, but the phase of the actuation on the top/bottom wall pair was shifted relative to the left/right wall pair by $\phi = \pi/2$. The resulting resonance curve is the same; however, as we will see below, the second-order steady acoustic streaming velocity field changes significantly by introducing this phase shift.

We now study the acoustophoretic motion of 0.5 μm-diameter particles in the nearly-square channel cross section, shown in Fig. 2, for each of the four actuations shown in Fig. 1. This particle motion results from the acoustic radiation force and the streaming-induced drag force, both second-order acoustic effects.[28] Given the small particle diameter, the acoustophoretic motion is dominated by the drag force from the acoustic streaming.[29] Fig. 2 contains four rows (a–d) corresponding to the four cases in Fig. 1. The actuation frequency was f_1 in (a), f_2 in (b), and f_m in (c–d). For each case, column 1 shows the first-order acoustic pressure, column 2 shows the acoustic radiation force together with streamlines of the steady streaming velocity field, and column 3 shows the acoustophoretic trajectories of 0.5 μm-diameter particles.

For the two cases (a–b) the weak radiation force acts to focus the particles towards a center line, but as the particle motion is dominated by the streaming-induced drag force, they follow the quadrupolar streaming flow of the 1D half-wavelength resonance. For the two cases (c–d) both the horizontal and the vertical half-wavelength resonances are exited simultaneously at the single frequency f_m, and the streaming flow is qualitatively different from the usual quadrupolar structure. For $\phi = 0$ (c), the streaming flow consists of two larger

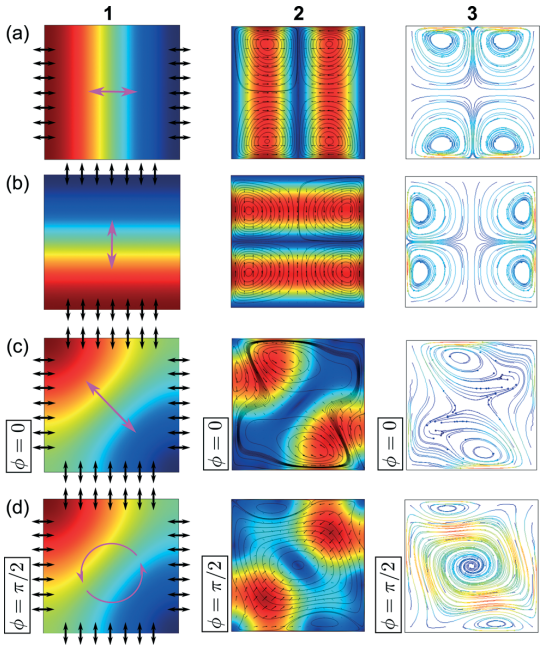

Fig. 2 Acoustophoretic motion of 0.5 μm-diameter particles in the nearly-square microchannel cross section. The rows (a–d) corresponds to the four cases shown in Fig. 1. The actuation frequency was f_1 in (a), f_2 in (b), and f_m in (c–d). For each case, column 1 is a snapshot in time of the amplitude of the oscillating first-order acoustic pressure (color plot where red is positive, green is zero, and blue is negative). Column 2 is the acoustic radiation force (color plot and arrows where red is positive and blue is zero) together with streamlines (black contour lines) of the steady streaming velocity field. Column 3 is the acoustophoretic trajectories (colors indicate the speed where red is positive and blue is zero) of 0.5 μm-diameter particles released from a regular grid in the channel cross section. To best illustrate the qualitative results, the color scale is set by the maximum value in each plot individually. For the color plots 1(a–c) the magenta arrow indicates that the pressure has an almost static nodal line (green) while the amplitude oscillates. For the color plot 1(d) the magenta arrows indicate that the nodal line (green) of the pressure field rotates in time.

flow rolls at the top and bottom walls along with two smaller flow rolls at the side walls. The small particles follow this streaming flow and are not focused in the center. For $\phi = \pi/2$ (d), the streaming flow consists of one large flow roll in the center of the channel and two smaller flow rolls at the top and bottom walls. The combined effect of the weak radiation force towards the centre and the strong streaming-induced drag force acts to focus the particles at the centre of the channel cross section following a spiralling motion. This allows for focusing of sub-micrometer particles, which is not possible in the standard one-dimensional half-wavelength resonance (a–b). By numerically tuning the phase shift ϕ a solution was obtained where the large centred flow roll covered the whole channel cross section without any smaller bulk flow rolls, allowing all particles to be focused at the centre. Changing the phase shift ϕ by π results in a counter-rotating streaming flow. The acoustic radiation force in Fig. 2(c–d) is similar to that reported for acoustic focusing of large particles in cylindrical channels.[39] It should be stressed that the steady streaming is a boundary driven second-order flow, it is not driven by the rotation of the first-order pressure in Fig. 2(d) first column.

This numerical analysis is a generic study not aimed at direct simulation of the following experiments. Experimentally it is very difficult to control, even to measure, the vibration of the channel walls. Moreover, the wall oscillation presumably varies along the length of the channel, by analogy with what has already been verified experimentally for the acoustic field of the half-wavelength resonance.[40] However, the numerical results indicate the existence of a streaming flow that enables focusing of sub-micrometer particles, which is impossible with the well-known quadrupolar Rayleigh streaming. This new streaming flow strongly depends on the relative phase of the vibrations of the walls, *i.e.* the boundary conditions for the first-order acoustic field. Moreover, the spatial variation of the actuation, which has not been investigated, will presumably also influence the streaming flow and thus the focusability. This calls for a more in-depth numerical study of the dependency of the acoustic streaming on the actuation boundary condition which will be included in future work, as for the present work the main emphasis is on the experimental results.

Materials and experimental methods

Design and fabrication of the device

The chips were fabricated from <110> oriented silicon using photolithography and anisotropic wet etching in KOH (400 g L^{-1} H_2O, 80 °C). Inlets and outlets were drilled through the silicon using a diamond drill (Tools Sverige AB, Lund, Sweden) and the chips were sealed by anodic bonding to a glass lid. The two chips had one trifurcation inlet and outlet split each, of which only a single inlet was used and the unused one was sealed (Fig. 3). The square-cross-section channel had a width

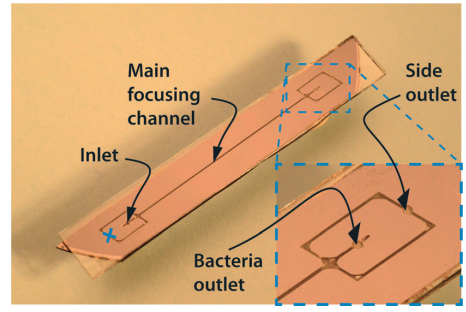

Fig. 3 Photograph of the chip design. The main focusing channel is 35 mm long and 230 μm wide, while its height is either 230 μm (square channel) or 150 μm (flat rectangular channel). After the trifurcation, the side channels are connected to one outlet. The inlet marked with a blue cross is not used.

and height of 230 μm and was operated at 3.19 MHz. The rectangular-cross-section channel had a width of 230 μm and a height of 150 μm, and was operated at 3.24 MHz and 5.09 MHz, respectively. The piezo-ceramic ultrasound transducers (PZ26; Ferroperm piezoceramics, Kvistgaard, Denmark) actuating the chips were glued to the chips with cyanoacrylate glue (Loctite Super Glue, Henkel Norden AB, Stockholm, Sweden). The 3 MHz ultrasound transducer was glued to the silicon and the 5 MHz transducer was glued to the glass lid, both at the middle of the chip. To control the temperature, a Peltier element (Farnell, London, UK) was glued underneath the 3 MHz ultrasound transducer and a Pt100 or Pt1000 resistance temperature detector (Farnell, London, UK) was glued to the glass lid.

Instrument set-up

The transducers were actuated using a dual-channel function generator (AFG 3022B; Tektronix UK Ltd., Bracknell, UK), the signals were amplified using in-house built power amplifiers based on an LT1012 power amplifier (Linear Technology Corp., Milpitas, CA, USA) and the applied voltage was monitored using an oscilloscope (TDS 2120; Tektronix). The temperature was controlled using a Peltier-controller (TC2812; Cooltronic GmbH, Beinwil am See, Switzerland) and the temperature was set to 37 °C throughout all experiments. Fluorescent microscopy images were obtained using a Hamamatsu camera (Hamamatsu Photonics KK, Hamamatsu, Japan) installed on an Olympus microscope (BX51WI; Olympus Corporation, Tokyo, Japan).

Experimental set-up

The flow rates were controlled using syringe pumps (neMESYS; Cetoni GmbH, Korbussen, Germany) mounted with glass syringes (Hamilton Bonaduz AG, Bonaduz, Switzerland) connected to the inlet and the outlet of the side channels. The center outlet was kept open and sample was collected from a short piece of tubing directly into an Eppendorf tube. While the inlet and outlet flow rates were varied, the outlet flow rates were kept at a split ratio of 40 : 60 at the center outlet and the outlet connected to the side channels. To minimize errors caused by sedimentation in the syringes and tubing, which would vary with the flow rate, sample collection with the ultrasound either on or off (for each flow rate) was compared. Particles and bacteria were quantified using a Coulter counter (Multiziser III; Beckman Coulter, Brea, CA, USA). Flow rates and voltage settings are given in Table 1.

Microparticles

Polystyrene microparticles of various sizes were used to characterize the system: 7.11 μm, 4.99 μm, and 3.17 μm diameter particles were obtained from Sigma-Aldrich (Buchs, Switzerland), and 0.992 μm and 0.591 μm particles and 0.49 μm and 0.24 μm fluorescent particles were obtained from Kisker (Kisker Biotech GmbH & Co. KG, Steinfurt, Germany). Fluorescent particles 0.78 μm in diameter were obtained from Bangs Laboratories (Bangs Laboratories, Fishers, IN, USA). Particle concentrations were kept below 10^9 mL^{-1}, to minimize the effect of acoustic and hydrodynamic interaction forces between particles.

Bacteria

For biological evaluation of the system, *Escherichia coli* (*E. coli*) DH5-α (containing a plasmid that carries the ampicillin-resistance gene), a kind gift from Åsa Janfalk Carlsson, was used. *E. coli* was cultured in liquid LB medium or LB plates containing 10 g L^{-1} tryptone (T1332; Saveen & Werner, Limhamn, Sweden), 5 g L^{-1} yeast extract (Hy-Yeast 412; Sigma-Aldrich), 10 g L^{-1} NaCl (Sigma-Aldrich) and 100 mg L^{-1} ampicillin (A9518-5G; Sigma-Aldrich) or agar (bacteriology-grade, A0949; Saveen & Werner).

Experimental results and discussion

In what follows, a system is presented that reduces the lower particle size focusing limit for acoustophoresis to the sub-micrometer range, thus enabling applications in research fields such as microbiology. The experiments were carried out on two variants of an acoustophoresis microfluidic chip, which had a straight square or rectangular channel with a single inlet for particle suspensions and a trifurcation outlet split (Fig. 3). Ideally, with the onset of continuous ultrasonic actuation, particles are focused in the center of the channel and exit through the central outlet—to an extent that depends on the acoustic energy density, the flow rate of the suspension, and the size and material properties of the particles relative to the suspending liquid. In the experiments particles with diameters ranging from 0.6 μm to 7 μm were used and for

Table 1 Nominal flow rates *Q* as set on the syringe pumps and voltage settings for the different experiments

Particle		Rectangular chip 1D		Rectangular chip 2D		Square chip 2D	
Diameter (μm)	Manufacturer	Voltage U_{pp} (V)	Flow rate Q (μL min^{-1})	Voltage $U_{pp,2}$ (V)	Flow rate Q (μL min^{-1})	Voltage U_{pp} (V)	Flow rate Q (μL min^{-1})
7	Sigma-Aldrich	2.5	50, 70, 90, 110, 130			3.16	50, 70, 90, 110, 130
5	Sigma-Aldrich	3.52	50, 70, 90, 110, 130			4.26	50, 60, 70, 80 90
3	Sigma-Aldrich	5.72	70, 80, 90, 100, 150, 200			5.73	50, 60, 70, 80, 90
1	Kisker	10.4	10, 20, 30, 40, 50, 60	0–4	10	10.6	15, 25, 35, 45, 55
0.6	Kisker	11	3, 5, 10, 15, 20	0–4	3	10.6	5, 10, 15, 20
0.5	Kisker	11	0.5, 0.8, 1.2, 2			10.6	0.5, 0.8, 1.2, 2

each particle size the flow rate was varied while keeping the peak-to-peak voltage applied to the transducer constant.

In the experiments the relative focusability R of the suspended particles, was measured. The relative focusability is defined as the proportion of particles moved by the ultrasound to the center outlet, particles which would otherwise end up in the side outlets if the ultrasound was not turned on. A relative focusability of $R = 1$ therefore corresponds to a recovery of 100% of the particles at the center outlet while a relative focusability of $R = 0$ corresponds to a recovery of $Q_c/(Q_c + Q_s) = 40\%$, where Q_c and Q_s are the flow rates of the center and side outlets, respectively. The 40% recovery corresponds to the fraction of particles that would be obtained at the center outlet when the ultrasound is turned off, depending on the flow split ratio between the center and side outlets.

The transverse focusing velocity u_{rad} due to the acoustic radiation force is proportional to the square of the transducer peak-to-peak voltage U_{pp} and the square of the particle radius a, *i.e.* $u_{rad} \propto U_{pp}{}^2 a^2$.[29] To be able to acquire data for different particle sizes while still maintaining a reasonable flow rate in the system, the applied voltage U_{pp} and therefore the acoustic energy density, was set higher in experiments involving smaller (weakly focusing) particles than in experiments with larger (strongly focusing) particles. To compare the results, the flow rates were normalized with respect to the transverse focusing velocity u_{rad}. The 7 μm particle was used as a normalization reference, as this was the largest particle used in the experiments, and it shows an almost ideal radiation force-dominated motion. The normalized flow rate Q_{norm} in a particular experiments with nominal flow rates Q is thus given by

$$Q_{norm} = Q\frac{(u_{rad})_{7\mu m}}{u_{rad}} = Q\frac{(U_{pp}{}^2 a^2)_{7\mu m}}{U_{pp}{}^2 a^2}. \quad (2)$$

One-dimensional focusing in a channel of rectangular cross-section

The small size of many bioparticles such as bacteria inherently makes them less suitable for acoustic standing wave focusing in microfluidic systems without experiencing severe losses, a problem that is prominent when handling highly dilute species in situations where recoveries of more than 90% are needed.

Fig. 4(a) shows the results of one-dimensional focusing in a rectangular channel (230 μm × 150 μm in cross section) where relatively large polystyrene particles with diameters of 7 μm, 5 μm, and 3 μm (red, purple, and green) could all be focused, with a relative focusability of more than 0.9 (R = 0.98 ± 0.10, 0.93 ± 0.003, and 0.98 ± 0.006, respectively). Throughout the paper, the stated uncertainty in the value of R is the standard deviation of three repeated measurements. The smaller polystyrene particles with diameters of 1 μm and 0.6 μm (blue and turquoise) could not be focused under the given conditions, and the focusability measured was only R = 0.52 ± 0.17 and R = 0.48 ± 0.07, respectively. For these particles, the relative focusability R will not approach unity (*i.e.* improve) as the flow rate is decreased further because of

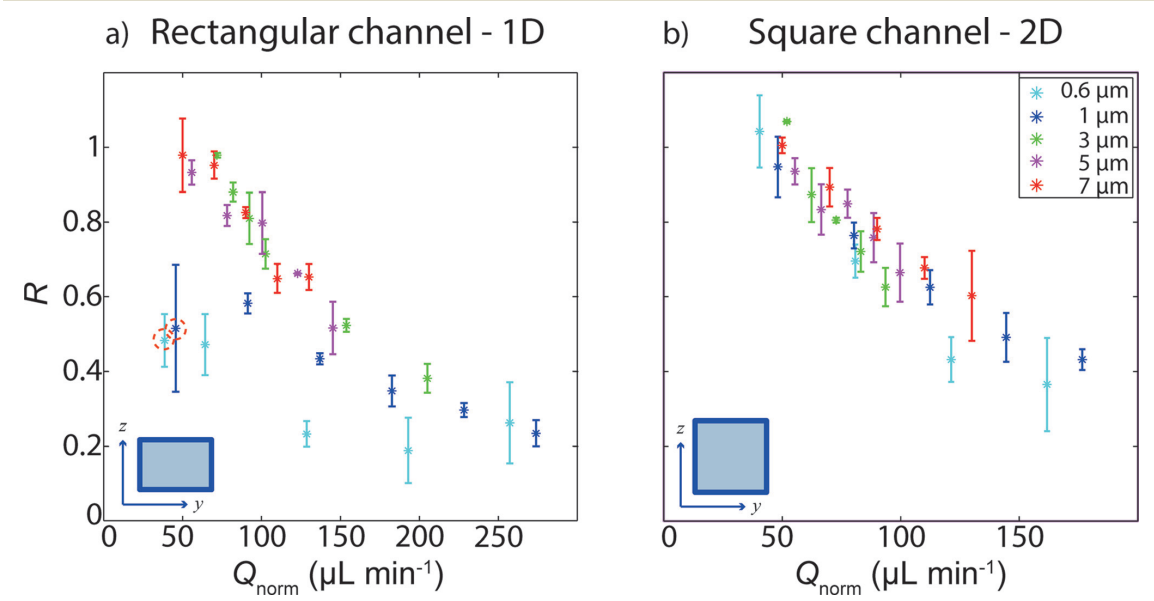

Fig. 4 (a) One-dimensional focusing in the rectangular channel. The relative focusability R plotted against the normalized flow rate Q_{norm}. (b) Two-dimensional single-frequency focusing in the square channel. The relative focusability R plotted against Q_{norm}. All error bars are standard deviations from three repeated measurements. The nominal flow rates for each data point are collected in Table 1.

the acoustic streaming-induced drag force. This is reflected in the saturation of R for the 1 μm and 0.6 μm particles seen for the data points obtained at the two lowest flow rates. The smaller the particle diameter, the more influence the streaming will have in comparison to the primary acoustic radiation force. This is also reflected in the fact that the focusability was generally lower for the 0.6 μm diameter particles than for the 1 μm diameter particles. Increasing the acoustic energy or decreasing the flow rate through the channel will not increase the focusability, since both the acoustic streaming and the acoustic radiation force depend linearly on the acoustic energy density.

For one-dimensional acoustophoretic focusing in this system, the acoustic streaming-induced drag force limits the focusability of particles less than 1.6 μm in diameter. This is caused by the streaming, counteracting the radiation force in the top and bottom regions of the channel, whereby the particles are pushed outwards from the center of the channel instead of inwards.[28] This can be avoided by using two-dimensional focusing, without compromising the channel size or sample throughput, as presented in the following section.

Two-dimensional dual-frequency focusing in a channel of rectangular cross-section

To enable focusing of the particles in the vertical direction as well, a second piezo-ceramic ultrasound transducer was added to the rectangular channel with a half-wavelength matched to the height of the channel. This resulted in a significantly improved focusability of the 1 μm and 0.6 μm particles of R = 0.87 ± 0.10 and R = 0.92 ± 0.34, respectively (Fig. 5). The voltage $U_{pp,2}$ applied to the second transducer was varied at an interval from 0 V to 4 V, while maintaining the settings for the flow rate and voltage of the first transducer in the corresponding one-dimensional focusing experiment at the lowest flow rate, indicated by dashed rings in Fig. 4(a). The relative focusability R increased steadily as the voltage $U_{pp,2}$ approached the maximum achievable in the current system configuration. The increase in the value of R for the small particles demonstrates the benefit of introducing a second orthogonal acoustic standing wave. Increasing the voltage $U_{pp,2}$ above 4 V may result in higher focusability, but it also caused the temperature of the system to rise above the dynamic range of the temperature regulator. An improvement in the focusability of the small particles was seen visually when the flow rate was reduced further.

Two-dimensional single-frequency focusing in a channel of square cross-section

A more straightforward way to generate two-dimensional focusing in an acoustophoresis microchannel is by using a square cross-section geometry. In this way, the same transducer operated at a single frequency can excite both the vertical and horizontal component of the standing waves. Even though the strict square symmetry is broken slightly, *e.g.* due to fabrication inaccuracies, the two resonances can still be excited simultaneously due to their finite width of approximately 10 kHz.[38]

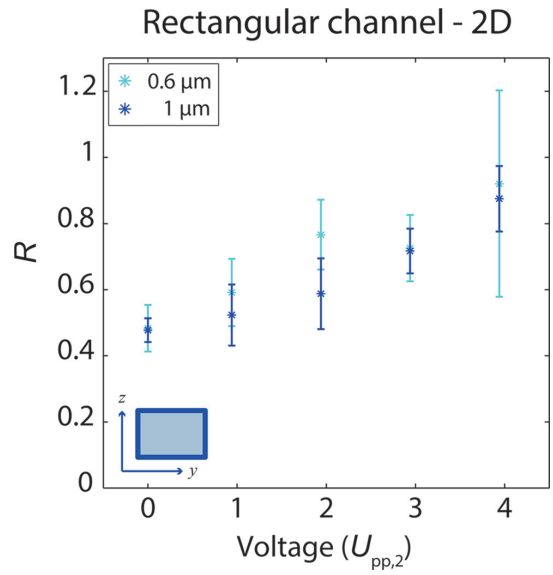

Fig. 5 Two-dimensional dual-frequency focusing in the rectangular channel. The relative focusability R plotted against the voltage $U_{pp,2}$ on the second (5 MHz) piezo transducer focusing the particles vertically in the rectangular channel. The voltage U_{pp} on the first (2 MHz) transducer and the flow rate were kept constant at the same value as used to focus the particles giving the data points surrounded by the dashed red rings in Fig. 4 for the 1 μm (10 μL min^{-1}) and 0.6 μm-particles (3 μL min^{-1}), respectively.

In the square channel (230 μm × 230 μm in cross section), which supports a two-dimensional resonance, again the large particles with diameters of 7 μm, 5 μm, and 3 μm reached high focusability of R = 1.01 ± 0.02, 0.94 ± 0.04, and 1.07 ± 0.004, respectively (Fig. 4(b)). The smaller particles with diameters of 1 μm and 0.6 μm also reached high focusability (R = 0.95 ± 0.08 and 1.04 ± 0.10, respectively), thus demonstrating improved focusability compared to the one-dimensional focusing experiment. This is evident from the fact that the normalized focusability data for all the different particles now collapsed onto a single line (Fig. 4(b)) as compared to the one-dimensional focusability data (Fig. 4(a)).

The square channel cross section offers a simpler system configuration with only one frequency. In contrast, the rectangular channel required the use of two different piezo-ceramic transducers and therefore of two electronic driving systems (signal generators and power amplifiers), adding both cost and complexity to the system. Also, two transducers complicate the design of the temperature controller and are more likely to cause overheating, leading to a shift in frequency of the acoustic resonance and therefore poor focusing performance.

To investigate the performance of the three systems for particles less than 0.6 μm in diameter, fluorescence

microscopy was employed as these particles were too small to be quantified in the Multisizer 3 Coulter Counter used in this study. Visually, it could be observed that 0.5 μm diameter fluorescent polystyrene particles could be focused in both the square (Fig. 6, Table 2) at 2 μL min^{-1} and the rectangular cross-section channels at 0.5 μL min^{-1} when using two-dimensional focusing (data not shown). When using one-dimensional focusing in the rectangular cross-section channel, the particles could not be completely focused, which is consistent with our previous results. The focusability of 0.24 μm fluorescent particles was also investigated, but these particles could only be seen to stream and they could not be focused in any channel (data not shown), placing the new critical particle diameter somewhere between 0.24 μm and 0.5 μm.

Bacteria focusing

A suspension of *E. coli* was also investigated to evaluate the biological relevance of the systems. The bacteria showed a relative focusability $R = 0.95 \pm 0.35$ in the square channel with two-dimensional focusing, whereas it was only $R = 0.40 \pm 0.13$ in the rectangular channel using one-dimensional focusing (Table 3).

In these experiments, we deliberately kept the concentration of particles and bacteria below 10^9 mL^{-1} to avoid the complication of particle-particle interaction due to hydrodynamic coupling of the particles.[41] Also, in future microbiological applications, the need for bacterial enrichment is most evident in samples with very low concentrations of bacteria. In contrast, previously reported focusing of *E. coli* based on a one-dimensional standing wave used a high sample concentration of 10^{10} mL^{-1}, which caused the bacteria to agglomerate and effectively act as larger particles.[42]

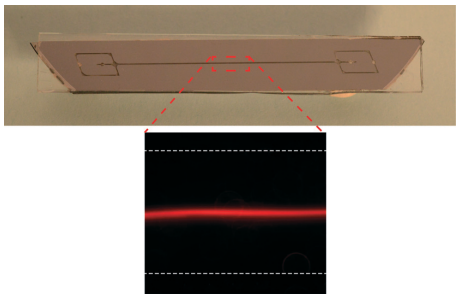

Fig. 6 Fluorescent image of 0.5 μm particles (red) focusing in the square-cross-section channel at a flow rate of 2 μL min^{-1} and at the same voltage as used for the 0.6 μm particles in the square-cross-section channel focusing experiments. The broken gray lines show the edges of the channel.

Table 2 Highest relative focusability achieved for 0.5 μm and 0.6 μm diameter polystyrene particles

Focusing method	Particle	Relative focusability	Flow rate Q
1D rectangle	0.6 μm	0.48 ± 0.07	3 μL min^{-1}
2D rectangle	0.6 μm	0.92 ± 0.34	3 μL min^{-1}
2D square	0.6 μm	1.04 ± 0.1	5 μL min^{-1}
2D square	0.5 μm	1[a]	2 μL min^{-1}
SAW[14,c]	0.5 μm	0.79[b]	1.8 μL min^{-1}
SAW[15]	0.5 μm	1[a]	0.2 μL min^{-1}

[a] No recovery data obtained. Visual focus of particles shown. [b] Recovery, no focusability data available. [c] Device uses a combination of dielectrophoretic and acoustic forces.

Table 3 Highest relative focusability achievable for *E. coli* and 1 μm and 0.6 μm diameter polystyrene particles

Particle	1D rectangular	2D rectangular	2D square
E. coli	0.40 ± 0.13		0.95 ± 0.35
1 μm	0.52 ± 0.17	0.87 ± 0.1	0.95 ± 0.08
0.6 μm	0.48 ± 0.07	0.92 ± 0.34	1.04 ± 0.1

Comparison of the experimental and numerical streaming flow

The experimental data demonstrate that sub-micrometer particles as small as 0.5 μm can be focused using two-dimensional acoustic focusing, which indicates that these systems are dominated by a streaming velocity field similar to that in Fig. 2(d) rather than Fig. 2(c). Importantly, the centred streaming roll derived in Fig. 2(d) has also been observed visually in some parts of the channel (video S1 of ESI†), while other parts appear to be "quieter" (*i.e.* not showing much streaming activity). This is consistent with the assumption that the vibration of the walls most likely changes along the channel. At different positions along the channel, the streaming rolls observed did not all move in the same direction: both clockwise and counter-clockwise streaming rolls were seen. Analogous streaming patterns have also been observed in acoustic resonance cavities with almost square geometry.[43]

Based on the experimental data and the numerical simulation, we hypothesise that the centred streaming roll in combination with two-dimensional focusing is the predominant effect along the full length of the channel, which enables focusing of sub-micrometer particles in the experimental square channel system presented in this paper.

Conclusions

This paper reports the successful use of acoustophoresis to focus sub-micrometer cells and particles. The use of two-dimensional actuation of a square channel was found to enable two-dimensional focusing of *E. coli* and polystyrene particles as small as 0.5 μm in diameter with recovery above 90%, something that could not be achieved using one-dimensional focusing. This sets the experimental limiting particle diameter for continuous-flow half-wavelength resonators operated at about 3 MHz to somewhere between 0.25 μm and 0.5 μm for particles and bacteria with acoustic properties similar to those of polystyrene suspended in water. The focusing of sub-micrometer particles is enabled by a streaming velocity field consisting of a large centered flow roll that does not counteract the weak two-dimensional focusing,

in contrast to the standard quadrupolar flow roll structure generated by a one-dimensional half-wavelength resonance.

The ability to manipulate bacteria and other sub-micrometer particles in a half-wavelength ultrasound standing wave field opens up the acoustophoresis research field to new applications in microbiology. Future research will concentrate on using the new method to generate systems capable of reducing diagnosis and detection times in the biomedical field, and in environmental and food applications.

Acknowledgements

We thank Åsa Janfalk Carlsson for the kind gift of *E. coli*. The work was supported by the Swedish government agency for innovation systems, Vinnova, CellCARE (grant no. 2009-00236), the Swedish Research Council (grant no. 621-2010-4389 and 2012-6708), the Royal Physiographic Society, the Crafoord Foundation, the Carl Trygger Foundation, and the Danish Council for Independent Research, Technology, and Production Sciences (grant no. 11-107021).

References

1 P. M. Dark, P. Dean and G. Warhurst, *Crit. Care*, 2009, **13**, 217.
2 L. A. Huber, K. Pfaller and I. Vietor, *Circ. Res.*, 2003, **92**, 962–968.
3 C. Pasquali, I. Fialka and L. A. Huber, *J. Chromatogr. B: Biomed. Sci. Appl.*, 1999, **722**, 89–102.
4 C. Lay, C. Y. Teo, L. Zhu, X. L. Peh, H. M. Ji, B.-R. Chew, R. Murthy, H. H. Feng and W.-T. Liu, *Lab Chip*, 2008, **8**, 830–833.
5 L. Zhu, Q. Zhang, H. Feng, S. Ang, F. S. Chau and W.-T. Liu, *Lab Chip*, 2004, **4**, 337–341.
6 D. Chen and H. A. Du, *Microfluid. Nanofluid.*, 2009, **9**, 281–291.
7 B. H. Lapizco-Encinas, B. A. Simmons, E. B. Cummings and Y. Fintschenko, *Anal. Chem.*, 2004, **76**, 1571–1579.
8 S. Bhattacharya, S. Salamat, D. Morisette, P. Banada, D. Akin, Y.-S. Liu, A. K. Bhunia, M. Ladisch and R. Bashir, *Lab Chip*, 2008, **8**, 1130–1136.
9 Z. Wu, B. Willing, J. Bjerketorp, J. K. Jansson and K. Hjort, *Lab Chip*, 2009, **9**, 1193–1199.
10 N. Xia, T. P. Hunt, B. T. Mayers, E. Alsberg, G. M. Whitesides, R. M. Westervelt and D. E. Ingber, *Biomed. Microdevices*, 2006, **8**, 299–308.
11 J. D. Adams, U. Kim and H. T. Soh, *Proc. Natl. Acad. Sci. U. S. A.*, 2008, **105**, 18165–18170.
12 L. R. Huang, E. C. Cox, R. H. Austin and J. C. Sturm, *Science*, 2004, **304**, 987–990.
13 J. Shi, D. Ahmed, X. Mao, S.-C. S. Lin, A. Lawit and T. J. Huang, *Lab Chip*, 2009, **9**, 2890–2895.
14 D. J. Collins, T. Alan and A. Neild, *Lab Chip*, 2014, **14**, 1595–1603.
15 V. Yantchev, J. Enlund, I. Katardjiev and L. A. Johansson, *J. Micromech. Microeng.*, 2010, **20**, 035031.
16 B. Hammarström, T. Laurell and J. Nilsson, *Lab Chip*, 2012, **12**, 4296–4304.
17 T. Laurell, F. Petersson and A. Nilsson, *Chem. Soc. Rev.*, 2007, **36**, 492–506.
18 M. Wiklund, *Lab Chip*, 2012, **12**, 2018–2028.
19 M. A. Burguillos, C. Magnusson, M. Nordin, A. Lenshof, P. Augustsson, M. J. Hansson, E. Elmér, H. Lilja, P. Brundin, T. Laurell and T. Deierborg, *PLoS One*, 2013, **8**, e64233.
20 J. D. Adams, C. L. Ebbesen, R. Barnkob, A. H. J. Yang, H. T. Soh and H. Bruus, *J. Micromech. Microeng.*, 2012, **22**, 075017.
21 A. Ahmad-Tajudin, K. Petersson, A. Lenshof, A.-M. Swärd-Nilsson, L. Åberg, G. Marko-Varga, J. Malm, H. Lilja and T. Laurell, *Lab Chip*, 2013, **13**, 1790–1796.
22 F. Petersson, A. Nilsson, C. Holm, H. Jonsson and T. Laurell, *Analyst*, 2004, **129**, 938–943.
23 A. Lenshof, A. Ahmad-Tajudin, K. Järås, A.-M. K. Swärd-Nilsson, L. Åberg, G. Marko-Varga, J. Malm, H. Lilja and T. Laurell, *Anal. Chem.*, 2009, **81**, 6030–6037.
24 C. Grenvall, P. Augustsson, J. R. Folkenberg and T. Laurell, *Anal. Chem.*, 2009, **81**, 6195–6200.
25 P. Augustsson, C. Magnusson, M. Nordin, H. Lilja and T. Laurell, *Anal. Chem.*, 2012, **84**, 7954–7962.
26 M. Nordin and T. Laurell, *Lab Chip*, 2012, **12**, 4610–4616.
27 S. Radel, A. J. McLoughlin, L. Gherardini, O. Doblhoff-Dier and E. Benes, *Ultrasonics*, 2000, **38**, 633–637.
28 P. B. Muller, R. Barnkob, M. J. H. Jensen and H. Bruus, *Lab Chip*, 2012, **12**, 4617–4627.
29 R. Barnkob, P. Augustsson, T. Laurell and H. Bruus, *Phys. Rev. E: Stat., Nonlinear, Soft Matter Phys.*, 2012, **86**, 056307.
30 M. S. Limaye, J. J. Hawkes and W. T. Coakley, *J. Microbiol. Methods*, 1996, **27**, 211–220.
31 M. Zourob, J. J. Hawkes, W. T. Coakley, B. J. Treves Brown, P. R. Fielden, M. B. McDonnell and N. J. Goddard, *Anal. Chem.*, 2005, **77**, 6163–6168.
32 R. J. Townsend, M. Hill, N. R. Harris and M. B. McDonnell, *Ultrasonics*, 2008, **48**, 515–520.
33 O. Manneberg, J. Svennebring, H. M. Hertz and M. Wiklund, *J. Micromech. Microeng.*, 2008, **18**, 095025.
34 S. Oberti, A. Neild and J. Dual, *J. Acoust. Soc. Am.*, 2007, **121**, 778–785.
35 O. J. E. Jakobsson, C. Grenvall, M. Nordin, M. Evander and T. Laurell, *Lab Chip*, 2014, **14**, 1943–1950.
36 M. Settnes and H. Bruus, *Phys. Rev. E: Stat., Nonlinear, Soft Matter Phys.*, 2012, **85**, 016327.
37 P. B. Muller, M. Rossi, Á. G. Marín, R. Barnkob, P. Augustsson, T. Laurell, C. J. Kähler and H. Bruus, *Phys. Rev. E: Stat., Nonlinear, Soft Matter Phys.*, 2013, **88**, 023006.
38 R. Barnkob, P. Augustsson, T. Laurell and H. Bruus, *Lab Chip*, 2010, **10**, 563–570.
39 G. Gregory and K. Gregory, *J. Acoust. Soc. Am.*, 2005, **117**, 3440–3447.
40 P. Augustsson, R. Barnkob, S. T. Wereley, H. Bruus and T. Laurell, *Lab Chip*, 2011, **11**, 4152–4164.
41 C. Mikkelsen and H. Bruus, *Lab Chip*, 2005, **5**, 1293–1297.
42 J. J. Hawkes, M. S. Limaye and W. T. Coakley, *J. Appl. Microbiol.*, 1997, **82**, 39–47.
43 M. Wiklund, R. Green and M. Ohlin, *Lab Chip*, 2012, **12**, 2438–2451.

Paper III

A single inlet two-stage acoustophoresis chip enabling tumor cell enrichment from white blood cells

Maria Antfolk, Christian Antfolk, Hans Lilja, Thomas Laurell, and Per Augustsson

Lab on a Chip, 2015, 15(9), 2102-2109.

Paper III

Lab on a Chip

PAPER

Cite this: *Lab Chip*, 2015, **15**, 2102

A single inlet two-stage acoustophoresis chip enabling tumor cell enrichment from white blood cells†

Maria Antfolk,*[a] Christian Antfolk,[a] Hans Lilja,[bcd] Thomas Laurell[a] and Per Augustsson*[ae]

Received 21st January 2015,
Accepted 20th March 2015

DOI: 10.1039/c5lc00078e

www.rsc.org/loc

Metastatic disease is responsible for most cancer deaths, and hematogenous spread through circulating tumor cells (CTC) is a prerequisite for tumor dissemination. CTCs may undergo epithelial–mesenchymal transition where many epithelial cell characteristics are lost. Therefore, CTC isolation systems relying on epithelial cell markers are at risk of losing important subpopulations of cells. Here, a simple acoustophoresis-based cell separation instrument is presented. Cells are uniquely separated while maintained in their initial suspending medium, thus eliminating the need for a secondary cell-free medium to hydrodynamically pre-position them before the separation. When characterizing the system using polystyrene particles, 99.6 ± 0.2% of 7 μm diameter particles were collected through one outlet while 98.8 ± 0.5% of 5 μm particles were recovered through a second outlet. Prostate cancer cells (DU145) spiked into blood were enriched from white blood cells at a sample flow rate of 100 μL min^{-1} providing 86.5 ± 6.7% recovery of the cancer cells with 1.1 ± 0.2% contamination of white blood cells. By increasing the acoustic intensity a recovery of 94.8 ± 2.8% of cancer cells was achieved with 2.2 ± 0.6% contamination of white blood cells. The single inlet approach makes this instrument insensitive to acoustic impedance mismatch; a phenomenon reported to importantly affect accuracy in multi-laminar flow stream acoustophoresis. It also offers a possibility of concentrating the recovered cells in the chip, as opposed to systems relying on hydrodynamic pre-positioning which commonly dilute the target cells.

Introduction

The incidence rate of cancer in the world is increasing, largely due to an aging population and changes in lifestyle factors.[1] Early diagnosis can improve outcomes, but metastatic spread of the cancer to secondary tissues still contributes the majority of cancer deaths.[2] Metastases are formed when cells are disseminated from the primary tumor into the blood circulation (where they are referred to as circulating tumor cells [CTC]), until they reach remote organs and tissues where they may establish secondary tumors.[3] To improve survival, it is critical to monitor the cancer's propensity to metastasize; CTC enumeration in blood is prognostic for survival.[4] Several techniques to enumerate and detect CTCs, including the FDA-approved system CellSearch®, are based on the use of immunolabels for specific epithelial cell markers such as EpCAM, or cytokeratins.[5] However, epithelial cell markers are frequently lost in the epithelial–mesenchymal transition, which the cells undergo to escape the primary epithelial tumor and become CTCs.[6,7] Therefore, the effectiveness of using only epithelial cell markers to isolate a purified CTC population prior to the enumeration process is questionable since subpopulations of CTCs may remain undetected.

Microfluidic technology offers a large number of cell separation principles, all relying on the deterministic behavior of laminar flow.[8–11] Since the dimensions of microchannels match the length scales of cells, microfluidics has the potential to contribute to cell separation by the ability to accurately control the position of the cells within the channels.[12] Microfluidic systems also offer potential for lower sample and reagent consumption.[13] To date, many microfluidic separators process cells by moving them from one laminar flow stream into a second with cell-free medium, as originally presented by Giddings.[14] This can be beneficial, for example

[a] *Department of Biomedical Engineering, Lund University, Box 118, SE-221 00 Lund, Sweden. E-mail: maria.antfolk@bme.lth.se, per.augustsson@bme.lth.se*
[b] *Departments of Laboratory Medicine, Surgery, and Medicine, Memorial Sloan Kettering Cancer Center, 1275 York Avenue, New York, NY, 10065, USA*
[c] *Nuffield Department of Surgical Sciences, University of Oxford, Oxford, OX3 7DQ, UK*
[d] *Department of Translational Medicine, Lund University, SE-205 02 Malmö, Sweden*
[e] *Department of Electrical Engineering and Computer Science, Massachusetts Institute of Technology, Cambridge, MA, USA*

† Electronic supplementary information (ESI) available. See DOI: 10.1039/c5lc00078e

when processing crude samples that need to be washed.[15–18] Multiple laminar flow streams are also used in cell separation to hydrodynamically pre-position the cells in the channel to increase resolution[19,20] or as part of the separation mechanism itself.[21,22] However, in many applications the inclusion of several laminar flow streams complicates the fluidic system of the chip, involving extra inlets, outlets and pumps, and an increased need for flow control. Furthermore, hydrodynamic pre-positioning of cells leads to high flow velocities in the separation channel, which is often a major limiting factor in terms of throughput and detector accuracy. Assuming that the separation channel is run at its limiting flow velocity, the sample volume throughput can be increased by replacing the hydrodynamic pre-positioning with an external field acting directly on the cells.

Acoustophoresis has been shown to be a robust, accurate and high-throughput method for performing unit operations on cells in suspension.[23] Furthermore, it is a gentle cell handling method that does not compromise cell viability or function, and allows for culturing and phenotypic characterization of the extracted cells.[24,25] In acoustophoresis-based cell separation, the sample is commonly laminated to the channel sides by a central stream of cell-free medium and the cells are then acoustically pushed into this cell-free medium. Cells are separated based on their acoustophoretic mobility, resulting in a cell-specific lateral displacement while flowing through the channel.[26–31]

However, the use of multiple inlet streams in acoustophoresis becomes complicated by the need to match the acoustic impedances of the fluids. The fluid with the highest acoustic impedance must be located where the acoustic standing wave pressure node is positioned. If not, the liquids themselves may relocate while flowing through the channel.[32] This relocation hampers the separation capabilities of the device, thus the acoustic impedance of the cell-free central laminar flow stream must be matched relative to the sample to be processed.

An optimal microfluidic system for isolation of CTCs should offer unbiased, label-free separation, simplicity in the fluidic setup and no need for matching the acoustic properties of liquids. Furthermore, it should perform high-throughput separation that can process clinically relevant sample volumes typically within an hour, yielding high recovery and purity of the collected sample. To meet this need, an acoustophoresis-based cell or particle sorter is now presented that is capable of separating cancer cells from white blood cells from a single inlet laminar flow stream. The separation is enabled through acoustic pre-alignment of the cells or particles in two dimensions[33,34] into well-defined positions and flow velocities before separation.

Separating or concentrating cells or particles using two-dimensional acoustic pre-alignment has previously been shown to be superior to separating without acoustic pre-alignment.[27,35,36] Here, instead of using a separate cell-free laminar flow stream for hydrodynamic pre-positioning of cells, ultrasound is used to acoustically pre-align the cells prior to separation while they remain in their initial suspending medium. This simplifies the fluidic setup, and also paves the way for an increased sample throughput since the sample input flow rate equals the total system flow rate during separation. This study demonstrates how both cancer cells and particles can be separated in this system.

Materials and methods

Device design

The chip was fabricated in <100> silicon using standard photolithography and anisotropic wet etching in KOH (0.4 g mL^{-1} H_2O, 80 °C). Holes for the inlet and outlets were drilled in the silicon using a diamond drill (Tools Sverige AB, Lund, Sweden) before sealing the chip by anodic bonding to a borosilicate lid. The microfluidic chip has a single inlet for cell suspension and two outlets for the separated cells (Fig. 1A).

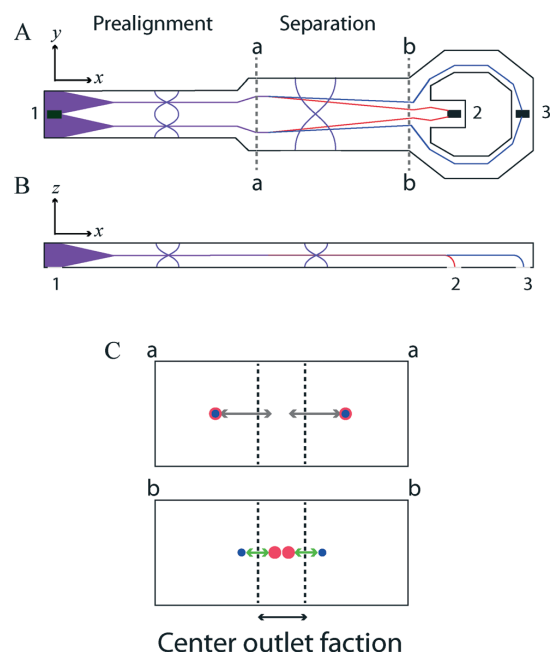

Fig. 1 Illustration of the chip and particle trajectories from (A) the top and (B) the side. Cells or particles are infused at (1) and are acoustically pre-aligned in two dimensions to two positions along the width (*y*-axis) of the chip and are at the same time levitated to mid-height (*z*-axis) of the channel (purple lines). The pre-aligned cells then enter the wider separation channel at (a–a), where the larger, denser, or less compressible cells are focused faster towards the center of the channel (red line). Thus, these cells or particles are separated from smaller, less dense, or more compressible cells (blue line) and the two different fractions can be collected in the two outlets (2) and (3). (C) The cross sections at (a–a) and (b–b) in A, where the grey arrows indicate the necessary sideways shift of a cell to exit through the central outlet and the green arrows indicate the cell–cell distance at (b–b). The dashed black lines indicate the center outlet flow stream, which can be tuned by adjusting the relative flow rates in the center outlet (2) with respect to the flow rate in (3).

The first part of the chip is a 23 mm long cell pre-alignment channel, etched to a width of 310 μm and a depth of 150 μm. The second part of the chip, the cell separation channel, is 22 mm long and etched to a width of 375 μm and a height of 150 μm. At the end of the channel, the flow is split in a trifurcation outlet where the central branch exits through the central outlet while the two side branches are recombined to a single side outlet. A photograph of the chip has been included as ESI† S1.

Underneath the pre-alignment and separation channels, piezoceramic transducers (PZ26, Ferroperm Piezoceramics, Kvistgaard, Denmark) were bonded to the back of the chip by cyanoacrylate glue (Loctite Super glue, Henkel Norden AB, Stockholm, Sweden). The pre-alignment channel was actuated at a frequency of 4.530 MHz and the separation channel was actuated at 2.001 MHz. To drive the ultrasound actuation, a dual-channel function generator (AFG 3022B, Tektronix UK Ltd., Bracknell, UK) was used and the signals were amplified using an in-house built power amplifier based on an LT1012 power amplifier (Linear Technology Corp., Milpitas, CA, USA) and a commercial amplifier (AG Series Amplifier, T&C Power Conversion Inc., Rochester, NY, USA). The applied voltage amplitudes over the piezoceramic transducers were monitored using an oscilloscope (TDS 2120, Tektronix UK Ltd.).

A constant temperature of 37 °C was maintained throughout all experiments through a feedback control loop using a Peltier-controller (TC2812, Cooltronic GmbH, Beinwil am See, Switzerland). A Peltier element (Farnell, London, UK) was glued underneath the 2 MHz actuator and a Pt1000 resistance temperature detector (Farnell) was glued to the chip surface.

Driving the flow

The flows in the inlet and outlets were controlled by glass syringes (Hamilton Bonaduz AG, Bonaduz, Switzerland) mounted on syringe pumps (Nemesys, Cetoni GmbH, Korbussen, Germany). The inlet flow rate was set to 100 μL min^{-1}, while the center outlet flow rate was set to 25 μL min^{-1} or 10 μL min^{-1} and the side outlet flow rate was correspondingly set to 75 μL min^{-1} or 90 μL min^{-1}, throughout the whole experiment. Samples were collected using two 2-position, 6-port valves connected in series with the center and side outlets. 100 μL of sample was collected in the loops of the valves.

Microparticles

The system was characterized using polystyrene particles of diameters 7 (7.11) μm and 5 (4.99) μm (Sigma-Aldrich, Buchs, Switzerland). The particles were suspended in PBS, with 0.002% Triton-X100 (Sigma-Aldrich, Switzerland) added to avoid aggregation, at a particle concentration on the order of 10^5 mL^{-1}.

Prostate cancer cells

Prostate cancer cell line DU145 was obtained from the American Type Culture Collection (ATCC, Manassas, VA, USA) and grown according to their recommendations. Briefly, RPMI-1640 medium (Sigma-Aldrich, Switzerland) was supplemented with 10% fetal bovine serum (Sigma-Aldrich, Switzerland), 55 IU mL^{-1} penicillin and 55 μg mL^{-1} streptomycin (Sigma-Aldrich, Switzerland). The cells were cultured at 37 °C in a humid atmosphere containing 5% CO_2. Before the experiments, 5×10^5 cells were detached using trypsin/EDTA, washed and resuspended in 80 μL FACS buffer (PBS supplemented with 1% BSA and 2 mM EDTA [pH 7.4]) to which was added 20 μL of direct conjugated EpCAM-PE antibody (BD Bioscience, San Jose, CA, USA) and incubated on ice for 25 minutes. The cells were then fixated using 2% PFA and incubated on ice for 10 minutes. Finally, the cells were resuspended in 50 μL FACS buffer and stored on ice until spiked in the white blood cell sample prior to experiments. The final concentration of the cancer cells was 5×10^4 cells per mL.

Blood samples

Blood was obtained, with informed consent, from healthy volunteers at the Lund University Hospital (Lund, Sweden) using vacutainer tubes (BD Bioscience) containing EDTA as an anticoagulant. Aliquots of 200 μL whole blood were incubated with 20 μL of direct conjugated CD45-APC (BD Bioscience) antibody for 25 minutes at room temperature. The red blood cells were then lysed using 2 mL BD FACS lysis buffer (BD Bioscience), diluted 1 : 10 in MilliQ H_2O, and incubated for 15 minutes at room temperature. The lysis was followed by fixation by incubating the cells in 2% PFA for 10 minutes on ice. Finally, the sample was resuspended in FACS buffer and stored on ice. The samples were diluted 10 times in FACS buffer and spiked with the cancer cells just prior to the acoustophoresis experiments.

Sample analysis

The samples collected from the center and side outlets during each run through the acoustophoresis chip were stored on ice until analysis with FACS Canto or FACS Canto II (BD Bioscience). White blood cells were characterized as CD45-positive and EpCAM-negative, and the cancer cells were characterized as CD45-negative and EpCAM-positive. To calculate the separation efficiency, the number of cells collected in the central outlet was compared to the total number of collected cells from the central and the side outlets during each run.

Flow and separation simulations

Matlab2014a (MathWorks, Natick, MA, USA) was used to calculate the flow profile and particle trajectories as they were subjected to an acoustic field.

Results and discussion

In this paper an acoustophoresis system is presented that is able to separate 5 *versus* 7 μm particles or cancer cells from white blood cells from a single inlet laminar flow stream. Our main objective was to investigate how the reduced complexity of the acoustofluidic set-up affected the separation performance compared to previously described systems for acoustic separation, which use multiple inlet hydrodynamic pre-positioning.

Operating principle

The chip utilizes an acoustic pre-alignment channel of width w = 300 μm to position the cells or particles to be separated to two points in the plane transverse to the flow. The acoustic field of the pre-alignment channel has two pressure minima located at distances 1/4w away from each side-wall (Fig. 1A) and which are elevated to mid-height above the channel floor (Fig. 1B). The pre-alignment of the cells is vital for the operation of this system, as only a modest acoustic separation result can be achieved if the cells are randomly distributed in the transverse cross-section upon entering the separation channel. This initial acoustic pre-alignment of the sample eliminates the need for the otherwise essential central inlet cell-free liquid used to hydrodynamically pre-position the cells towards the channel walls prior to the separation step. We have provided a schematic functional comparison between this single-inlet acoustophoresis system and systems using hydrodynamic pre-positioning in the ESI† S2.

After acoustic pre-alignment the sample enters the separation channel where particles are focused towards the channel center in an acoustic field having a single centrally located pressure node. Particles or cells that are large, have high density or are of low compressibility move faster in the acoustic field than particles that are small, light and compressible. By correct matching of the flow rate and the acoustic amplitude, the particles of high mobility can be collected in the central outlet of the separation channel (outlet 2 in Fig. 1A & B) while slow-moving particles are collected in the combined side outlet (outlet 3 in Fig. 1A & B).

The acoustic pre-alignment of particles in two dimensions assures that all particles experience identical initial flow conditions, which leads to deterministic separation that is undistorted by the flow velocity distribution in the channel. That is, a particle's sideways deflection in the acoustic field will truly reflect its acoustofluidic mobility, which depends on particle, size morphology, density and compressibility as well as the viscosity, density and compressibility of the suspending liquid.

Without acoustic pre-alignment, the retention time of a particle in the acoustic field depends strongly on its position in the width and height of the channel, due to the flow velocity profile in the channel (see ESI† S3). For instance, in a system without acoustic pre-alignment, a particle of low acoustic mobility that flows slowly near the bottom of the channel experiences the acoustic field for a longer time than a particle of high acoustic mobility flowing in a high flow rate region. Since the sideways deflection is then a function of both the acoustic mobility of the cell and the retention time in the field, the two different particles could end up in the same outlet.[27]

Numerical separation optimization

To find the optimal separation conditions, particle trajectories were computed taking into account both the flow velocity distribution in the microchannel and the acoustic radiation force acting transversely to the flow. Such trajectories were first described by Mandralis and Feke[37] for a parallel-plate channel geometry. A comprehensive theoretical framework governing the motion of a particle in an acoustic field inside a channel with the dimensions used in this work can be found in Barnkob *et al.*,[38] for a no-flow condition.

The microchannel flow is governed by the Hagen–Poiseuille equation, for which there exists no exact analytical solution for a rectangular geometry, so the positions of the particles were computed numerically in short time-steps. The fundamental assumptions were that the velocity of a particle in the direction of the channel is always the same as the flow velocity at that point, and that the particle velocity orthogonal to the flow is only governed by the acoustic radiation force. A code example for execution in MATLAB® is shown in the supplementary files *exampletrajectory.m*, *poiseuille.m*, and *acoustopath.m*.

Fig. 2A shows the trajectories of a 5 and a 7 μm particle for identical starting positions after acoustic pre-alignment. For a given outlet flow rate configuration, the optimal separation can be assumed to occur when the two particles are located on opposite sides and at an equal distance from the virtual interface between the central and the side outlet flow

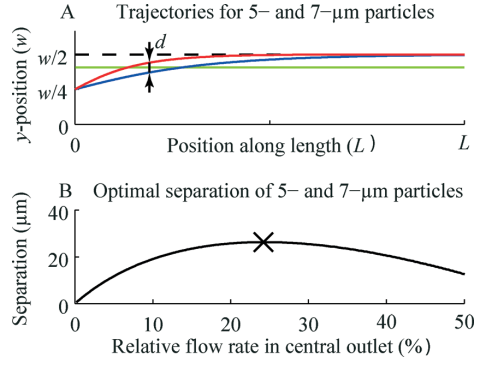

Fig. 2 (A) Simulated trajectories of 5 μm (blue) and 7 μm (red) polystyrene microparticles starting from an initial position of ideal acoustic pre-alignment in width and height. Arrows indicate the point of maximal separation (d), the dashed black line indicates the channel center, and the green line indicates the interface between the side and central outlet flow streams. (B) Plot showing the maximum achievable particle–particle distance *versus* the relative center outlet flow rate when separating pre-aligned 5 and 7 μm particles.

streams. For each point along the length of the channel in Fig. 2A, the mean transverse position of each of the two particles was calculated. The central outlet volume flow rate, corresponding to these mean positions, was then derived by integrating the flow velocity profile from each position to the center of the channel.

Fig. 2B shows the result of a simulation of the separation distance of 5 μm and 7 μm particles at the end of the separation channel *versus* the relative central outlet volume flow rate. The longest particle–particle distance after separation will be reached when the center outlet flow rate is set to 24.2% of the total flow. The particle–particle distance after separation is in this case 26.3 μm. The reason that the separation optimum does not correspond to the longest sideways deflection is explained by considering the acoustophoretic velocity with which the particles travel towards the channel center. The acoustic radiation force on a particle varies sinusoidally over the width w of the channel and produces maximum velocity for a particle at the symmetrically equivalent positions $1/4w$ and $3/4w$.[39] After passing this position ($1/4w$ or $3/4w$), the velocity gradually decreases until it reaches zero at the channel center. As the larger particle reaches the central region of the channel, its velocity will at some point become lower than that of a smaller trailing particle, thus reducing the inter–particle distance. Hence, a maximum inter–particle distance can be found with respect to exposure time in the acoustophoresis zone.

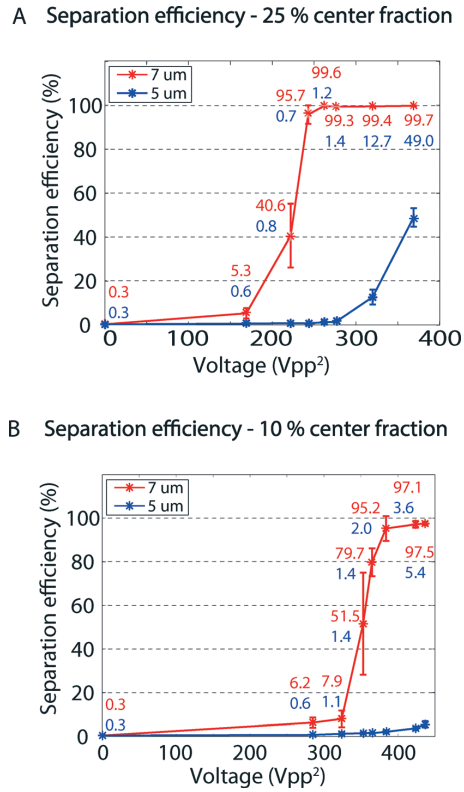

Fig. 3 (A) Separation efficiency of 5 μm *versus* 7 μm polystyrene particles when extracting 25% of the total flow in the center outlet. The total sample flow rate was 100 μL min^{-1} and the particles were collected through the center outlet with a flow rate of 25 μL min^{-1}. (B) Separation efficiency of 5 μm and 7 μm polystyrene particles when taking out 10% of the total fluid flow in the center outlet. The total sample flow rate was 100 μL min^{-1} and the particles were collected through the center outlet with a flow rate of 10 μL min^{-1}. The error bars represents the standard deviation for n = 3.

Characterization

5 and 7 μm polystyrene particles were used because they have been observed to move at rates similar to those of white blood cells and cancer cells, respectively, when influenced by an acoustic field.[27] Therefore, to determine the system separation characteristics, we used equal number concentrations of the two sizes of particles. The outlet flows were configured according to the optimal settings from the simulations withdrawing 25% of the total flow from the central outlet. The separation efficiency of 5 and 7 μm polystyrene particles was investigated by gradually increasing the applied voltage to the transducer.

Increasing the sound intensity leads to a higher acoustic migration velocity, which has been shown to increase linearly with the square of the applied transducer voltage.[38,40] Since the acoustic migration velocity is also proportional to the square of the particle diameter[39,40] the 7 μm particles can be expected to move towards the channel center with approximately twice the velocity as that of the 5 μm particles.

Fig. 3A shows the separation efficiency as the proportion of particles collected in the center outlet (outlet 2 in Fig. 1) compared to the total number of collected particles of that type in the center and side outlets combined (outlets 2 and 3, respectively, in Fig. 1). The larger 7 μm particles have a lower transition voltage, above which they exit through the central outlet, than do the 5 μm particles. At voltage amplitudes (peak to peak) between about 240 V^2 and 275 V^2, the vast majority of the 7 μm particles could be collected in the center outlet while the majority of the 5 μm particles were collected through the side outlet. At 262 V^2, 99.6 ± 0.2% of the 7 μm particles were collected through the center outlet while 98.8 ± 0.5% of the 5 μm particles were collected through the side outlet. The initial purity of 50% for each particle size leads to enrichment factors of 10^2, reflecting this system's deterministic separation capability. In acoustophoresis, this high enrichment factor in combination with the 2 μm particle size difference has previously only been achieved using a combination of multiple-inlet hydrodynamic pre-positioning and acoustic pre-alignment.[27]

According to the simulations, a lower central outlet flow rate, *i.e.*, a larger sideways shift for the particles, should not further improve the separation efficiency since the particle–particle distance after separation will not be greater. To investigate this, the separation experiments of 5 μm and 7 μm

particles were repeated. The center outlet flow rate was now set to 10 μL min^{-1} and the side outlet flow rate was set to 90 μL min^{-1}, and thus a total sample flow rate of 100 μL min^{-1} was maintained.

Fig. 3B shows the proportion of particles recovered in the center outlet for the narrow central outlet stream. The transition voltage of the 7 μm particles is now higher and the best separation was achieved for voltage amplitudes ranging from 380 V^2 to 420 V^2. At 380 V^2, 95.2 ± 5.7% of the 7 μm particles are collected in the center outlet while 98 ± 0.7% of the 5 μm particles exit through the side outlet. The higher transition voltage can be explained by the longer sideways shift that the particles have to make to exit the central outlet when only 10% instead of 25% of the total flow rate is extracted through the center outlet. As anticipated, the longer separation distance did not further improve the separation efficiency.

A system dependent on both hydrodynamic pre-positioning and acoustic pre-alignment has the apparent advantage that the cell-free liquid places the pre-positioned cells closer to the channel walls, which theoretically increases the resolution. However, the experimental separation efficiency presented in this paper is comparable to that reported by Augustsson *et al.*,[27] using combined acoustic pre-alignment and hydrodynamic pre-positioning. This suggests that the shorter sideways shift is compensated for by the more stable flow system, something that is more easily attainable with fewer inlets and outlets.

Enrichment of tumor cells spiked into white blood cells

The system was further evaluated for its ability to enrich tumor cells from white blood cells to assess whether this system may be useful to isolate CTCs from patient samples. In this *in vitro* model prostate cancer cells (cell line, DU145) were spiked at final concentrations of 5×10^4 mL^{-1} into white blood cell fractions from red blood cell-lysed whole blood. Although the levels of CTCs anticipated in patient samples, as measured by epithelial cell maker-affinity based capture, are commonly two to three magnitudes lower (1–1000 cells per mL) the higher cell concentrations used herein enables the use of conventional flow cytometry to determine tumor cell recovery and purity. Also, from a mechanistic perspective, tumor cell recovery as reported herein is not compromised by 10–100 fold lower concentrations of cancer cells. The total sample flow rate was set to 100 μL min^{-1} and the center outlet flow rate was set to 25 μL min^{-1} as determined from simulations and experiments using particles. To save sample and reagents, the level of white blood cells in the samples was one tenth of that of whole blood; however, it has previously been shown that there was no difference in the performance of the acoustophoretic separation using a ten-fold dilution of white blood cells as compared with undiluted samples.[27]

Fig. 4 shows the results from the cell separation experiment. The transition voltage for cancer cells to exit through the center outlet is lower than for the white blood cells,

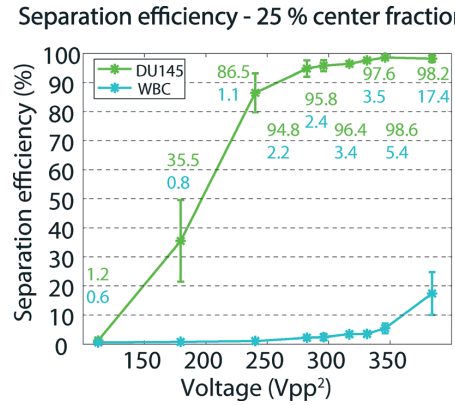

Fig. 4 Separation efficiency of prostate cancer cell line, DU145, and white blood cells (WBC) when extracting 25% of the total flow in the center outlet. The total sample flow rate was 100 μL min^{-1} and the cells were collected through the center outlet with a flow rate of 25 μL min^{-1}. The error bars represents the standard deviation for $n = 3$.

which are smaller. The two cell populations displayed partially overlapping acoustophoretic mobility and could thus not be perfectly separated by this system. Even so, by proper adjustment of the transducer voltage, high recovery of cancer cells could be accomplished while discriminating them from the white blood cells. At 240 V^2, 86.5 ± 6.7% of the cancer cells were collected in the center outlet with a contamination of only 1.1 ± 0.2% white blood cells. At 280 V^2, there was two-fold higher white blood cell contamination (2.2 ± 0.6%), but 94.8 ± 2.8% of the cancer cells could be recovered in the center outlet. These separation levels are comparable to previous results using acoustophoresis together with hydrodynamic pre-positioning.[27] The current system, however, provides a simpler microfluidic setup as well as faster sample processing flow rate of 6 mL h^{-1}, even though the flow rate has not been fully optimized. The simpler fluidic setup, not involving a second liquid flow, leads to a concentration of the cells instead of a dilution as will most often happen when hydrodynamic pre-positioning is used. When separating rare cells such as circulating tumor cells the sample will most likely need to be concentrated before analysis. The possibility to concentrate the sample directly on the chip instead of diluting it is thus a further advantage.

The acoustophoretic velocity of a cell scales with the size to the power of two.[41] The leukocyte size distribution, as previously measured by impedance cytometry (Coulter counter), range from 7–14 μm while the cancer cells range from 15–25 μm (data not shown), and are thus not overlapping in size. Given the strong size dependence and the distinct size difference of the populations, the separation is likely predominantly based on size.

The experiments and simulations presented here indicate that this method in its current manifestation holds promise,

in terms of throughput and accuracy, for further development toward isolation of CTC from patient blood samples. Given the relative rareness of CTCs in patient blood, a 100- to 1000-fold reduction of white blood cells will not allow for direct label-free enumeration of CTCs but the method can be an important unit in a sequence of isolation steps. Further refinements to increase the purity of the isolated cells relative to the white blood cells would be of value to expand its applicability.

Based on the findings, two measures may be taken to further improve the accuracy and throughput to shorten the sample-to-answer time and to make the separation truly deterministic. First, the acoustic pre-alignment channel can be elongated at the expense of the separation channel. In the separation channel, the cells of higher acoustic migration rate must be deflected sideways only a short distance while in the pre-alignment channel all cells must be transferred from their initial random positions in the channel cross-section to the two pre-alignment locations. Second, the separation channel can be widened to improve the separation performance. By doing this, the sideways displacement of the cells increases, leading to a longer absolute distance between separated cells at the outlet. Simulations show that increasing the width of the separation channel to 750 μm, and actuating at the corresponding frequency of 1 MHz, leads to a doubled distance between the separated particles at the outlet (see ESI† S4). This increased distance is anticipated to improve overall separation performance and reduce the sensitivity to phenomena such as flow fluctuations or long-term drift.

Conclusions

This paper presents a simple microfluidic cell sorter for continuous-flow, unbiased, label-free separation of cancer cells from white blood cells based on acoustophoresis. Even though the lateral displacement of a particle in the acoustic field is less than 50 μm, the platform can separate cells and particles with high precision. The single inlet approach leads to simple and robust flow conditions for acoustic pre-alignment and separation of cells.

An advantage of this system is that separation is carried out directly in the particles' suspending medium and thus does not require matching of the acoustic properties of the sample relative to a system using multiple laminar flow streams.

This system also paves the way for increased sample throughput, currently enabling clinical sample processing up to 6 mL h^{-1}, since the sample inflow rate equals the total flow rate of the system. This is in contrast to devices relying on hydrodynamic pre-positioning of cells where the volume flow of cell-free medium adds to the net flow velocity of the particles in the separation channel, limiting the sample throughput.

Acknowledgements

The authors would like to thank Dr. Cecilia Magnusson for the generous gift of the DU145 cells. The work was supported by the Swedish governmental agency for innovation systems, VINNOVA, CellCARE (grant no. 2009-00236), Knut and Alice Wallenberg Foundation (grant no. KAW 2012.0023), the Swedish Research Council (grants no. 621-2010-4389, 2012-6708, and 637-2013-444), Swedish Cancer Society (grants no. 11-0624 and 14-0722) the Sten K Johnson Foundation, the Royal Physiographic Society, the Crafoord Foundation, and the Carl Trygger Foundation, the National Cancer Institute at the National Institutes of Health (P50 CA092629); the Sidney Kimmel Center for Prostate and Urologic Cancers; David H. Koch through the Prostate Cancer Foundation; the National Institute for Health Research (NIHR) Oxford Biomedical Research Centre Program in UK; and Fundacion Federico SA The funding sources did not have any role in the design or conduct of the study; the collection, management, analysis, or interpretation of the data; or the preparation, review, or approval of the manuscript.

References

1 K. Christensen, G. Doblhammer, R. Rau and J. W. Vaupel, *Lancet*, 2009, **374**, 1196–1208.
2 P. Mehlen and A. Puisieux, *Nat. Rev. Cancer*, 2006, **6**, 449–458.
3 K. Pantel, R. H. Brakenhoff and B. Brandt, *Nat. Rev. Cancer*, 2008, **8**, 329–340.
4 D. C. Danila, A. Anand, N. Schultz, G. Heller, M. Wan, C. C. Sung, C. Dai, R. Khanin, M. Fleisher, H. Lilja and H. I. Scher, *Eur. Urol.*, 2014, **65**, 1191–1197.
5 M. Cristofanilli, G. T. Budd, M. J. Ellis, A. Stopeck, J. Matera, M. C. Miller, J. M. Reuben, G. V. Doyle, W. J. Allard, L. W. M. M. Terstappen and D. F. Hayes, *N. Engl. J. Med.*, 2004, **351**, 781–791.
6 A. D. Rhim, E. T. Mirek, N. M. Aiello, A. Maitra, J. M. Bailey, F. McAllister, M. Reichert, G. L. Beatty, A. K. Rustgi, R. H. Vonderheide, S. D. Leach and B. Z. Stanger, *Cell*, 2012, **148**, 349–361.
7 T. M. Gorges, I. Tinhofer, M. Drosch, L. Röse, T. M. Zollner, T. Krahn and O. von Ahsen, *BMC Cancer*, 2012, **12**, 178.
8 W. Zhang, K. Kai, D. S. Choi, T. Iwamoto, Y. H. Nguyen, H. Wong, M. D. Landis, N. T. Ueno, J. Chang and L. Qin, *Proc. Natl. Acad. Sci. U. S. A.*, 2012, **109**, 18707–18712.
9 L. Mazutis, J. Gilbert, W. L. Ung, D. A. Weitz, A. D. Griffiths and J. A. Heyman, *Nat. Protoc.*, 2013, **8**, 870–891.
10 M. G. Lee, J. H. Shin, C. Y. Bae, S. Choi and J.-K. Park, *Anal. Chem.*, 2013, **85**, 6213–6218.
11 J. P. Beech, S. H. Holm, K. Adolfsson and J. O. Tegenfeldt, *Lab Chip*, 2012, **12**, 1048–1051.
12 A. A. S. Bhagat, H. Bow, H. W. Hou, S. J. Tan, J. Han and C. T. Lim, *Med. Biol. Eng. Comput.*, 2010, **48**, 999–1014.
13 H. Tsutsui and C.-M. Ho, *Mech. Res. Commun.*, 2009, **36**, 92–103.
14 J. C. Giddings, *Sep. Sci. Technol.*, 1985, **20**, 749–768.
15 P. Augustsson, J. Persson, S. Ekström, M. Ohlin and T. Laurell, *Lab Chip*, 2009, **9**, 810–818.
16 D. R. Gossett, H. T. K. Tse, J. S. Dudani, K. Goda, T. A. Woods, S. W. Graves and D. Di Carlo, *Small*, 2012, **8**, 2757–2764.
17 F. Petersson, A. Nilsson, H. Jönsson and T. Laurell, *Anal. Chem.*, 2005, **77**, 1216–1221.

18 J. Persson, P. Augustsson, T. Laurell and M. Ohlin, *FEBS J.*, 2008, **275**, 5657–5666.
19 B. D. Plouffe, M. Mahalanabis, L. H. Lewis, C. M. Klapperich and S. K. Murthy, *Anal. Chem.*, 2012, **84**, 1336–1344.
20 S. H. Ling, Y. C. Lam and K. S. Chian, *Anal. Chem.*, 2012, **84**, 6463–6470.
21 J. Takagi, M. Yamada, M. Yasuda and M. Seki, *Lab Chip*, 2005, **5**, 778–784.
22 Z. Wu, B. Willing, J. Bjerketorp, J. K. Jansson and K. Hjort, *Lab Chip*, 2009, **9**, 1193–1199.
23 A. Lenshof, C. Magnusson and T. Laurell, *Lab Chip*, 2012, **12**, 1210–1223.
24 M. Burguillos, C. Magnusson, M. Nordin, A. Lenshof, P. Augustsson, M. Hansson, E. Elmér, H. Lilja, P. Brundin, T. Laurell and T. Deierborg, *PLoS One*, 2013, **8**, e64233.
25 M. Wiklund, *Lab Chip*, 2012, **12**, 2018–2028.
26 J. Dykes, A. Lenshof, I.-B. Åstrand-Grundström, T. Laurell and S. Scheding, *PLoS One*, 2011, **6**, e23074.
27 P. Augustsson, C. Magnusson, M. Nordin, H. Lilja and T. Laurell, *Anal. Chem.*, 2012, **84**, 7954–7962.
28 F. Petersson, L. B. Åberg, A.-M. K. Swärd-Nilsson and T. Laurell, *Anal. Chem.*, 2007, **79**, 5117–5123.
29 Y. Ai, C. K. Sanders and B. L. Marrone, *Anal. Chem.*, 2013, **85**, 9126–9134.
30 J. Nam, H. Lim, D. Kim and S. Shin, *Lab Chip*, 2011, **11**, 3361–3364.
31 X. Ding, Z. Peng, S.-C. S. Lin, M. Geri, S. Li, P. Li, Y. Chen, M. Dao, S. Suresh and T. J. Huang, *Proc. Natl. Acad. Sci. U. S. A.*, 2014, **111**, 12992–12997.
32 S. Deshmukh, Z. Brzozka, T. Laurell and P. Augustsson, *Lab Chip*, 2014, **14**, 3394–3400.
33 G. R. Goddard and G. Kaduchak, *J. Acoust. Soc. Am.*, 2005, **117**, 3440.
34 O. Manneberg, J. Svennebring, H. M. Hertz and M. Wiklund, *J. Micromech. Microeng.*, 2008, **18**, 095025.
35 O. J. E. Jakobsson, C. Grenvall, M. Nordin, M. Evander and T. Laurell, *Lab Chip*, 2014, **14**, 1943–1950.
36 M. Nordin and T. Laurell, *Lab Chip*, 2012, **12**, 4610–4616.
37 Z. I. Mandralis and D. L. Feke, *Chem. Eng. Sci.*, 1993, **48**, 3897–3905.
38 R. Barnkob, P. Augustsson, T. Laurell and H. Bruus, *Lab Chip*, 2010, **10**, 563–570.
39 R. Barnkob, P. Augustsson, T. Laurell and H. Bruus, *Phys. Rev. E: Stat., Nonlinear, Soft Matter Phys.*, 2012, **86**, 056307.
40 M. Antfolk, P. B. Muller, P. Augustsson, H. Bruus and T. Laurell, *Lab Chip*, 2014, **14**, 2791–2799.
41 R. Barnkob, P. Augustsson, T. Laurell and H. Bruus, *Lab Chip*, 2010, **10**, 563–570.

Paper IV

Acoustofluidic, label-free separation and simultaneous concentration of rare tumor cells from white blood cells
Maria Antfolk, Cecilia Magnusson, Per Augustsson, Hans Lilja, and Thomas Laurell
Analytical Chemistry, 2015, 87(18): 9322-9328.

Paper IV

analytical chemistry

Article

pubs.acs.org/ac

Acoustofluidic, Label-Free Separation and Simultaneous Concentration of Rare Tumor Cells from White Blood Cells

Maria Antfolk,*[,†] Cecilia Magnusson,[‡] Per Augustsson,[†,§] Hans Lilja,[‡,∥,⊥,#] and Thomas Laurell*[,†]

[†]Department of Biomedical Engineering, Lund University, Ole Römers väg 3, 22363 Lund, Sweden

[‡]Department of Translational Medicine, Lund University, Jan Waldenströms gata 35, 205 02 Malmö, Sweden

[§]Department of Electrical Engineering and Computer Science, Massachusetts Institute of Technology, 77 Massachusetts Avenue, Cambridge, Massachusetts 02139, United States

[∥]Department of Laboratory Medicine, Surgery (Urology), and Medicine (GU Oncology), Memorial Sloan Kettering Cancer Center, 1275 York Avenue, New York, New York 10065, United States

[⊥]Nuffield Department of Surgical Sciences, University of Oxford John Radcliffe Hospital, Headington, Oxford OX3 9DU, United Kingdom

[#]Institute for Biosciences and Medical Technology, University of Tampere, Biokatu 10, 33520 Tampere, Finland

Supporting Information

ABSTRACT: Enrichment of rare cells from peripheral blood has emerged as a means to enable noninvasive diagnostics and development of personalized drugs, commonly associated with a prerequisite to concentrate the enriched rare cell population prior to molecular analysis or culture. However, common concentration by centrifugation has important limitations when processing low cell numbers. Here, we report on an integrated acoustophoresis-based rare cell enrichment system combined with integrated concentration. Polystyrene 7 μm microparticles could be separated from 5 μm particles with a recovery of 99.3 ± 0.3% at a contamination of 0.1 ± 0.03%, with an overall 25.7 ± 1.7-fold concentration of the recovered 7 μm particles. At a flow rate of 100 μL/min, breast cancer cells (MCF7) spiked into red blood cell-lysed human blood were separated with an efficiency of 91.8 ± 1.0% with a contamination of 0.6 ± 0.1% from white blood cells with a 23.8 ± 1.3-fold concentration of cancer cells. The recovery of prostate cancer cells (DU145) spiked into whole blood was 84.1 ± 2.1% with 0.2 ± 0.04% contamination of white blood cells with a 9.6 ± 0.4-fold concentration of cancer cells. This simultaneous on-chip separation and concentration shows feasibility of future acoustofluidic systems for rapid label-free enrichment and molecular characterization of circulating tumor cells using peripheral venous blood in clinical practice.

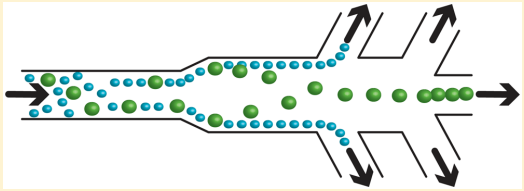

Microfluidics has been extensively used for cell separation and processing.[1] Separation of rare cells, such as separation of nucleated fetal cells from maternal blood or circulating tumor cells (CTCs) from the blood of cancer patients, is an area of emerging interest.[2] CTCs are very rare cells that have been shed from a cancer tumor, mostly found in quantities of only 1−10 CTC/mL in blood, but higher quantities have been reported. They can travel to secondary tissues, but only few of them may have the potential to form metastases. CTCs are of interest as prognostic and diagnostic markers. However, they also reflect the evolution of the tumor during disease progression, and they are used as an indicator of response to treatment. Hence, CTC containing blood samples provide a noninvasive means for studying the primary tumor as well as for studying metastasis biology: they can thereby provide information that helps to target and personalize treatment.[3,4] CTCs can be detected in blood from patients harboring all major cancer types at advanced metastatic stages but are very rarely or never detected in healthy subjects.[4−6] In many types of cancer, the quantity of CTCs found in the blood has been shown to be an independent predictor of disease progression.[3]

Most investigations attempting to isolate and enumerate CTCs have focused on carcinoma patients, due to the common nature of these cancers and because they express markers that can enable their detection. So far, other cancer forms have not provided any universal markers for detection although vimentin expressed at the cell surface has recently been reported as a marker for sarcoma.[7] Although some CTCs stemming from carcinomas can be detected using epithelial cell specific markers, such as EpCAM in combination with cytokeratins, the use of these markers may allow subpopulations expressing low EpCAM or cytokeratins to remain undetected. For epithelial cancers, the epithelial-mesenchymal transition is

Received: May 30, 2015
Accepted: August 26, 2015
Published: August 26, 2015

DOI: 10.1021/acs.analchem.5b02023
Anal. Chem. 2015, 87, 9322−9328

considered to be the crucial event in the shedding of circulating tumor cells from the primary site of the tumor. In this transition, the cells adopt a more mesenchymal-like migratory phenotype, which might include loss of epithelial cell markers and thereby disabling detection by clinical routine assays.[8]

Microfluidics has been extensively used as a means of isolating CTCs.[9,10] These systems provide low sample and reagent consumption, which reduces sample processing costs. The microchannel length scale matches the cells' length scale, providing the opportunity to more accurately control cell position within the channels and thereby better facilitate cell separation.[11] However, most microfluidic isolation systems rely upon epithelial cell markers such as EpCAM or more specific markers that target a specific phenotype. Techniques used include microvortex-generating herringbone chip using EpCAM antibodies,[12] nanostructured silicon with bound EpCAM antibodies and chaotic micromixers,[13] isolation using EpCAM-antibody-bound magnetic beads,[14] and prostate specific membrane antigen antibody-covered microposts.[15] Others have used negative selection in combination with inertial focusing and magnetophoresis to deplete nucleated white blood cells from samples using specific antibodies.[16] Due to imperfect binding chemistry caused by under-expression of target cell surface molecules, both positive and negative selection schemes can lead to either the loss of tumor cells or contamination of unwanted subpopulations. Efficient, label-free methods would eliminate these problems, potentially to a lower cost per sample.

Label-free methods for CTC isolation include Dean flow in combination with a slanted microchannel,[17] microvortices,[18] optically induced-dielectrophoresis,[19] acoustophoresis,[20,21] and flow fractionation.[22] Although these techniques show promise in isolating all tumor cells in blood without cell-type specific markers, further analysis of the collected samples still poses challenges, as the exceedingly rare cells are collected in a highly dilute sample aliquot. In an attempt to solve this problem, Mach et al.[18] used fluid vortices to trap cells passively. Despite a relatively low capture efficiency of 20% of cancer cells, the system had the advantage of being able to simultaneously concentrate the cells 20-fold. Still, there is a need for a label-free system that can simultaneously separate and concentrate target cells with both high efficiency and concentration factors.

In an attempt to address this problem, this paper presents a label-free, gentle[23−25] cell handling method based on acoustophoresis[26−29] using ultrasound to simultaneously prealign, separate, and concentrate cancer cells from nucleated white blood cells. The method isolates cells primarily by size but also by density and compressibility[30] and is applicable to all cancer forms, with different properties than white blood cells, that undergo vascular invasion. This new method integrates in a single unit the functionality of two previously reported devices for microfluidic chip-based tumor cell separation[25] and tumor cell concentration[31] offering simultaneous separation and concentration of rare target cells from a mixed population. The system demonstrates well the flexibility offered in acoustofluidic systems to combine multiple unit operations and highlights that subunit matching is feasible for flow rates ranging up to 2 orders of magnitude within one device.

MATERIALS AND METHODS

Device Design and Chip Fabrication. A chip was fabricated in ⟨100⟩ oriented silicon using photolithography and anisotropic wet etching in KOH (0.4 g/mL H_2O, 80 °C). Subsequently, holes for the inlets and outlets were drilled using a diamond drill (Tools Sverige AB, Lund, Sweden), and the chip was sealed by anodic bonding of a glass lid.

The chip was supplied with two inlets, a sample inlet and a subsequent sheath buffer inlet, and three outlets. The sample inlet channel comprised an acoustic prealignment zone of width and height dimensions ∼310 μm by 150 μm, followed by a separation zone after the sheath buffer inlet of dimensions 375 μm by 150 μm. This continued into a concentration zone of dimensions 375 μm by 150 μm. The prealignment zone, the separation zone, and the concentration zone were 20, 25, and 10 mm long, respectively. The prealignment zone was actuated using an ultrasound frequency of 4.91 MHz and a voltage of 10 V. The separation and concentration zone was actuated using a frequency of 1.99 MHz and varying voltage. Actuation was accomplished using piezoceramic transducers (PZ26, Ferroperm piezoceramics, Kvistgaard, Denmark). Chip temperature was controlled using a Peltier element (Farnell, London, UK) and a Pt1000 temperature sensor (Farnell, London, UK).

Instrument Setup. To drive the actuation, a dual-channel function generator (AFG 3022B; Tektronix UK Ltd., Bracknell, UK) was used and signals were amplified using two power amplifiers built in-house and based on an LT1012 power amplifier (Linear Technology Corp., Milpitas, CA, USA). The applied voltages were monitored using an oscilloscope (TDS 2120, Tektronix), and temperature was controlled using a Peltier-controller (TC2812; Cooltronic GmbH, Beinwil am See, Switzerland). Flow rates were controlled using a pressure system built in-house and in which a sample could be infused and collected in 5 mL FACS tubes.[32] The temperature of the system was set to 37 °C throughout the experiment.

Microparticles. The system was characterized using polystyrene particles 7 μm (Sigma-Aldrich, Buchs, Switzerland) and 5 μm (Sigma-Aldrich) in diameter. The particles were suspended in PBS with 0.002% Triton-X100 added to avoid aggregation, at a particle concentration on the order of 10^5 /mL.

Cell Culture and Blood Samples. Prostate cancer cell line DU145 and breast cancer cell line MCF7 were used for the experiments. The cell lines were acquired from ATCC and cultured according to their guidelines. Blood was collected from healthy donors, with informed consent, at Skåne University Hospital in Lund, Sweden.

Cell Preparations. Cultured cancer cells were harvested with trypsin/EDTA and stained with EpCAM-PE (BD Biosciences) for 25 min in room temperature. Cells were fixed with 1% ice cold PFA, then washed, and suspended in FACS buffer (1× PBS, 1% FBS, 2 mM EDTA). The cells were stored on ice until acoustophoresis processing.

Daily fresh blood from healthy donors, obtained in vacutainer tubes containing EDTA as anticoagulant, was used for the separation experiments. Red blood cells were lysed with BD FACS lysing solution (BD Biosciences) for 15 min in room temperature. White blood cells (WBCs) were stained with CD45-APC (BD Biosciences) for 25 min in room temperature and fixed with 1% PFA. Cells were washed, suspended in FACS buffer, and stored on ice until acoustophoresis processing.

Separation and Volume Concentration Experiments. The separation efficiency was determined by prealigning the cells or particles at a fixed voltage of 10 V throughout the experimental series. The voltage in the separation zone varied between 0 and 12 V to obtain different cells or particles in the center and side outlets, respectively.

DOI: 10.1021/acs.analchem.5b02023
Anal. Chem. 2015, 87, 9322−9328

In the volume concentration experiments, a fixed voltage where separation was considered optimal was chosen for the separation zone and the flow rates in the outlets were varied to obtain different concentration factors (Table 1). The final concentration of the cells and particles were obtained by measuring the sample input and output volumes and take into account the recovery. The relative particle composition between the outlets was then investigated using a FACS (FACS Canto II, BD Bioscience).

Table 1. Flow Rates Used in the Different Concentration Experiments[a]

concentration	inlet (a) (μL/min)	inlet (b) (μL/min)	outlet (1) (μL/min)	outlet (2) (μL/min)	outlet (3) (μL/min)
5-fold	100	120	200	0	20
10-fold	100	120	200	10	10
20-fold	100	120	200	15	5
50-fold	100	120	200	18	2

[a]The outlets are numbered according to Figure 1.

RESULTS AND DISCUSSION

An integrated separation and concentration device for label-free rare cell separation was developed. To characterize the platform, mixed populations of either microbeads of different sizes or cells from blood and culture were processed and subsequently analyzed off chip.

Chip Design and Operating Principle. The device used ultrasound standing waves to prealign, separate, and concentrate cells and particles (Figure 1). The sample was infused through inlet (a) and prealigned both horizontally and vertically (*y*- and *z*-directions Figure 1) into two acoustic nodes. The nodes were located at one-quarter of the channel width away from each sidewall and at one-half the channel height between the bottom of the channel and the glass lid. Two-dimensional prealignment ensured that all of the particles were located in the same flow velocity regime within the parabolic flow profile: this made separation more efficient than the one-dimensional hydrodynamic prealignment commonly used in acoustophoresis.[21,25,33] Thus, all of the particles had the same retention time in the separation zone, which limited any decrease in separation efficiency caused by particles moving with different velocities.

After prealigment, the particles entered the separation channel. By infusing a cell-free liquid through inlet (b), the prealigned particles were hydrodynamically laminated close to the sidewalls. A single node standing wave deflected particles toward the channel center so that at the end of the channel the sideways location reflects the acoustic contrast and size of the particle. To avoid medium switching, in which the sample-containing liquid and the cell-free liquid change place, the cell-free liquid must have equal or higher acoustic impedance than the sample-containing liquid.[26,32] In the experiments reported herein, to avoid this, the suspending liquid for the particles was the same as the cell-free central sheath liquid.

At the end of the separation channel, particles of small acoustic sideways displacement were discarded through outlet (1) (Figure 1, blue trajectories). The target particles proceeded into the concentration channel, where they were refocused to the channel center by a single node standing wave before entering the concentration zone (Figure 1, red trajectories). At the end of this channel, the liquid at each side is branched off through outlet (2) which leads to an increased particle concentration in the central outlet (3) flow stream. (The Supporting Information contains SI movies 1−3 of 5 and 7 μm particles separating and concentrating.)

The particles were focused toward the center of the concentration channel by the acoustic field generated by the 2 MHz transducer that also controls the separation unit. The two-dimensional focusing in the concentration zone of the chip ensures that the particles are positioned in the highest velocity region of the parabolic flow profile. This ensured they would move as fast as possible through the second trifurcation in the concentration zone thus avoiding deflection by the uncontrolled nonsymmetrical local acoustic field that is commonly interfering with cells flowing at low velocities.[31]

Since the separation and concentration parts of the device are operated using the same piezoceramic transducer, the acoustic amplitude and flow rates in the different modules must be chosen with care. As reported previously,[31] target particles can be lost in the trifurcation outlet region (3) due to an uncontrolled acoustic field that deflects the particles to the side outlets (2). Further, high acoustic amplitude in

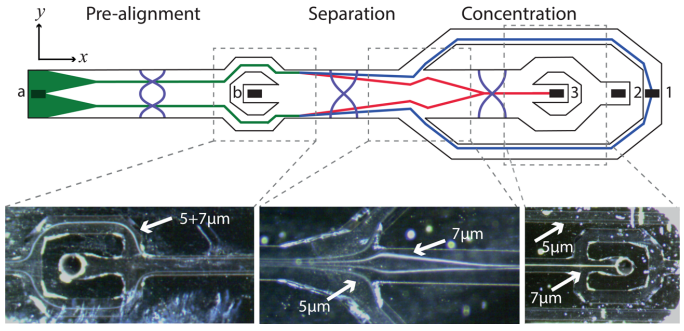

Figure 1. Illustration of the chip from the top showing particle trajectories and inset photographs, showing the separation of 5 and 7 μm polystyrene particles. Particles were infused through inlet (a) and prealigned in two dimensions, horizontally and vertically (*y*- and *z*-directions). A cell-free liquid was infused through inlet (b) where the cells of interest were isolated in the separation channel. Waste cells were discarded through outlet (1) as the target cells were refocused in the concentration channel. Concentrated cells were then collected through outlet (3), and cell-free liquid was discarded through outlet (2).

DOI: 10.1021/acs.analchem.5b02023
Anal. Chem. 2015, 87, 9322−9328

combination with low flow velocity can lead to trapping of particles on the walls of the concentration zone. On the other hand, too low acoustic amplitude will require a low flow rate in the separation zone to fulfill the separation condition and limits throughput of the device. To accommodate for this, the separation zone was designed to be two times longer than the concentration zone, taking into account both the 10-fold difference in flow velocity and the demand for larger sideways shift in the concentration zone to fully focus the cells or particles. Hence, using a single transducer for multiple operations comes at the cost of a more elaborate flow and actuation optimization.

Separation and Volume Concentration Efficiency of 5 and 7 μm Polystyrene Particles. The integrated system was further evaluated by its ability to separate and concentrate polystyrene particles of 5 and 7 μm diameters. The particle concentrations used were higher than what one would expect to find in rare-cell samples as the particles were used to characterize the system. First, the separation efficiency was determined by comparing the amount of particles collected from outlets (2) and (3) versus those collected from outlet (1). The efficiency of the device's separation zone is illustrated in Figure 2. To determine the optimal separation settings, the applied voltage was gradually increased to find the transition voltage where the particles enter outlets (2) or (3) instead of outlet (1). An increased voltage will lead to a higher acoustic migration velocity toward the channel center. Because the acoustic migration velocity is proportional to the square of the particle diameter, the 7 μm particles will migrate approximately twice as fast as the 5 μm particles.[21,34] Between applied voltages of 6.25 to 6.75 V, the majority of the faster moving 7 μm particles could be collected through the center outlets (2) or (3) while the majority of the 5 μm particles were collected through the side outlet (1). At an applied voltage of 6.5 V, 99.8 ± 0.04% of the 7 μm particles entered the center outlets (2) or (3) while 99.7 ± 0.1% of the 5 μm particles entered the side outlet (1).

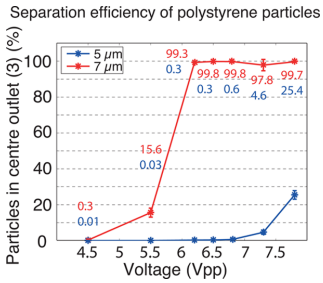

Figure 2. Separation efficiency of the device using 5 and 7 μm particles. The sample inflow rate was 100 μL/min, and outflow rate in the center outlet (3) was 20 μL/min. The error bars represent the standard deviation for $n = 3$.

The volume concentration ability of the device was investigated by maintaining the voltage setting that provided optimal separation and varying flow rates through outlets (2) and (3) (Table 2). The flow rate of the particles moving from the separation to the concentration parts of the device was kept at 20 μL/min to ensure that the separation conditions were constant. This resulted in a 5-fold concentration compared to the sample inflow rate of 100 μL/min and corresponds to the 6.5 V-data point in Figure 2 as well as the first row in Table 1. The resulting concentration factor was 5.6 ± 0.04. This differed slightly from the anticipated concentration, likely because the measured flow rates differed slightly from the actual flow rates, seen as the input sample was processed faster than anticipated according to the set flow rate. Setting the flow rates for outlet (2) and (3) to 10 μL/min each, a 2-fold concentration would be expected after the separation step multiplying up to an attempted 10-fold concentration after the concentration step. At these settings, 98.3 ± 0.6% of 7 μm particles were recovered and were concentrated 11.5 ± 0.4-fold. Efforts to further increase the output concentration using flow rates for outlets (2) and (3) set at 15 and 5 μL/min, respectively, would correspond to a tentative 20-fold concentration. While collecting 99.3 ± 0.3% of the 7 μm particles through outlet (3), they were simultaneously concentrated 25.7 ± 1.7-fold.

Attempting to concentrate the particles 50-fold, the flow rates for outlets (2) and (3) were set to 18 and 2 μL/min, respectively. Almost 20% of the target 7 μm particles were lost through outlet (2), and this resulted in a recovery of only 80.1 ± 7.4% of the 7 μm particles while concentrating them 57.5 ± 6.4-fold. The particle loss was due to the limitations in the pressure-regulated flow system and the performance of the flow rate sensors and not due to insufficient acoustic performance. As all of the pressure system flow rates are controlled in a loop, a small fluctuation in the higher flows led to major relative fluctuations of the flow rate of the center outlet (3), which in turn caused particles to spill over to outlet (2) instead. Hence, using a system with improved ability to control a larger range of flow rates at high precision would enable higher concentration factors. E.g. a previously described, the syringe pump-based system for cell concentration allowed higher differences between the system flow rates because each syringe was precisely and separately controlled.[25,31]

Separation and Volume Concentration of Cancer Cells and White Blood Cells. The presented device aims to simultaneously separate and concentrate rare cells such as circulating tumor cells from an abundance of nucleated white blood cells. To investigate this potential, DU145 prostate

Table 2. Volume Concentration Ability for 7 μm Polystyrene Particles Attempting to Concentrate the Particles 5-, 10-, 20-, and 50-Fold[a]

separation experiment	attempted concentration	7 μm loss outlet (1) (%)	7 μm loss outlet (2) (%)	7 μm collected outlet (3) (%)	5 μm contamination outlet (3) (%)	7 μm concentration
7 μm/5 μm polystyrene particles	5-fold	0.2 ± 0.04	0	99.8 ± 0.04	0.3 ± 0.1	5.6 ± 0.04
	10-fold	1.7 ± 0.6	0	98.3 ± 0.6	0.1 ± 0.06	11.5 ± 0.4
	20-fold	0.7 ± 0.3	0	99.3 ± 0.3	0.1 ± 0.03	25.7 ± 1.7
	50-fold	1.7 ± 0.2	18.2 ± 7.4	80.1 ± 7.4	0.1 ± 0.02	57.5 ± 6.4

[a]The standard deviations were derived for $n = 3$.

DOI: 10.1021/acs.analchem.5b02023
Anal. Chem. 2015, 87, 9322−9328

cancer and MCF7 breast cancer cell lines were used, separately, spiked into red blood cell-lysed white blood cells, to serve as model systems. To save reagents and sample, the white blood cells were diluted 10-fold as compared to whole blood. It has previously been shown that, compared to using an undiluted sample, this dilution factor does not cause any measurable difference in performing the acoustophoretic separation.[25] To facilitate enumeration of the cancer cells using conventional flow cytometry, the cancer cells were spiked at a concentration of 2.5×10^5 cells/mL. The levels of cancer cells anticipated in patient samples are commonly low (1−10 cells/mL). However, acoustophoretic tumor cell recovery is not compromised by lower concentrations of cancer cells. As was done with the polystyrene particles, the separation efficiency for isolating the cancer cells from the white blood cells was obtained by gradually increasing the voltage to find the cells respective side-to-center outlet transition voltages.

The separation efficiencies attained for the two cell-line preparations are shown in Figure 3. The transition voltage of the cancer cells to exit through the center outlet (3) is lower than for most white blood cells. The two cell populations display somewhat overlapping acoustic mobility and did not separate completely. Nevertheless, a large proportion of the cancer cells was collected while largely avoiding white blood cell contamination. At 6.5 V, 80.8 ± 9.5% of the DU145 cancer cells could be collected with 0.1 ± 0.025% contamination of white blood cells. At 7 V, 88 ± 3.7% of the DU145 cancer cells were recovered with 0.4 ± 0.3% contamination of white blood cells. A similar recovery rate was obtained for MCF7 cancer cells: at 7 V, 88.6 ± 5.5% of the cancer cells were recovered with 0.7 ± 0.4% contamination from the white blood cells.

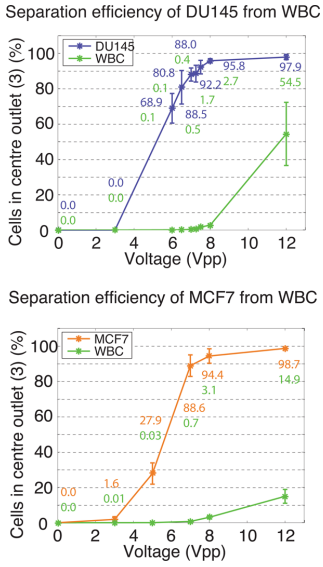

Figure 3. Separation efficiency of cancer cells and white blood cells. The sample inflow rate was 100 μL/min, and the outflow rate in the center outlet (3) was 20 μL/min. The error bars represent the standard deviation for $n = 3$.

The acoustic velocity moving the cells toward the microchannel center scales with the cell size to the power of two, the density, and the compressibility. The size distribution of the leukocytes measures from 7 to 14 μm and the cancer cells from 15 to 25 μm (Coulter counter data not shown). Given the size differences between the two populations and the size dependence of the acoustic velocity, the separation is likely predominantly based on size, although the overlap of the separated populations indicates that the density or compressibility also affects the separation efficiency.

The performance of the cell volume concentration step was obtained as previously described for the particles. Data for the cancer cell separation from WBCs is presented in Table 3. The voltage of the transducer regulating the separation and concentration was set at 7 V for the separation of both cancer cell types, which possibly corresponds to acceptable levels of white blood cell contamination while yielding high cancer cell recoveries. Assuming 100% tumor cell recovery, the anticipated discriminatory capability at this voltage and flow rate would result in an approximate 5-fold concentration. At this voltage and with these flow rates, the recovered MCF7 cancer cells were concentrated 4.7 ± 0.6-fold and the DU145 were concentrated 5.0 ± 0.4-fold. Attempting to obtain 10-fold concentration of the targeted cancer cells, using similar settings as were used during the polystyrene trials, 90.8 ± 3.1% MCF7 cancer cells were collected and concentrated 10.2 ± 0.2-fold with 0.3 ± 0.01% contamination of white blood cells. At the same settings, 84.1 ± 2.1% of DU145 cancer cells were recovered and concentrated 9.6 ± 0.4-fold at 0.2 ± 0.04% contamination of white blood cells. Using settings designed to achieve a 20-fold concentration, a 23.8 ± 1.3-fold concentration of MCF7 cancer cells was obtained while recovering 91.8 ± 1.0% of the cancer cells at 0.6 ± 0.1% contamination of white blood cells. Likewise, a 20.8 ± 1.8-fold concentration of DU145 cells was obtained while recovering 76.8 ± 2.5% of the cancer cells at 0.3 ± 0.3% contamination of white blood cells. Similar

Table 3. Volume Concentration Ability for Cancer Cells (CC) Attempting to Concentrate the Cells 5-, 10-, 20-, and 50-Fold[a]

separation experiment	approx attempted conc	CC loss outlet 1 (%)	CC loss outlet 2 (%)	CC collected outlet 3 (%)	WBC contamination outlet 3 (%)	CC concentration outlet (3)
MCF7/WBC	5-fold	11.4 ± 5.5	0	88.6 ± 5.5	0.7 ± 0.4	4.7 ± 0.6
	10-fold	9.2 ± 3.1	0	90.8 ± 3.1	0.3 ± 0.01	10.2 ± 0.2
	20-fold	7.6 ± 1.5	0.6 ± 0.6	91.8 ± 1.0	0.6 ± 0.1	23.8 ± 1.3
	50-fold	16.9 ± 3.5	16.1 ± 2.1	67.0 ± 3.4	0.2 ± 0.02	44.4 ± 4.6
DU145/WBC	5-fold	12 ± 3.7	0	88.0 ± 3.7	0.4 ± 0.3	5.0 ± 0.4
	10-fold	15.9 ± 2.1	0	84.1 ± 2.1	0.2 ± 0.04	9.6 ± 0.4
	20-fold	19.8 ± 3.8	3.3 ± 1.3	76.8 ± 2.5	0.3 ± 0.3	20.8 ± 1.8
	50-fold	21.1 ± 8.0	14.7 ± 10.5	64.2 ± 17.9	0.2 ± 0.1	26.8 ± 9.7

[a]The standard deviations are derived for $n = 3$.

DOI: 10.1021/acs.analchem.5b02023
Anal. Chem. 2015, 87, 9322−9328

to the trials using polystyrene particles, a few target cells were lost through outlet (2). As that which occurred with the particles, when attempting to obtain 50-fold concentration of cancer cells, losses of cancer cells increased through outlet (2). Hence, 44.4 ± 4.6-fold concentration was obtained while recovering 67 ± 3.4% of the MCF7 at 0.2 ± 0.02% contamination of white blood cells. While recovering 64.2 ± 17.9% of the DU145 cancer cells, the cancer cells were concentrated 26.8 ± 9.7-fold at only 0.2 ± 0.1% contamination of white blood cells. Losses in tumor cell recovery while attempting to obtain higher concentrations of tumor cells were again due to the insufficient flow control possibilities of the pressure system used.

The current data on separation of cancer cells from white blood cells confirms previously reported data.[25] However, the previous device diluted the sample during the separation process instead of concentrating it, and while aiming to isolate rare cells, diluting the purified sample is a clear disadvantage. Subsequent analysis becomes difficult because rare cells may be lost and their analysis distorted by concentration through conventional centrifugation. To use centrifugation to concentrate the small sample volumes collected, the centrifuged cells would need to be resuspended in even smaller volumes that are not practically possible to handle. Concentration of low cell numbers also increases the risk of sample loss if the formed pellet is to small to be seen or if a pellet does not form at all. A system offering simultaneous separation and concentration also offers the further advantage of integration with analysis modules, where the cancer cells could be detected directly on chip.

In contrast to the previously described system,[25] the device developed here reliably concentrates target cells up to about 20-fold, facilitating subsequent analysis or further culture while maintaining acceptable recoveries. Fundamentally important, the current system can process a sample at a rate of 6 mL/h, making it suitable for handling clinical samples. Furthermore, as seen in Figure 3, the current device makes it possible to further suppress the white blood cell contamination although this is accomplished at the expense of target cell recovery.

To further improve the throughput and concentration ability of the presented device, two measures can be taken. First, increasing the length of the prealignment zone may increase the throughput. The prealignment zone limits the current device because the particles must be focused from every possible random location in the channel cross section to the two prealignment nodal points. Furthermore, the acoustic radiation force has a sinusoidal distribution such that the force is zero on the walls and at the pressure nodes. In the separation zone, on the other hand, particles are already prealigned to a region of maximal acoustic radiation force and do not have to be moved all the way to the single nodal point to be successfully separated. Second, improving the flow stability of the flow system can increase the concentration performance of the device. Recently published findings suggest that excluding the central inlet for cell-free medium (Figure 1, inlet (b)) from the design reduces flow fluctuations, has minimal negative effect on the separation performance, and prevents dilution of the cell sample.[21] This will also eliminate the need for acoustic impedance matching of the sample and the cell-free liquids.[32]

CONCLUSIONS

The device presented in this paper enables label-free simultaneous separation and volume concentration, facilitating subsequent analysis or cell culture. The on-chip concentration of the target sample is especially suitable for rare cell samples that are not always suitable for concentration by common centrifugation. Cells and particles can be concentrated up to 20-fold while maintaining a high separation efficiency at sample flow rates that can process a 6 mL clinical sample in 1 h. Future work will aim to further increase the concentration factors and to integrate the present device with an analysis unit. Also, by extending the prealignment zone, it is anticipated that the throughput could be increased. The presented device has the potential to contribute to the development of targeted therapies specific to an individual patient's tumor biology.

ASSOCIATED CONTENT

Supporting Information

The Supporting Information is available free of charge on the ACS Publications website at DOI: 10.1021/acs.analchem.5b02023.

Summary of the content in the movies (PDF)
SI movie 1 (AVI)
SI movie 2 (AVI)
SI movie 3 (AVI)

AUTHOR INFORMATION

Corresponding Authors

*E-mail: maria.antfolk@bme.lth.se.
*E-mail: thomas.laurell@bme.lth.se.

Notes

The authors declare no competing financial interest.

ACKNOWLEDGMENTS

This work was supported by the Swedish governmental agency for innovation systems, VINNOVA, CellCARE (Grant No. 2009-00236), the Swedish Research Council (Grant Nos. 621-2010-4389 and 2012-6708), Knut and Alice Wallenberg Foundation (Grant No. KAW 2012.0023), the Sten K Johnsson Foundation, the Royal Physiographic Society, the Crafoord Foundation, and the Carl Trygger Foundation. This work was also supported in parts by grants from the Sidney Kimmel Center for Prostate and Urologic Cancers; David H. Koch through the Prostate Cancer Foundation; the National Institute for Health Research (NIHR) Oxford Biomedical Research Centre Program; the Cancer Research UK Oxford Centre; the Swedish Cancer Society (project no. 14-0722); the Finnish Funding Agency for Technology and Innovation Finland Distinguished Professor program, and Fundacion Federico SA.

REFERENCES

(1) Gossett, D. R.; Weaver, W. M.; Mach, A. J.; Hur, S. C.; Tse, H. T. K.; Lee, W.; Amini, H.; Di Carlo, D. *Anal. Bioanal. Chem.* **2010**, *397* (8), 3249−3267.
(2) Chen, Y.; Li, P.; Huang, P.-H.; Xie, Y.; Mai, J. D.; Wang, L.; Nguyen, N.-T.; Huang, T. J. *Lab Chip* **2014**, *14* (4), 626−645.
(3) Cohen, S. J.; Punt, C. J. A.; Iannotti, N.; Saidman, B. H.; Sabbath, K. D.; Gabrail, N. Y.; Picus, J.; Morse, M.; Mitchell, E.; Miller, M. C.; Doyle, G. V.; Tissing, H.; Terstappen, L. W. M. M.; Meropol, N. J. *J. Clin. Oncol.* **2008**, *26* (19), 3213−3221.
(4) Allard, W. J.; Matera, J.; Miller, M. C.; Repollet, M.; Connelly, M. C.; Rao, C.; Tibbe, A. G. J.; Uhr, J. W.; Terstappen, L. W. M. M. *Clin. Cancer Res.* **2004**, *10* (20), 6897−6904.
(5) Cristofanilli, M.; Budd, G. T.; Ellis, M. J.; Stopeck, A.; Matera, J.; Miller, M. C.; Reuben, J. M.; Doyle, G. V.; Allard, W. J.; Terstappen, L. W. M. M.; Hayes, D. F. *N. Engl. J. Med.* **2004**, *351* (8), 781−791.

DOI: 10.1021/acs.analchem.5b02023
Anal. Chem. 2015, 87, 9322−9328

(6) Ghossein, R.; Scher, H.; Gerald, W.; Kelly, W.; Curley, T.; Amsterdam, A.; Zhang, Z.; Rosai, J. *J. Clin. Oncol.* **1995**, *13* (5), 1195−1200.
(7) Satelli, A.; Mitra, A.; Cutrera, J. J.; Devarie, M.; Xia, X.; Ingram, D. R.; Dibra, D.; Somaiah, N.; Torres, K. E.; Ravi, V.; Ludwig, J. A.; Kleinerman, E. S.; Li, S. *Cancer Res.* **2014**, *74* (6), 1645−1650.
(8) Aktas, B.; Tewes, M.; Fehm, T.; Hauch, S.; Kimmig, R.; Kasimir-Bauer, S. *Breast Cancer Res.* **2009**, *11* (4), R46.
(9) Li, P.; Stratton, Z. S.; Dao, M.; Ritz, J.; Huang, T. J. *Lab Chip* **2013**, *13* (4), 602−609.
(10) Alix-Panabières, C.; Pantel, K. *Lab Chip* **2014**, *14* (1), 57−62.
(11) Bhagat, A. A. S.; Bow, H.; Hou, H. W.; Tan, S. J.; Han, J.; Lim, C. T. *Med. Biol. Eng. Comput.* **2010**, *48* (10), 999−1014.
(12) Stott, S. L.; Hsu, C.-H.; Tsukrov, D. I.; Yu, M.; Miyamoto, D. T.; Waltman, B. A.; Rothenberg, S. M.; Shah, A. M.; Smas, M. E.; Korir, G. K.; Floyd, F. P.; Gilman, A. J.; Lord, J. B.; Winokur, D.; Springer, S.; Irimia, D.; Nagrath, S.; Sequist, L. V.; Lee, R. J.; Isselbacher, K. J.; Maheswaran, S.; Haber, D. A.; Toner, M. *Proc. Natl. Acad. Sci. U. S. A.* **2010**, *107* (43), 18392−18397.
(13) Wang, S.; Liu, K.; Liu, J.; Yu, Z. T.-F.; Xu, X.; Zhao, L.; Lee, T.; Lee, E. K.; Reiss, J.; Lee, Y.-K.; Chung, L. W. K.; Huang, J.; Rettig, M.; Seligson, D.; Duraiswamy, K. N.; Shen, C. K.-F.; Tseng, H.-R. *Angew. Chem., Int. Ed.* **2011**, *50* (13), 3084−3088.
(14) Kang, J. H.; Krause, S.; Tobin, H.; Mammoto, A.; Kanapathipillai, M.; Ingber, D. E. *Lab Chip* **2012**, *12* (12), 2175−2181.
(15) Gleghorn, J. P.; Pratt, E. D.; Denning, D.; Liu, H.; Bander, N. H.; Tagawa, S. T.; Nanus, D. M.; Giannakakou, P. A.; Kirby, B. J. *Lab Chip* **2010**, *10* (1), 27−29.
(16) Ozkumur, E.; Shah, A. M.; Ciciliano, J. C.; Emmink, B. L.; Miyamoto, D. T.; Brachtel, E.; Yu, M.; Chen, P.; Morgan, B.; Trautwein, J.; Kimura, A.; Sengupta, S.; Stott, S. L.; Karabacak, N. M.; Barber, T. A.; Walsh, J. R.; Smith, K.; Spuhler, P. S.; Sullivan, J. P.; Lee, R. J.; Ting, D. T.; Luo, X.; Shaw, A. T.; Bardia, A.; Sequist, L. V.; Louis, D. N.; Maheswaran, S.; Kapur, R.; Haber, D. A.; Toner, M. *Sci. Transl. Med.* **2013**, *5* (179), 179ra47.
(17) Warkiani, M. E.; Guan, G.; Luan, K. B.; Lee, W. C.; Bhagat, A. A. S.; Chaudhuri, P. K.; Tan, D. S.-W.; Lim, W. T.; Lee, S. C.; Chen, P. C. Y.; Lim, C. T.; Han, J. *Lab Chip* **2014**, *14* (1), 128−137.
(18) Mach, A. J.; Kim, J. H.; Arshi, A.; Hur, S. C.; DiCarlo, D. *Lab Chip* **2011**, *11* (17), 2827−2834.
(19) Huang, S.-B.; Wu, M.-H.; Lin, Y.-H.; Hsieh, C.-H.; Yang, C.-L.; Lin, H.-C.; Tseng, C.-P.; Lee, G.-B. *Lab Chip* **2013**, *13* (7), 1371−1383.
(20) Li, P.; Mao, Z.; Peng, Z.; Zhou, L.; Chen, Y.; Huang, P.-H.; Truica, C. I.; Drabick, J. J.; El-Deiry, W. S.; Dao, M.; Suresh, S.; Huang, T. J. *Proc. Natl. Acad. Sci. U. S. A.* **2015**, *112* (16), 4970−4975.
(21) Antfolk, M.; Antfolk, C.; Lilja, H.; Laurell, T.; Augustsson, P. *Lab Chip* **2015**, *15*, 2102−2109.
(22) Hyun, K.-A.; Kwon, K.; Han, H.; Kim, S.-I.; Jung, H.-I. *Biosens. Bioelectron.* **2013**, *40* (1), 206−212.
(23) Wiklund, M. *Lab Chip* **2012**, *12*, 2018.
(24) Burguillos, M. A.; Magnusson, C.; Nordin, M.; Lenshof, A.; Augustsson, P.; Hansson, M. J.; Elmér, E.; Lilja, H.; Brundin, P.; Laurell, T.; Deierborg, T. *PLoS One* **2013**, *8* (5), e64233.
(25) Augustsson, P.; Magnusson, C.; Nordin, M.; Lilja, H.; Laurell, T. *Anal. Chem.* **2012**, *84* (18), 7954−7962.
(26) Augustsson, P.; Laurell, T. *Lab Chip* **2012**, *12*, 1742−1752.
(27) Lenshof, A.; Magnusson, C.; Laurell, T. *Lab Chip* **2012**, *12* (7), 1210−1223.
(28) Glynne-Jones, P.; Boltryk, R. J.; Hill, M. *Lab Chip* **2012**, *12* (8), 1417−1426.
(29) Bruus, H. *Lab Chip* **2012**, *12* (9), 1578−1586.
(30) Laurell, T.; Petersson, F.; Nilsson, A. *Chem. Soc. Rev.* **2007**, *36* (3), 492−506.
(31) Nordin, M.; Laurell, T. *Lab Chip* **2012**, *12*, 4610−4616.
(32) Deshmukh, S.; Brzozka, Z.; Laurell, T.; Augustsson, P. *Lab Chip* **2014**, *14*, 3394−3400.
(33) Grenvall, C.; Magnusson, C.; Lilja, H.; Laurell, T. *Anal. Chem.* **2015**, *87*, 5596.
(34) Barnkob, R.; Augustsson, P.; Laurell, T.; Bruus, H. *Phys. Rev. E* **2012**, *86* (5), 056307.

DOI: 10.1021/acs.analchem.5b02023
Anal. Chem. 2015, 87, 9322−9328

Paper V

Highly efficient single cell arraying by integrating acoustophoretic cell pre-concentration and dielectrophoretic cell trapping

Soo Hyeon Kim*, Maria Antfolk*, Marina Kobayashi, Shohei Kaneda, Thomas Laurell, and Teruo Fujii

Lab on a Chip, 2015, 15(22), 4356-4363.

*Authors contributed equally to this work

Paper V

Lab on a Chip

PAPER

View Article Online
View Journal | View Issue

Cite this: *Lab Chip*, 2015, **15**, 4356

Highly efficient single cell arraying by integrating acoustophoretic cell pre-concentration and dielectrophoretic cell trapping†

Soo Hyeon Kim,‡[ab] Maria Antfolk,‡[c] Marina Kobayashi,[ab] Shohei Kaneda,[ab] Thomas Laurell*[cd] and Teruo Fujii*[ab]

Received 8th September 2015,
Accepted 23rd September 2015

DOI: 10.1039/c5lc01065a

www.rsc.org/loc

To array rare cells at the single-cell level, the volumetric throughput may become a bottleneck in the cell trapping and the subsequent single-cell analysis, since the target cells per definition commonly exist in a large sample volume after purification from the original sample. Here, we present a novel approach for high throughput single cell arraying by integrating two original microfluidic devices: an acoustofluidic chip and an electroactive microwell array. The velocity of the cells is geared down in the acoustofluidic chip while maintaining a high volume flow rate at the inlet of the microsystem, and the cells are subsequently trapped one by one into the microwell array using dielectrophoresis. The integrated system exhibited a 10 times improved sample throughput compared to trapping with the electroactive microwell array chip alone, while maintaining a highly efficient cell recovery above 90%. The results indicate that the serial integration of the acoustophoretic pre-concentration with the dielectrophoretic cell trapping drastically improves the performance of the electroactive microwell array for highly efficient single cell analysis. This simple and effective system for high throughput single cell arraying with further possible integration of additional functions, including cell sorting and downstream analysis after cell trapping, has potential for development to a highly integrated and automated platform for single-cell analysis of rare cells.

Introduction

Analysis of rare cells, *e.g.* circulating tumor cells (CTCs) and circulating fetal cells, holds promise for the diagnosis and prognosis of many cancers, and non-invasive prenatal diagnosis. For instance, counting the number of CTCs in peripheral blood makes it possible to monitor the therapeutic effect of a treatment and to give prognosis without tissue biopsies.[1] Microfluidic devices are suitable for sorting and analyzing rare cells and enable processing of complex cellular fluids. Several groups have been developing microfluidic devices for continuous flow-based rare cell isolation using the physical properties,[2–6] biochemical properties[7,8] or dielectric properties[9–11] of rare cells. Although previous methods using microfluidic devices successfully demonstrated separation of rare cells, the separated cells have to be collected and arrayed for downstream analysis. The rare cells should preferably be analyzed at the single-cell level for the improvement of the understanding of cellular heterogeneity, and for clinical applications. For instance, characterization of individual CTCs would help to profile a disseminated tumor at the molecular level, and to further guide diagnostic and therapeutic strategies since CTCs may be shed from different locations within tumors, and even from metastases.[12]

A microfluidic approach has been employed to array single cells using additional forces, *i.e.* hydrodynamic force,[13,14] gravity[15] or dielectrophoresis.[16] Recently, highly improved single-cell arraying efficiency was realized by optimizing flow profiling.[17] However, there are some practical problems of the method – trapped cells can be easily deformed due to a hydrodynamic pressure and microfluidic channels can be easily clogged since the dimension of the channel is comparable with that of the target cells. In order to overcome the drawbacks of the method, we have developed a microfluidic device containing an electroactive microwell array (EMA) for trapping single cells using dielectrophoresis (DEP) followed by on-chip single-cell analysis.[18] Although we successfully demonstrated the feasibility of the EMA device for on-chip single-cell analysis,[18,19] the main drawbacks of the EMA chip for single cell analysis laid in the difficulty to analyze large sample volumes in a short time period, since the optimal inlet flow rate of the EMA chip was 2 μL min^{-1}. Higher flow

[a] *Institute of Industrial Science, The University of Tokyo, Japan. E-mail: tfujii@iis.u-tokyo.ac.jp; Tel: +81 3 5452 6211*
[b] *CREST, Japan Science and Technology Agency, Japan*
[c] *Lund University, Sweden. E-mail: thomas.laurell@bme.lth.se; Tel: +46 46 222 7540*
[d] *Dongguk University, South Korea*

† Electronic supplementary information (ESI) available. See DOI: 10.1039/c5lc01065a

‡ These authors contributed equally to this work.

velocities in the EMA device prevent efficient trapping of the target cells, yielding a lower cell recovery.

A practical problem on the rare cell analysis is that the isolated target cells are usually suspended in a large sample volume as shown in Table S1 in the ESI.† For instance, collected rare cells, sorted by Dean flow fractionation, were suspended in a 3 times larger volume of buffer.[3] In this case, if 10 cells exist in 1 mL of blood sample, 10 cells would be suspended in 3 mL of buffer after isolation. Although centrifugation is widely used to concentrate a sample, centrifugation of a sample with a low cell number will increase the risk of critical sample losses since a pellet of sample is too small to be seen or even no pellet forms at all with such a low number of cells,[20] and may induce a possible damage to cell viability[21] as well as cell function[22] because of the strong centrifugal forces acting on a cell. Moreover, during the sample transfer process from the tube to the device for downstream analysis, the small number of cells could be nonspecifically bound on a surface of a centrifugal tube or a pipet tip.

An effective strategy to overcome this would be to decrease the volume flow rate in the device while maintaining a high flow rate at the inlet of the microsystem. Microfluidic devices have previously been demonstrated to decrease the sample volume using gravity,[23] hydrodynamic forces,[24,25] electrical forces,[26–29] magnetic forces[30] and acoustophoresis.[31] Although the methods efficiently decrease the volume of the samples, there is a lack of continuous flow-based systems yielding high concentration factors while maintaining a high recovery and throughput.[20] Recently, we have developed an acoustofluidic chip to concentrate dilute cells into a smaller volume with concentration factors of several orders of magnitude of dilute samples.[20] The chip focuses the cells in a confined liquid volume by utilizing acoustic standing waves formed in the microchannel. The chip allows us to drastically decrease the volume flow rate of the sample, prior to entering the EMA device, by collecting the cells focused in the channel center while discarding the cell-free liquid volume along the channel sides.

Here, we present a novel approach for high throughput arraying of single cells supplemented in a large sample volume by integrating two original microfluidic devices: 1) an acoustofluidic chip for sample pre-concentration and 2) an EMA chip for single-cell arraying. The integration was achieved by directly bonding the sample outlet of the acoustofluidic chip to the inlet of the EMA chip to deliver a focused cell stream into the EMA chip. First, we improved the inherent cell trapping efficiency of the EMA to accommodate trapping of single cells, where the cell trapping efficiency of the older version was 10%.[18] The inherent cell trapping efficiency of the EMA was improved up to 98 ± 1.7% for the inlet flow rate of 4 μL min^{-1} by modifying the geometry of the microwell array, while moderate trapping efficiencies of 64 ± 5.3% and 23 ± 3.8% were observed with the higher flow rates of 10 and 20 μL min^{-1}, respectively, without pre-concentration. Next, the feasibility of the integrated system was demonstrated by arraying diluted DU145 cells, a human prostate cancer cell line, after acoustophoretic pre-concentration. The integrated system showed a good recovery of 96 ± 0.8%, 96 ± 3.7%, 88 ± 6% and 65 ± 13% for the high inlet flow rates of 20, 40, 60 and 100 μL min^{-1}, respectively. We successfully improved sample throughput by implementing an acoustic pre-concentration step prior to entering the EMA chip which allowed a 10-fold increase of the system throughput without any impact on the cell recovery.

Design of the device

Acoustofluidic device

Acoustophoresis utilizes ultrasound standing waves to focus cells and particles into the pressure node or anti-node by the primary acoustic radiation force, F_{rad}, approximated as

$$F_{rad} = 4\pi a^3 \phi k_y E_{ac} \sin(2k_y y) \quad (1)$$

$$\phi = \frac{\kappa_o - \kappa_p}{3\kappa_o} + \frac{\rho_p - \rho_o}{2\rho_p + \rho_o} \quad (2)$$

where ϕ is the acoustic contrast factor, a is the particle radius, $k_y = 2\pi/\lambda$ is the wavenumber, E_{ac} is the acoustic energy density, y is the distance from the wall, κ_p is the isothermal compressibility of the particle, κ_o is the isothermal compressibility of the suspending fluid, ρ_p is the particle density, and ρ_o is the suspending fluid density.[32] From the equations, it can be seen that particles are focused depending on their volume, density and compressibility, indicating that the F_{rad} is strongly dependent on the particle size.[33]

In the acoustofluidic chip, dilute cells are focused into the microchannel centre in two dimensions. The wavelength of the ultrasound is matched to the width and height of the microchannel, forming both horizontal and vertical ultrasound standing waves operated at two different frequencies. The two-dimensional focusing is crucial for the ability to obtain high concentration factors. When focusing the cells in two dimensions, they will all be collected in the fastest moving central fluid regime in the laminar flow profile. This ensures a fast transit through the outlet region where the microfluidic channel widens. In this location, the channel width no longer corresponds to the frequency of the applied ultrasound. Instead, other resonance modes and vigorous acoustic streaming zones can be found, yielding unpredictable particle trajectories that divert slower moving particles along the channel walls, from their original trajectory. When two-dimensional focusing (levitation) is active, these artifacts can be efficiently circumvented.[20]

Electroactive microwell array

An electroactive microwell array utilizes dielectrophoresis (DEP) to attract the cells to the bottom of the microwells. The

time-averaged DEP force, $\mathbf{F}_{DEP}$, acting on a spherical cell of radius a can be approximated as

$$\mathbf{F}_{DEP} = 2\pi\varepsilon_e a^3 \mathrm{Re}[K(2\pi f)]\nabla|E_e|^2, \quad (3)$$

$$K(2\pi f) = \frac{\varepsilon^*_{cell} - \varepsilon^*_e}{\varepsilon^*_{cell} + 2\varepsilon^*_e}, \quad (4)$$

where ε_e, f and E_e are the permittivity of the external medium, the frequency of the applied ac field and the amplitude of the electric field, respectively. $\mathrm{Re}[K(2\pi f)]$ is the real part of the polarization factor called the Clausius–Mossotti (CM) factor, where ε^*_{cell} is the complex electrical permittivity of the cell and ε^*_e is the complex electrical permittivity of the external medium. Since DEP allows stable and precise manipulation of cells, DEP has been widely used for manipulation of cells.[34]

To attract the cells into the microwells using DEP, each electroactive microwell has patterned electrodes at the bottom of the microwell. The distance between the electrodes is 10 μm, which is smaller than the diameter of the target cells. A thin insulation layer (4 μm in thickness, made with a negative-type photoresist) was coated on the electrodes to block the electric fields except for the area where the microwells are patterned. The diameter of the microwell is 22 μm. A polydimethylsiloxane (PDMS) microfluidic channel is formed on the EMA substrate for the efficient delivery of target cells.

Integration of the devices

Two original microfluidic devices, the acoustofluidic chip for sample pre-concentraion and the EMA chip for single-cell analysis, were integrated to improve the sample throughput capability (Fig. 1A). For the integration, the sample outlet of the acoustofluidic chip was directly connected with the inlet of the EMA chip by plasma activation of the surfaces and direct bonding of the PDMS-based EMA chip to the glass surface of the acoustofluidic chip. The cells, introduced into the inlet of the acoustofluidic chip, were focused in two-dimensions in the centre of the channel. The main stream of the acoustofluidic chip with the focused cells flowed into the EMA chip and cell-free fractions of the flow stream in the acoustofluidic chip were discarded into the waste outlet. Since only a small fraction of the main stream with cells flowed into the EMA chip (gearing down the flow rate), we could operate the EMA chip at an optimal flow rate (Q_o) with respect to the DEP trapping efficiency even at a high inlet flow rate (Q_i), which allowed high throughput collection of dilute cell suspensions. The cells flowing into the EMA chip were trapped into the microwells in an array with the DEP force at the single-cell level.

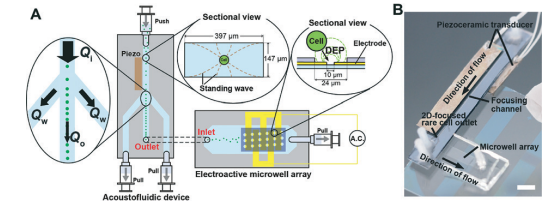

Fig. 1 Integration of the acoustofluidic chip and the EMA chip. (A) Schematic image of the integration. The target cells introduced from the inlet of the acoustofluidic chip are focused at the center of the channel using ultrasound standing waves. The central stream of the chip with the focused cells flows into the EMA chip. The cells are trapped into the microwell array using DEP in the EMA chip. (B) Photo of the integrated device. The outlet of the acoustofluidic device is directly connected with the inlet of the EMA chip. Scale bar is 4 mm.

Materials and methods

Device fabrication

The EMA chip for single cell trapping was fabricated using the conventional photolithography and etching process. The shape of the electrodes were patterned on a indium tin oxide (ITO) coated glass substrate (GEOMATEC Co., Japan) using a positive-type photoresist (S1813, Shipley Far East Ltd., Japan), followed by etching of ITO by a 0.2 M $FeCl_3$ + 6 M HCl solution for 30 min at room temperature. After that, the substrate was cleaned and rinsed with acetone and isopropyl alcohol to remove the photoresist layer remaining on the substrate. The microwell array structure was fabricated with a negative-type photoresist (SU-8 3005, MicroChem Corp., USA) on top of the patterned ITO electrodes. The microfluidic channel for the microwell array was fabricated using polydimethylsiloxane (PDMS, Silopt 184, Dow Corning Toray, Co. Ltd., Japan) through the standard replica molding process. The height and width of the PDMS microchannel were 50 and 3600 μm, respectively. The PDMS channel and microwell array substrate were exposed to O_2 plasma using a reactive ion etching machine (RIE-10NR, Samco Co., Japan) and bonded together.

The fluidic channel for acoustophoresis was fabricated on a silicon substrate using photolithography and anisotropic wet etching in KOH (40 g per 100 mL of H_2O, 80 °C). A hole for the sample outlet was drilled in the silicon and holes for the inlet and waste outlets were drilled in the glass lid using a diamond drill. The silicon chip was sealed by anodic bonding of the glass lid. The focusing channel was 397 μm wide and 147 μm deep. Since the channel width and height corresponded to half a wavelength of ultrasound at 1.89 MHz and 5.08 MHz, piezoceramic transducers (PZ26, Ferroperm Piezoceramics, Kvistgaard, Denmark) resonant at 2 MHz and 5 MHz were attached by using cyanoacrylate glue (Loctite Super glue, Henkel Norden AB, Stockholm, Sweden) to the front and backside of the chip, respectively.

In order to assemble the microwell array chip with the acoustofluidic chip, each of their surfaces for bonding was activated in an O_2 plasma using the reactive ion etching machine. Both were aligned and brought into contact, and spontaneously bonded together without applying any external pressure. Fig. 1B shows the combined device, where the outlet of the acoustofluidic device is directly connected with the inlet of the EMA chip.

Experimental setup

The integrated device was placed on the x–y translational stage located on an inverted microscope (IX 71, Olympus, Japan). The cells were monitored with a digital CCD camera (ORCA-R2, Hamamatsu Photonics, Japan) installed on the microscope. The two transducers bonded on the acoustofluidic chip were actuated using a two-channel function generator (WF1974; NF Corp., Japan). The electric potential for DEP trapping was applied to the ITO electrodes using a function generator (WF1948; NF Corp., Japan). The flow rates in the chip were controlled by connecting the inlets and outlets to gastight glass syringes (Hamilton Company, USA) mounted on a precisely controlled syringe pump (MFS-SP1, Microfluidic System Works Inc., Japan).

Cells and reagents

The human prostate cancer cell line, DU145 (obtained from the RIKEN Bio Resource Center, Japan), was used for the demonstration. The DU145 cells were cultured in a humidified incubator (37 °C in an atmosphere of 5% CO_2). The culture medium was RPMI 1640 (Invitrogen Corp., USA) supplemented with fetal bovine serum (10%, Gemini Bio-products, USA) and a penicillin–streptomycin solution (1%, Sigma Chemical Co., USA). The cultured cells were stained with a fluorescent probe (Calcein AM; Wako Pure Chemical Industries Ltd., Japan) and harvested. To adjust the conductivity of the cell suspension medium, a low-conductivity buffer (10 mM HEPES, 0.1 mM $CaCl_2$, 59 mM D-glucose and 236 mM sucrose) was used, where BSA (Sigma Chemical Co., USA) was added to block nonspecific cell adhesion (2% wt/vol). The final conductivity of the buffer was 22.4 mS m^{-1}. Before injecting the cells into the device, the culture medium was gently removed after centrifugation at 190g for 3 minutes, and the low-conductivity buffer was added to adjust the conductivity of the cell suspension medium to induce positive DEP.

Results and discussion

Single cell trapping with the electroactive microwell array

The electroactive microwells utilize an electrostatic force, DEP, to actively attract single cells flowing over the microwell array. To investigate the DEP force acting on the cells, 2D simulation of the electric fields was carried out by using a commercially available code (Comsol Multiphysics, COMSOL Group, USA). Fig. 2A shows the simulated E_e contours and $\nabla|E_e|^2$ vectors, where the magnitude of the DEP force is proportional to $\nabla|E_e|^2$ as shown in eqn (3). The direction of $\nabla|E_e|^2$ is toward the inside of the microwell and the magnitude of the $\nabla|E_e|^2$ decreases with increasing distance from the electrodes. To evaluate the DEP trapping force, we considered the partial derivative of $|E_e|^2$ with respect to the y direction, which represents a magnitude of the y directional DEP force, along the red dashed line in Fig. 2A. The magnitude of the partial derivative rapidly decreases with the distance from the electrodes as shown in Fig. 2B. Hence, we fabricated thin (4 μm) microwell structures on the electrodes, which increased the magnitude of the DEP force acting on a cell flowing over the microwell array compared to previously used thicker microwell structures.[18]

The improved EMA was evaluated by trapping DU145 cells. Diluted DU145 cells were introduced into the integrated system and the cells were trapped with DEP by applying a 4 V_{p-p} sinusoidal electric potential at 8 MHz to the electrodes. The acoustophoresis was turned off and the waste outlet was closed (Q_w = 0 μL min^{-1}) to investigate the inherent trapping efficiency of the EMA. Fig. 3A displays time-lapse images of the DU145 cells during DEP trapping. Cells flowing over the microwell array were attracted to the bottom of the microwells with the positive DEP. When a cell was already trapped into a microwell, a second could not be trapped into the same microwell due to space restrictions. The trapping efficiency (recovery), a percentage ratio of the number of trapped cells to the number of cells flowing over the microwell array, was 98 ± 1.7% with a 4 μm microwell array structure at the flow rate of 4 μL min^{-1} (Fig. 3B). The trapping efficiency of the present EMA was drastically improved, compared to that of the older version of the chip having a thicker microwell array (15 μm in thickness),[18] where the trapping efficiency was only 10%. This result indicates that the thin microwells on the electrodes allow a highly efficient DEP trapping since the cells are exposed to a strong attractive DEP force when flowing over the microwell array.

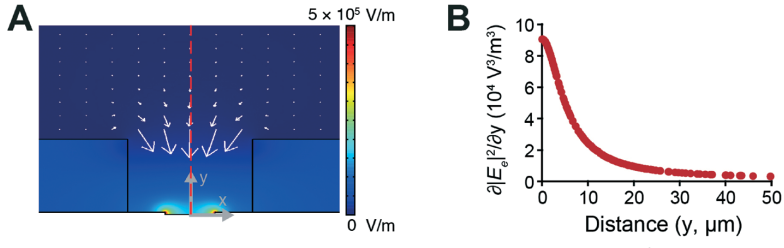

Fig. 2 Simulation of the electric fields for the evaluation of DEP. (A) Simulated E_e contours and $\nabla|E_e|^2$ vectors, where the electric potential is assigned at the boundaries of the electrodes. (B) Partial derivative of $|E_e|^2$ with respect to the y direction along the red dashed line in (A).

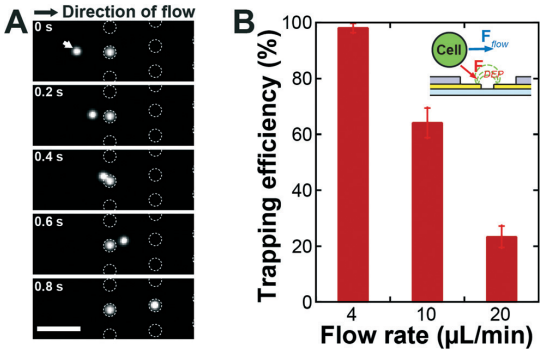

Fig. 3 Single-cell trapping with DEP. (A) Time-lapse image of microwell array during DEP trapping, where the white dotted circles indicate the positions of microwells. The white arrow indicates a cell flowing over the microwell array. Scale bar is 100 μm. (B) Cell trapping efficiency depending on the inlet flow rate without acoustophoretic focusing of cells. The cell suspension, introduced into the inlet of the integrated device, was directly delivered to the microwell array device without focusing. A flow rate of 4 μL min^{-1} corresponded to the average velocity of 370 μm s^{-1} in the EMA chip, where the height and width of the PDMS microchannel were 50 μm and 3600 μm, respectively.

Effect of flow rate on the single-cell trapping

The inlet flow rate of the chip determines the sample throughput capability: one can analyze large sample volumes within a shorter time at a higher inlet flow rate, a prerequisite for applications of rare cell analysis. The cell trapping efficiency of the EMA is, however, affected by the fluid velocity (Stokes drag) when the cells pass over the microwells. To investigate the cell trapping efficiency with respect to the average velocity of the flow which delivers the target cells, we fixed all experimental parameters except for the inlet flow rate. The average velocity in the EMA chip was proportional to the inlet flow rate since the cross-sectional area of the channel was fixed and the waste outlets of the acoustofluidic chip were closed. The trapping efficiencies were 98 ± 1.7%, 64 ± 5.3% and 23 ± 3.8% for the inlet flow rates of 4, 10 and 20 μL min^{-1} (Fig. 3B), respectively, where the flow rate of 4 μL min^{-1} corresponded to the average velocity of 370 μm s^{-1} in the EMA chip. The data showed the expected decrease in trapping efficiency with the increase in average velocity. When the target cells flow over the EMA, the DEP force attracting the cells is dependent on the exposure time of the cells to the electric field gradient above the microwells. Since the exposure time is shortened at higher flow rates, the trapping efficiency drops rapidly with an elevated flow rate.

To enable a high sample throughput capability at an unchanged cell trapping efficiency, one should increase the inlet flow rate while maintaining a constant average velocity in the microfluidic channel of the EMA chip. An increase of the cross-sectional area by widening the microfluidic channel of the EMA chip allows an increase of the inlet flow rate without a change of the average velocity. However, it takes a longer time to observe the microwell array since the area of the microwell array becomes larger and this strategy does not support a large scalability. An effective strategy is rather to decrease the volume flow rate in the EMA chip without decreasing the inlet flow rate by integrating a preconcentration sample preparation function, as proposed here by acoustophoretic cell concentration, directly onto the EMA chip to enable high throughput analysis.

Acoustophoretic cell focusing

The acoustophoretic cell concentration chip utilized ultrasonic standing wave forces, in two dimensions, to focus target cells in the acoustic pressure node located in the microchannel centre. For the demonstration of the cell focusing, we introduced fluorescently labeled DU145 cells into the inlet of the acoustofluidic chip (Q_i = 20 μL min^{-1}, Q_w = 8 μL min^{-1} and Q_o = 4 μL min^{-1}). To form a half-wavelength resonance mode in the acoustofluidc chip, we applied a 10 V_{p-p} sinusoidal electric potential at 1.89 MHz to the piezoceramic transducer, resonant at 2 MHz, and 20 V_{p-p} at 5.08 MHz to the transducer, resonant at 5 MHz. As we activated the acoustophoresis, all of the cells flowing in the acoustofluidic channel were focused into the center of the channel (Fig. 4A). The center fraction of the flow with the acoustophoretically focused cells, which was directly connected to the EMA chip

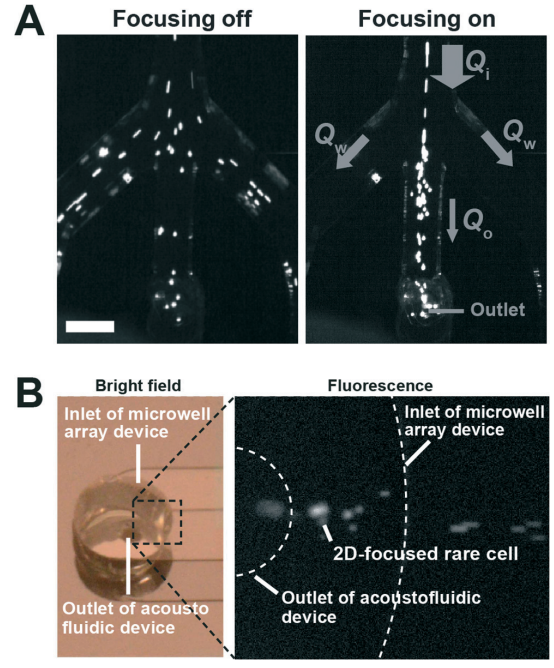

Fig. 4 Acoustophoretic cell focusing. (A) Fluorescence images of the acoustofluidic chip. Acoustophoresis allowed cell focusing at the centre of the channel. Scale bar is 300 μm. (B) Bright field and fluorescence images of the connected area. The cells focused by acoustophoresis flows into the EMA chip.

inlet, streamed into the EMA chip (Fig. 4B). The cell-free fraction of the flow in the acoustophoresis channel was discarded through the waste outlets.

The acoustofluidic chip allowed us to operate the EMA chip at a constant outlet flow rate, Q_o, without relying on the inlet flow rate, Q_i. Since the acoustofluidic chip focuses the cells in a confined liquid volume, one can drastically decrease the volume flow rate by extracting the confined volume with the focused cells and discard the cell-free liquid. This feature improves the sample throughput capability while maintaining the cell trapping efficiency of the EMA.

Single cell trapping using the integrated device

The feasibility of high sample throughput capability of the integrated system was demonstrated by trapping diluted DU145 cells with various inlet flow rates, Q_i. The outlet flow rate, Q_o, was fixed at 4 μL min^{-1} to operate the EMA chip with a moderate flow rate for the efficient single cell trapping and the waste flow rates, Q_w, were determined by $Q_w = (Q_i - Q_o)/2$. Fig. 5A shows a time-lapse image of the microwell array in the integrated system during cell trapping, where Q_i was 20 μL min^{-1}. The focused cells, streamed from the acoustofluidic chip into the EMA chip at a flow rate of 4 μL min^{-1}, were trapped into the electroactive microwells by DEP, applying an electric potential of 4 V_{p-p} at 8 MHz to the electrodes. The positions of the microwells were gradually occupied by single DU145 cells. After trapping the cells for a minute, we counted the number of trapped cells on the EMA, where we also counted the number of introduced cells for one minute by observing the fluidic channel. The cell recovery ratio, a percentage ratio of the number of trapped cells to the number of introduced cells, of the integrated system was 96 ± 0.8%, even at an inlet flow rate of 20 μL min^{-1} (Fig. 5B). The cell trapping efficiency of the integrated system was increased 4.2 times compared with the inherent trapping efficiency of the EMA chip for the inlet flow rate of 20 μL min^{-1}. Moreover, the integrated system showed a reasonably high trapping efficiency of 65 ± 13% for an inlet flow rate as high as 100 μL min^{-1}, where no cells were trapped into the EMA chip without acoustophoretic cell focusing at the same flow rate (data not shown). These results indicate that the integration of the acoustofluidic chip to the EMA chip allows us to array singe cells with a significantly improved sample throughput capability, approaching sample volumes of milliliters in the processing time of 10 minutes.

The integrated system shows good trapping efficiency at high inlet flow rates (20, 40, and 60 μL min^{-1}) since the flow rate at the EMA chip was maintained constant. The cell recovery ratio was, however, gradually decreased with a further increased flow rate (Fig. 5B). One main reason could be caused by the difficulty in precise control of the flow in the fluidic channel. The PDMS microfluidic channel of the EMA chip and the tube connector, made of silicone, have large elasticity compared with the silicon wafer or glass substrate. The elastic deformation of the PDMS microfluidic channel, or the tube connector at the higher flow rate could cause change of the flow rate at the EMA chip or the imbalance of the flow rate at the waste outlets, respectively. Moreover, the acoustofluidic chip has inherent limitation on the cell concentration caused by the width of the critical centre fraction, a minute fraction of the total flow which contains all the cells. In the present setup, the critical centre fraction is smaller than 4% of the width of the fluidic channel at the

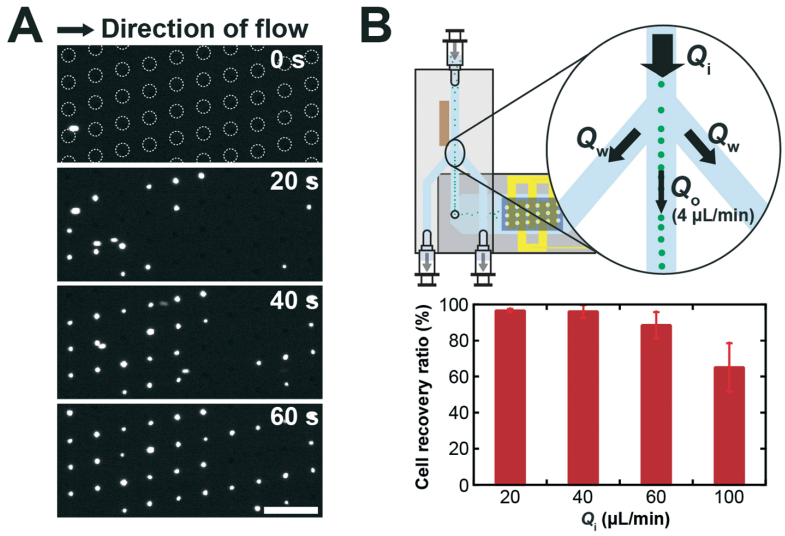

Fig. 5 DEP trapping after acoustophoretic concentration. (A) Fluorescence images of the microwell array during cell trapping. Scale bar is 200 μm. (B) Cell trapping efficiency depending on Q_i with acoustophoretic cell focusing. The outlet flow rate (Q_o) was fixed at 4 μL min^{-1} and Q_w was determined by $Q_w = (Q_i - Q_o)/2$.

flow rate of 100 μL min^{-1}. Since an acoustofluidic chip having two sequential trifurcation outlet regions can solve this limitation by splitting the critical centre fraction from the main flow sequentially,[20] one can further anticipate improvement of the sample throughput capability by using such sequential trifurcation outlets. Moreover, the width of the critical centre fraction could be widened by increasing the operation flow rate of the EMA chip.

Conclusions

In this paper, we have demonstrated the feasibility of the system integration of two original microfluidic devices having their unique functions. The integration of the acoustofluidic chip for sample pre-concentration and the EMA chip for single-cell analysis shows highly improved sample throughput, more than 10 times, on arraying of single cells while maintaining a highly efficient cell recovery ratio above 90%, compared to operating only the EMA chip. The integrated system is achieved simply by directly connecting an outlet of the acoustofluidic chip to an inlet of the EMA chip. Furthermore, the system holds potential for automation of the system for pre-concentration and trapping by controlling the electric potentials to the system. This kind of system integration of several original microfluidic devices holds promise to create a more advanced microfluidic system yet offering ease of use, and widen the scope of the field of applications in rare cell microfluidics. To further expand the feasibility of the presented integrated system, we aim to integrate a cell sorting function into the acoustofluidic chip to isolate target rare cells from blood samples based on their physical properties using acoustophoresis to build a highly integrated and automated platform for single-cell analysis of rare cells with high throughput.

Acknowledgements

This research was supported by the Japan Science and Technology Agency for Strategic International Research Cooperative Program (SICP) and the Core Research for Evolutional Science and Technology (CREST). This research was also supported by the Sten K. Johnson Foundation, the Swedish Foundation for Strategic Research and Vinnova, Multidisiplinary BIO (MBD10-0018), and the Swedish Government Agency for Innovation Systems, VINNOVA – CellCARE (2009-00236), and the Knut and Alice Wallenberg Foundation (grant no. KAW 2012.0023).

References

1 J. S. de Bono, H. I. Scher, R. B. Montgomery, C. Parker, M. C. Miller, H. Tissing, G. V. Doyle, L. W. Terstappen, K. J. Pienta and D. Raghavan, *Clin. Cancer Res.*, 2008, **14**, 6302–6309.
2 E. Sollier, D. E. Go, J. Che, D. R. Gossett, S. O'Byrne, W. M. Weaver, N. Kummer, M. Rettig, J. Goldman, N. Nickols, S. McCloskey, R. P. Kulkarni and D. Di Carlo, *Lab Chip*, 2014, **14**, 63–77.
3 H. W. Hou, M. E. Warkiani, B. L. Khoo, Z. R. Li, R. A. Soo, D. S. Tan, W. T. Lim, J. Han, A. A. Bhagat and C. T. Lim, *Sci. Rep.*, 2013, **3**, 1259.
4 P. Augustsson, C. Magnusson, M. Nordin, H. Lilja and T. Laurell, *Anal. Chem.*, 2012, **84**, 7954–7962.
5 M. Antfolk, C. Antfolk, H. Lilja, T. Laurell and P. Augustsson, *Lab Chip*, 2015, **15**, 2102–2109.
6 P. Li, Z. Mao, Z. Peng, L. Zhou, Y. Chen, P. H. Huang, C. I. Truica, J. J. Drabick, W. S. El-Deiry, M. Dao, S. Suresh and T. J. Huang, *Proc. Natl. Acad. Sci. U. S. A.*, 2015, **112**, 4970–4975.
7 N. M. Karabacak, P. S. Spuhler, F. Fachin, E. J. Lim, V. Pai, E. Ozkumur, J. M. Martel, N. Kojic, K. Smith, P. I. Chen, J. Yang, H. Hwang, B. Morgan, J. Trautwein, T. A. Barber, S. L. Stott, S. Maheswaran, R. Kapur, D. A. Haber and M. Toner, *Nat. Protoc.*, 2014, **9**, 694–710.
8 S. Choi, O. Levy, M. B. Coelho, J. M. Cabral, J. M. Karp and R. Karnik, *Lab Chip*, 2014, **14**, 161–166.
9 P. R. Gascoyne, J. Noshari, T. J. Anderson and F. F. Becker, *Electrophoresis*, 2009, **30**, 1388–1398.
10 S. Shim, K. Stemke-Hale, A. M. Tsimberidou, J. Noshari, T. E. Anderson and P. R. Gascoyne, *Biomicrofluidics*, 2013, **7**, 11807.
11 H. S. Moon, K. Kwon, S. I. Kim, H. Han, J. Sohn, S. Lee and H. I. Jung, *Lab Chip*, 2011, **11**, 1118–1125.
12 V. Plaks, C. D. Koopman and Z. Werb, *Science*, 2013, **341**, 1186–1188.
13 D. Di Carlo, L. Y. Wu and L. P. Lee, *Lab Chip*, 2006, **6**, 1445–1449.
14 D. Di Carlo, N. Aghdam and L. P. Lee, *Anal. Chem.*, 2006, **78**, 4925–4930.
15 J. R. Rettig and A. Folch, *Anal. Chem.*, 2005, **77**, 5628–5634.
16 B. M. Taff and J. Voldman, *Anal. Chem.*, 2005, **77**, 7976–7983.
17 S. Kobel, A. Valero, J. Latt, P. Renaud and M. Lutolf, *Lab Chip*, 2010, **10**, 857–863.
18 S. H. Kim, T. Yamamoto, D. Fourmy and T. Fujii, *Small*, 2011, **7**, 3239–3247.
19 S. H. Kim, X. He, S. Kaneda, J. Kawada, D. Fourmy, H. Noji and T. Fujii, *Lab Chip*, 2014, **14**, 730–736.
20 M. Nordin and T. Laurell, *Lab Chip*, 2012, **12**, 4610–4616.
21 D. I. C. Wang, T. J. Sinskey, R. E. Gerner and R. P. Defilipp, *Biotechnol. Bioeng.*, 1968, **10**, 641–649.
22 J. Yang, W. C. Hooper, D. J. Phillips, M. L. Tondella and D. F. Talkington, *Clin. Diagn. Lab. Immunol.*, 2002, **9**, 1142–1143.
23 J. Warrick, B. Casavant, M. Frisk and D. Beebe, *Anal. Chem.*, 2010, **82**, 8320–8326.
24 A. J. Mach, J. H. Kim, A. Arshi, S. C. Hur and D. Di Carlo, *Lab Chip*, 2011, **11**, 2827–2834.
25 M. Yamada and M. Seki, *Anal. Chem.*, 2006, **78**, 1357–1362.
26 A. K. Balasubramanian, K. A. Soni, A. Beskok and S. D. Pillai, *Lab Chip*, 2007, **7**, 1315–1321.
27 C. R. Cabrera and P. Yager, *Electrophoresis*, 2001, **22**, 355–362.
28 D. Puchberger-Enengl, S. Podszun, H. Heinz, C. Hermann, P. Vulto and G. A. Urban, *Biomicrofluidics*, 2011, **5**.

29 N. Gadish and J. Voldman, *Anal. Chem.*, 2006, **78**, 7870–7876.
30 P. Grodzinski, J. Yang, R. H. Liu and M. D. Ward, *Biomed. Microdevices*, 2003, **5**, 303–310.
31 J. J. Hawkes and W. T. Coakley, *Enzyme Microb. Technol.*, 1996, **19**, 57–62.
32 P. Augustsson, R. Barnkob, S. T. Wereley, H. Bruus and T. Laurell, *Lab Chip*, 2011, **11**, 4152–4164.
33 F. Petersson, L. Aberg, A. M. Sward-Nilsson and T. Laurell, *Anal. Chem.*, 2007, **79**, 5117–5123.
34 J. Voldman, *Annu. Rev. Biomed. Eng.*, 2006, **8**, 425–454.